

EXPERIMENTAL AND NUMERICAL TECHNIQUES  
RELATED TO THE STRESS ANALYSIS  
OF APPLES UNDER STATIC LOADS

A Dissertation  
for the Degree of Ph. D.  
MICHIGAN STATE UNIVERSITY  
Josse G. De Baerdemaeker  
1975

21098670

THESIS



This is to certify that the

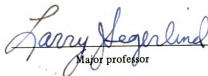
thesis entitled  
Experimental and Numerical Techniques  
Related to the Stress Analysis of  
Apples under Static Loads

presented by

Josse G. De Baerdemaeker

has been accepted towards fulfillment  
of the requirements for

Ph. D. degree in Agricultural Engineering

  
Major professor

Date 19 February 1975







## ABSTRACT

### EXPERIMENTAL AND NUMERICAL TECHNIQUES RELATED TO THE STRESS ANALYSIS OF APPLES UNDER STATIC LOADS

By

Josse G. De Baerdemaeker

The objective of this work was to develop a technique for studying the mechanical behavior of apples under static loading conditions. The apple flesh was assumed to have linear viscoelastic properties and isotropic constitutive equations were experimentally determined. These material properties were used in a numerical model which described the behavior of a spherical body under static loads.

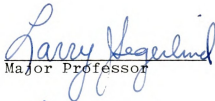
An experimental procedure for determination of bulk and shear relaxation functions and a time dependent Poisson's ratio were described. The bulk and shear relaxation functions and Poisson's ratio for Red Delicious apples exhibit time dependence. Suggestions were made for the determination of dynamic material properties and for the inclusion of a ripeness factor in the constitutive equations.

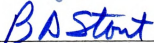
The finite element method was used to obtain numerical solutions to the viscoelastic boundary value problem of a viscoelastic sphere loaded by a rigid flat plate. The experimental relaxation functions were used. Experimental and calculated force-deformation curves at low deformation rates were compared and the differences were discussed.

An iterative procedure was developed for the study of creep behavior of a sphere under a constant load. The stress distribution in the sphere at the initial loading and at a later time were compared. The location of maximum compressive stresses was shown to be at the center of the contact area while maximum shear and tensile stresses were found near the circular boundary of the surface of contact.

This thesis concludes with suggestions for the development of a failure criterion which should also include the proven effect of time in storage on the failure strength.

Approved:

  
Major Professor

  
Department Chairman

EXPERIMENTAL AND NUMERICAL TECHNIQUES  
RELATED TO THE STRESS ANALYSIS  
OF APPLES UNDER STATIC LOADS

By

Josse G. De Baerdemaeker

A DISSERTATION

Submitted to

Michigan State University

in partial fulfillment of the requirements

for the degree of

DOCTOR OF PHILOSOPHY

Department of Agricultural Engineering

1975



693210

## ACKNOWLEDGMENTS

The author sincerely appreciates the guidance and counsel he received during his graduate work. The close cooperation with Dr. Larry J. Segerlind, his major professor, was fruitful and agreeable. Discussions with Drs. D. H. Dewey (Horticulture), J. B. Gerrish (Agricultural Engineering) and W. N. Sharpe (Metallurgy, Mechanics, and Material Science) were very inspiring and constructive.

Appreciation is extended to the Agricultural Engineering Department for a research assistantship, and to the Commission for Educational Exchange between the United States of America, Belgium and Luxembourg for the scholarship at the beginning of this graduate work.

## TABLE OF CONTENTS

	<u>Page</u>
LIST OF FIGURES . . . . .	v
LIST OF TABLES . . . . .	ix
1. INTRODUCTION . . . . .	1
2. LITERATURE REVIEW . . . . .	4
2.1 Constitutive Equations or Stress-Strain Relations . . . . .	4
2.1.1 Viscoelastic Behavior of Agricultural Products . . . . .	4
2.1.2 Viscoelastic Constitutive Equations . . . . .	5
2.1.3 Constitutive Equations of Agricultural Products . . . . .	8
2.1.4 Some Other Experiments . . . . .	11
2.2 Analysis of Stress in Fruits Under Loading . . . . .	12
2.3 Criteria for Maximum Allowable Load . . . . .	13
2.4 Comments and Conclusions . . . . .	15
3. CONSTITUTIVE EQUATIONS OF APPLE FLESH . . . . .	18
3.1 Equations of the Linear Theory of Viscoelasticity . . . . .	18
3.1.1 Laplace Transform of Viscoelastic Equations . . . . .	18
3.1.2 Complex Modulus Representation . . . . .	20
3.2 Analysis of a Relaxation Experiment . . . . .	24
3.2.1 Experimental Determination of the Relaxation Functions $E(t)$ and $X(t)$ . . . . .	28

	<u>Page</u>
3.2.2 Numerical Interconversions of the Relaxation Functions: Approximate Laplace Transform Inversion . . .	34
3.2.3 Accuracy of the Method . . .	38
3.2.4 Summary of the Procedure . . .	42
3.3 Determination of Dynamic Properties . . .	43
3.4 Closure . . . . .	45
4. EXPERIMENTAL PROCEDURE . . . . .	47
4.1 Apple Selection and Storage . . . . .	47
4.2 Sample Preparation . . . . .	47
4.3 Relaxation Tests . . . . .	49
5. EXPERIMENTAL RELAXATION FUNCTIONS . . . . .	53
5.1 Relaxation Force Curves . . . . .	53
5.2 Relaxation Functions . . . . .	62
5.3 Average Values of Relaxation Functions . . . . .	68
6. FINITE ELEMENT FORMULATION IN VISCOELASTICITY . . . . .	75
6.1 Viscoelasticity Boundary Value Problem: Variational Theorem . . . . .	75
6.2 Axisymmetric Viscoelastic Solids . . . . .	78
6.3 Discretization of a Region: Finite Element Formulation . . . . .	81
6.3.1 Nodal Displacements . . . . .	81
6.3.2 Element Stresses . . . . .	87
7. NUMERICAL ANALYSIS OF MECHANICAL BEHAVIOR OF APPLES UNDER LOADS . . . . .	88
7.1 Division into Elements . . . . .	89

	<u>Page</u>
7.2 Special Techniques for the Solution of Contact Problems . . . . .	. 89
7.3 Material Properties . . . . .	. 94
7.4 Specimen Subjected to a Constant Deformation Rate . . . . .	.100
7.5 Behavior of Fruit Under a Constant Load	.108
7.5.1 Creep Behavior of a Cylindrical Specimen . . . . .	.108
7.5.2 Creep Behavior of a Spherical Specimen . . . . .	.110
7.6 Closure . . . . .	.124
8. SUMMARY AND CONCLUSIONS . . . . .	.125
9. FURTHER DEVELOPMENTS AND SUGGESTIONS FOR FUTURE RESEARCH . . . . .	.127
9.1 Change of Material Properties During Ripening . . . . .	.127
9.2 The Effect of the Skin . . . . .	.129
9.3 Dynamic Mechanical Properties . . . . .	.130
9.4 Development of a Failure Criterion . . . . .	.130
BIBLIOGRAPHY . . . . .	.134
APPENDIX A . . . . .	.142

## LIST OF FIGURES

<u>Figure</u>	<u>Page</u>
3.1      Uniaxial Compression and Constrained Compression of Cylindrical Samples      .      .	25
3.2      Ramp-Step Deformation Function      .      .      .	31
3.3      Force on a Specimen Subjected to a Ramp-Step Deformation Function      .      .      .      .      .	31
4.1      Sample Cutting Machine      .      .      .      .      .	48
4.2      Force and Deformation Measuring and Recording Equipment      .      .      .      .      .	48
4.3      Schematic Diagram of Equipment for a Relaxation Test      .      .      .      .      .      .	50
4.4      Analysis of Relaxation Test Data to Obtain Relaxation Functions and Poisson's Ratio      .	52
5.1      Uniaxial Relaxation Force; Model Not Through First Data Point      .      .      .      .      .	54
5.2      Constrained Relaxation Force; Model Not Through First Data Point      .      .      .      .      .	55
5.3      Uniaxial Relaxation Force; Model Through First Data Point      .      .      .      .      .      .	59
5.4      Constrained Relaxation Force; Model Through First Data Point      .      .      .      .      .      .	60
5.5      Uniaxial Relaxation Function      .      .      .      .	63
5.6      Constrained Relaxation Function      .      .      .	64
5.7      Bulk Relaxation Function      .      .      .      .      .	65
5.8      Shear Relaxation Function      .      .      .      .      .	66
5.9      Time Dependent Poisson's Ratio      .      .      .	67
5.10     Average and Standard Deviation of Uniaxial Relaxation Function for 24 Red Delicious Apples      .      .      .      .      .      .      .	70



	<u>Page</u>
5.11 Average and Standard Deviation of the Constrained Relaxation Function of 24 Red Delicious Apples . . . . .	71
5.12 Average and Standard Deviation of the Bulk Relaxation Function of 24 Red Delicious Apples . . . . .	72
5.13 Average and Standard Deviation of the Shear Relaxation Function of 24 Red Delicious Apples . . . . .	73
5.14 Average and Standard Deviation of the Poisson's Ratio of 24 Red Delicious Apples . . . . .	74
6.1 Stresses in Axially Symmetric Problems . . . . .	79
6.2 Triangular Axisymmetric Element and Nodal Displacements . . . . .	83
7.1 Finite Element Grid for a Cylindrical Specimen . . . . .	90
7.2 Finite Element Grid for a Spherical Specimen . . . . .	91
7.3 Spherical Sample in Contact with Rigid Flat Plate: Prescribed Displacement of the Contact Nodes . . . . .	93
7.4 Iterative Procedure for Determining the Deformation Under a Constant Load . . . . .	95
7.5 Uniaxial Relaxation Function for Sample I . . . . .	96
7.6 Constrained Relaxation Function for Sample I . . . . .	97
7.7 Bulk Relaxation Function for Sample I . . . . .	98
7.8 Shear Relaxation Function for Sample I . . . . .	99
7.9 Comparison of Analytical and Numerical Force Versus Time Curves of a Cylindrical Specimen Under Constant Deformation Rate of 2.54 mm/min . . . . .	101
7.10 Experimental and Calculated Force-Time Curves of a Cylindrical Specimen, Sample I. Deformation Rate = 2.54 mm/min . . . . .	103

	<u>Page</u>
7.11 Experimental and Calculated Force-Time Curves of a Cylindrical Specimen, Sample II. Deformation Rate = 2.54 mm/min . . .	104
7.12 Experimental and Calculated Force-Time Curves of a Spherical Specimen, Sample I. Deformation Rate = 2.54 mm/min . . .	106
7.13 Experimental and Calculated Force-Time Curves of a Spherical Specimen, Sample II. Deformation Rate = 2.54 mm/min . . .	107
7.14 Uniaxial Compliance (Sample I) . . .	109
7.15 Creep Response of a Cylindrical Specimen of 19.1 mm Length Subjected to a Constant Compressive Force of 80 N . . .	111
7.16 Calculated Creep Response of a Sphere with a 17.8 mm Radius Under Flat Plate Compressive Load of 50 N . . .	112
7.17 Lines of Constant Stress in the z-Direction at Time $t=0$ . . .	113
7.18 Lines of Constant Maximum Principal Stress at Time $t=0$ . . .	114
7.19 Lines of Constant Minimum Principal Stress at Time $t=0$ . . .	115
7.20 Lines of Maximum Shear Stress at Time $t=0$ .	116
7.21 Lines of Constant Stress in the z-Direction at Time $t=0.76$ . . .	118
7.22 Lines of Constant Maximum Principal Stress at Time $t=0.76$ . . .	119
7.23 Lines of Constant Minimum Principal Stress at Time $t=0.76$ . . .	120
7.24 Lines of Maximum Shear Stress at Time $t=0.76$	121
7.25 Maximum Compressive and Shear Stress in a Spherical Sample Under a 50 N Creep Load (Sample Diameter = 17.8 mm) . . .	122
7.26 Deformed Finite Element Grid of the Spherical Sample at Time $t=0.76$ . . .	123

	<u>Page</u>
9.1 Failure Locus of Parenchyma of Northern Spy Apples at Two Strain Rates (Calculated From Data by Miles and Rehkugler, 1971)	131

## LIST OF TABLES

<u>Table</u>	<u>Page</u>
3.1      Influence of the measurement errors on the values of the bulk and shear relaxation functions . . . . .	41
5.1      Variance-covariance matrices of parameters in a two-term exponential series . . . . .	57
5.2      Variance-covariance matrices of parameters in a two-term exponential series subjected to the linear restraint $C_1 = F(t'=0) - C_2$ . . . . .	61
5.3      Average values and standard deviations of the relaxation functions of 24 Red Delicious apples . . . . .	69

## 1. INTRODUCTION

Mechanization of fruit harvesting and handling operations has become widespread in recent years. A major design concern is the effect mechanical harvesting and handling has on the quality of the products, particularly the level of bruise damage that occurs during these operations.

One phase of the fruit handling process that is undergoing some major changes is the storage. A lumber shortage has stirred an interest in the bulk storage of apples, thereby eliminating the need for a large number of bulk bins.

Fresh market apples have to be (almost) completely bruise free, but bruise damage in apples for the processing industry is acceptable as long as most of the bruised tissue can be removed during the peeling operation. Larger bruises require bleaching and increase processing costs.

The increased interest in the bulk storage of apples for processing has raised the question of the allowable depth to which apples can be piled before excessive bruising occurs. The answer to this problem can be sought along two lines. First, experiments can be conducted to determine the maximum allowable drop height, the



relationship between drop height and bruise size, and the relationship between stack height and bruise size. The results of these experiments are valuable only for the practical applications they simulate because they do not furnish enough basic information for possible use in other applications. An alternate method is to approach apple bruising from a mechanics of deformable bodies point of view, using the laws that govern the static or dynamic behavior of the material.

The latter approach has become more acceptable in recent years. Most research in this area, however, has been limited either to attempts to formulate the constitutive equations of the tissue (Mohsenin and Goehlich, 1962), to solve viscoelastic boundary value problems (Hamann, 1967), or else to define a failure criterion (Miles and Rehkugler, 1971). While these are essential in the study of bruising of fruits, they are, by themselves, insufficient to completely describe the behavior of fruit during bruising. The study of bruising is hindered by two primary items: the difficulty in completely defining the time dependent material properties and the difficulty in calculating the stresses in the fruit which result from a contact type of loading.

The objective of this work was to develop some experimental and analytical techniques required in studying the behavior of fruit during loading. The specific objectives were:

- (1) To establish an experimental technique for determining the constitutive equations governing the mechanical behavior of apple tissue.
- (2) To use the experimental values of the constitutive equations in a finite element model for the solution of viscoelastic boundary value problems and to verify the numerical technique by comparing experimental and numerical force-deformation curves.
- (3) To study the stress distribution in apples under loading and gain some insight in the formation of a bruise.

It is important to note that this work was based on the assumption that the undamaged fruit tissue can be considered homogeneous and isotropic, a good macroscopic approximation. Other recent research has also approached the behavior of the tissue by considering its basic composition as a mixture of solids, liquids and gas (Brusewitz, 1969; Akyurt, 1969; Gustafson, 1974).

## 2. LITERATURE REVIEW

In a review of a decade of research on mechanical properties of fruits and vegetables, Mohsenin (1971) cited some immediate applications, among which were: characterizations of the material, optimum time to harvest, quality evaluation, damage in collecting, handling and storage. Mohsenin (1971) cites ample literature on the work done toward these applications. Some of this work relates to the characterization of the material and the use of the material properties in evaluating stresses in fruit under static and dynamic loading and the study of the bruise susceptibility of the product. The pertinent topics are summarized below.

### 2.1 Constitutive Equations or Stress-Strain Relations

#### 2.1.1 Viscoelastic Behavior of Agricultural Products

During the early experiments on mechanical behavior of fruits and vegetables, it was observed that force deformation relations include time effects (Finney, 1963; Mohsenin, 1963; Timbers *et al.*, 1966). Morrow and Mohsenin (1966) review some of these early investigations and conducted a study of their own. Their study led them to conclude that McIntosh apples can be considered as

viscoelastic bodies, with a nearly linear behavior. Chappell and Hamann (1968) also studied the viscoelastic behavior of apple flesh, but they found the material properties to be somewhat stress dependent and thus could not be exactly characterized as linear. Hamann (1967 and 1970) also noted the non-linear properties in apple flesh, but he made the assumption of linearity to facilitate his analysis. Clevenger and Hamann (1968) concluded from uniaxial tensile tests that the apple skin also has a viscoelastic behavior.

### 2.1.2 Viscoelastic Constitutive Equations

The theory of viscoelasticity is adequately described by several authors such as Flugge (1967), Christensen (1971), and Ferry (1970). There are several equivalent forms of the constitutive equations of viscoelastic materials: hereditary integral forms, differential operator form, complex modulus form. The integral form of the constitutive equations can be written as (Christensen, 1971)<sup>1</sup>

---

<sup>1</sup>The standard indicial system for a rectangular Cartesian reference frame is employed whenever applicable: Repeating the subscripts i, j, k or l implies summation, Kronecker's delta is denoted by  $\delta_{ij}$ , differentiation with respect to space is indicated by subscripts preceded by a comma.

$$s_{ij} = \int_{-\infty}^t G_1(t-\tau) \frac{de_{ij}(\tau)}{d\tau} d\tau \quad (2.1)$$

$$\sigma_{kk} = \int_{-\infty}^t G_2(t-\tau) \frac{d\epsilon_{kk}(\tau)}{d\tau} d\tau \quad (2.2)$$

where  $G_1(t)$  is a relaxation function appropriate to states of shear and  $G_2(t)$  is a relaxation function appropriate to states of dilatation. The deviatoric stress and strain tensors are

$$s_{ij} = \sigma_{ij} - \frac{1}{3} \delta_{ij} \sigma_{kk} \quad , \quad s_{ii} = 0 \quad (2.3)$$

and

$$e_{ij} = \epsilon_{ij} - \frac{1}{3} \delta_{ij} \epsilon_{kk} \quad , \quad e_{ii} = 0 \quad (2.4)$$

respectively with  $\sigma_{ij}$  = stress tensor

$\epsilon_{ij}$  = strain tensor

$\delta_{ij}$  = Kronecker delta, zero for  $i \neq j$

and  $\delta_{ii} = \delta_{11} + \delta_{22} + \delta_{33} = 3$

$\sigma_{kk}$  = first invariant of the stress tensor

$\epsilon_{kk}$  = first invariant of the strain tensor



In order to use the same notation as in elasticity, the relaxation functions in simple shear and dilation are taken as

$$G(t) = G_1(t)/2 \quad (2.5)$$

$$K(t) = G_2(t)/3 \quad (2.6)$$

These relaxation functions are equivalent to the elastic shear and bulk moduli, respectively.

An alternate form of the stress-strain relation is obtained by using creep functions to represent the current strain as determined by current value and past history of stress (Christensen, 1971)

$$e_{ij} = \int_{-\infty}^t J_1(t-\tau) \frac{d s_{ij}(\tau)}{d\tau} d\tau \quad (2.7)$$

$$\epsilon_{kk} = \int_{-\infty}^t J_2(t-\tau) \frac{d \tau_{kk}(\tau)}{d\tau} d\tau \quad (2.8)$$

where  $J_1(t)$  and  $J_2(t)$  are creep functions for states of shear and dilatation. They can be related to the relaxation functions by use of Laplace Transforms or other interconversion techniques (Knoff and Hopkins, 1972). Shear and bulk modulus are two independent constants characterizing a homogeneous elastic solid, and the relations between these and more commonly used engineering parameters like Young's modulus and Poisson's ratio have

been established (see Sokolnikoff, 1956). Similar relations exist between the Laplace transforms of the viscoelastic relaxation functions (Christensen, 1971). The commonly used relaxation function  $E(t)$  which characterizes a state of uniaxial extension and a viscoelastic Poisson's ratio  $\nu(t)$  can be defined as the viscoelastic equivalents to Young's modulus and Poisson's ratio in elasticity.

### 2.1.3 Constitutive Equations of Agricultural Products

Simple mechanical models of combinations of elastic and viscous elements have been used to represent viscoelastic behavior of fruits. These mechanical models are described in more detail in Flügge (1967) and Mohsenin (1970). They all represent a possible approximation for describing the viscoelastic behavior with an elastic or a viscous model as the limits. The material is often considered to be elastic in dynamic experiments (Fridley *et al.*, 1968; Horsfield *et al.*, 1972). Poisson's ratio has been evaluated both as an elastic constant (Finney, 1963; Morrow, 1965; Hughes and Segerlind, 1972) and a time dependent value (Chappell and Hamann, 1968).

Finney (1963) calculated an elastic Poisson's ratio for potatoes from a mean bulk modulus and mean uniaxial compression modulus. Morrow (1965) used an elastic bulk modulus and Boussinesq solution for a cylindrical plunger on a half space to simultaneously determine an elastic

uniaxial modulus and elastic Poisson's ratio. Hughes and Segerlind (1972) derived an elastic Poisson's ratio by comparing the axial force-deformation relation of two cylindrical samples, one specimen was free to expand in the radial direction while the other was not.

Bulk compression and uniaxial compression are most commonly used to determine the relaxation functions, while torsion and tension tests are very difficult to apply because of gripping problems (Morrow and Mohsenin, 1966). Morrow (1965) and Sharma and Mohsenin (1970) used hydrostatic compression for evaluation of the bulk creep function. Uniaxial compression has been extensively used for evaluation of the uniaxial relaxation function  $E(t)$  (Finney, 1963; Chappell and Hamann, 1968; Hammerle *et al.*, 1971; Morrow *et al.*, 1971).

Direct methods for measuring viscoelastic Poisson's ratio have been investigated. Chappell and Hamann (1968) measured lateral displacement of an axially compressed specimen using linear variable differential transformers (LVDT) on each side of the specimen. They observed that Poisson's ratio of apples decreased with increasing time. Mohsenin (1970) mentions the measuring microscope as well as a Nikon Shadowgraph for direct measurement of Poisson's ratio. No time dependency of this parameter is mentioned. Hammerle and McClure (1970) used a photomicrometer and found that Poisson's ratio of sweet potato flesh increased with time.

A widely used form of the relaxation function is an exponential series representation known as the generalized Maxwell Model

$$E(t) = \sum_{j=0}^n E_j e^{-\alpha_j t} \quad (2.9)$$

Several authors have discussed methods to determine the parameters  $E_j$  and  $\alpha_j$  from experimental relaxation curves (Gradowczyk and Moavenzadeh, 1969; Mohsenin, 1970; Hammerle and Mohsenin, 1970; Chen and Fridley, 1972; Bashford and Whitney, 1973).

Creep functions are sometimes approximated using elastic elements and viscous elements in parallel, as represented by the series (Gradowczyk and Moavenzadeh, 1969)

$$D(t) = \sum_{j=0}^m D_j (1 - e^{-\beta_j t}) \quad (2.10)$$

Models of this kind were used to approximate the bulk compressive behavior of apples (Morrow, 1965; Sharma and Mohsenin, 1970).

Hamann (1969) attempted to experimentally determine the dynamic axial compression relaxation function and the shear relaxation function by measuring complex moduli and the use of an approximate equation relating relaxation functions and complex moduli. He found that a simple Maxwell Model (spring and dashpot in series) is a good

approximation of uniaxial dynamic behavior, while the shear experiments gave no reliable results.

Peterson and Hall (1973) found no consistent interdependency of the complex modulus and temperature when studying potato flesh.

#### 2.1.4 Some Other Experiments

Theocaris (1964) has shown that the information obtained from a simple tension test along the whole response spectrum of the material together with an initial value of the lateral contraction ratio are sufficient for the complete description of the viscoelastic properties of the material. The lateral contraction ratio functions are monotonically increasing functions. Rigbi (1967) also recognized this delayed lateral deformation of viscoelastic materials. Gottenberg and Christensen (1964) demonstrated that the complex shear modulus function is a convenient property to experimentally determine and that the shear relaxation function may be obtained by direct conversion from the frequency to the time domain.

Parsons *et al.* (1969) used a specimen under tensile stress and a "shear-sandwich" specimen for the measurement of the complex uniaxial relaxation function and the complex shear relaxation function.

Laird and Kingsbury (1973) described an experiment for determining the longitudinal complex modulus function.

Their experimental setup consisted of a single degree of freedom system with the material specimen acting as a massless stiffness element, whose spring constant is represented by a complex number.

Hayes and Morland (1968) proposed different constrained compression tests for determination of response functions of anisotropic linear viscoelastic materials. Their derivations were based on the hereditary integral representation and no actual experiments were described.

Arridge (1974) determined the bulk or dilatational relaxation function of solid polymers from measuring the extensions of a tube of the material under internal pressure.

## 2.2 Analysis of Stress in Fruits Under Loading

Limited work has been done to analyze stresses in fruits under loading. Hamann (1970) solved the contact problem involving one viscoelastic spherical body falling onto another for the approach of the bodies, surface indentations, surface pressures and internal stresses. He used a simple Maxwell model for the uniaxial relaxation function and a constant Poisson's ratio when specifying the constitutive equations. The finite element method has been used to determine the stresses in apples subjected to a contact type load. Apaclla (1973) assumed an elastic material. Rumsey and Fridley (1974) used a

material with constant bulk modulus and time dependent shear relaxation function.

### 2.3 Criteria for Maximum Allowable Load

Considerable work has been done on experimental determination of loads that cause failure or rupture in fruits or vegetables. Nelson and Mohsenin (1968) have determined a relation between bruise volume and load. They report that bruises caused by dynamic loads are considerably larger than those caused by equivalent quasi-static loads. In an effort to understand the criteria associated with bruising, researchers have attempted to define parameters associated with damage of agricultural products. Some of those parameters are energy to bruising, maximum force during impact, maximum stresses within the product or maximum deformation. Energy required for bruising was reported greater under impact conditions than under quasi-static loading conditions for apples (Mohsenin and Göhlich, 1962), apples and peaches (Fridley *et al.*, 1964). However, others have found lower energy to damage under impact than under quasi-static conditions for sweet potatoes (Wright and Splinter, 1968) and pears (Fridley and Adrian, 1966). Fletcher *et al.* (1965) reported that energy force and deformation to rupture first decrease with increasing loading rate, then increase. Maximum force during impact

was studied by Davis and Rehkugler (1971) for apple-limb impact and by Hammerle and Mohsenin (1966) and Simpson and Rehkugler (1972) for cushioned impact of apples. Wright and Splinter (1968) reported that rupture forces of cylindrical samples of sweet potatoes during impact were about one-third of those under slow loading. Fluck and Ahmed (1972) studied impact bruising of whole fruits and concluded from their experiments that it was impossible to say whether energy or force is the more important parameter in bruising.

The location of the bruise has suggested that maximum shear stress can be a possible failure parameter (Fridley and Adrian, 1966). Horsfield *et al.* (1972) predicted damage of peaches caused by impact based upon the theory of elastic impact, the radii of curvature, the impact energy, the elastic modulus and the shear strength. The shear strength of the material was determined from calculating the shear stresses that exist in an impacting elastic sphere and the observation of whether or not a bruise had occurred.

Miles and Rehkugler (1971) attempted to define a failure criterion for apple flesh using a uniaxial compression force superimposed with a hydrostatic compression. The hydrostatic pressure was of the same order of magnitude as the mean normal stress at failure. They confirmed that stress at failure is a function of strain rate. They concluded that shear stress is the most significant failure parameter.



## 2.4 Comments and Conclusions

Several researchers have established the almost linear viscoelastic behavior of agricultural products. Attempts have been made to experimentally determine the relaxation or creep functions describing this viscoelastic behavior. It was noted that a uniaxial relaxation function can easily be found from a relaxation experiment. However, the determination of a second relaxation function to completely describe the properties of a linear material has been less successful. Assumptions have been made that either Poisson's ratio or the bulk modulus are constant. Other experiments were thereby based on the formulae of the theory of elastic contact in which the boundary conditions are only approximately described. Christensen (1971) states that the ideal experimental procedure is the one where the analysis, used to relate the mechanical property of interest to an observable quantity, must yield the exact solution of the field equations of the theory and represent the exact boundary conditions of the specimen. A torsion test of a cylindrical sample as used for the determination of the shear relaxation function satisfies the above conditions. However, the nature of the agricultural product makes the torsion test nearly impossible. Direct measurement of Poisson's ratio during a uniaxial compression test is an alternative solution, but no standard procedure has

evolved. This is also partially due to the nature of the material.

Stress analysis in fruits under loading has been limited either by the insufficient knowledge of the material properties or by the lack of analytical solutions to various -- sometimes complicated -- boundary conditions or by both. The recent introduction of the finite element technique in the agricultural field offers an excellent alternative to analytical solutions. However, some of the applications were restricted by the limited availability of material properties. Assumptions were made that one or both of the material property functions were elastic instead of viscoelastic.

The determination of the maximum allowable load on fruit under different loading conditions has been the subject of several experimental investigations while there have been no analytical approaches to it. The recent work of Miles and Rehkugler (1971) was a first attempt to establish a failure criterion for apple flesh. After analysis of their data, it remains unclear whether the maximum shear stress theory or the distortion energy theory or any variation of these can be used as a valid failure criterion.

In summary, many attempts have been made to describe the mechanical behavior of fruits. The determination of the constitutive equations as well as the stress analysis within the fruits subjected to a load have been based on

assumptions that limit their applicability, and a firm criterion for material failure is missing. No unified study which determines the material properties, and then uses these properties to determine the state of stresses at failure has been undertaken.

### 3. CONSTITUTIVE EQUATIONS OF APPLE FLESH

The determination of the material properties is a basic step in modeling the behavior of an apple subjected any loading. The review of literature indicated there are some difficulties in the experimental determination of the stress-strain relations of apple flesh due to the nature of the product. A new experimental technique which allows the determination of two relaxation functions for an isotropic homogeneous material is presented in this section.

#### 3.1 Equations of the Linear Theory of Viscoelasticity

##### 3.1.1 Laplace Transform of Viscoelastic Equations

The convolution integral form of the viscoelastic constitutive equations was given in Chapter 2, equations (2.1)-(2.8). The relationship between the different relaxation and creep functions can be established by introducing the Laplace transformation. Let  $f(t)$  be a continuous function over  $0 < t \leq \infty$ . The Laplace transform of this function is

$$\bar{f}(s) = L[f(t)] = \int_0^{\infty} f(t)e^{-st} dt \quad (3.1)$$

Application of the transformation to the convolution integrals (2.1), (2.2), (2.7) and (2.8) yields (Christensen, 1971)

$$\bar{s}_{ij}(s) = s\bar{G}_1(s) \bar{e}_{ij}(s) \quad (3.2)$$

$$\bar{\sigma}_{kk}(s) = s\bar{G}_2(s) \bar{\epsilon}_{kk}(s) \quad (3.3)$$

$$\bar{e}_{ij}(s) = s\bar{J}_1(s) \bar{s}_{ij}(s) \quad (3.4)$$

$$\bar{\epsilon}_{kk}(s) = s\bar{J}_2(s) \bar{\sigma}_{kk}(s) \quad (3.5)$$

In the case of simple uniaxial extension

$$\bar{\sigma}_{11}(s) = s \bar{E}(s) \bar{\epsilon}_{11}(s) \quad (3.6)$$

where  $\bar{E}(s)$  is the Laplace transform of the uniaxial relaxation function  $E(t)$ . The equation (3.6) is similar to the elastic uniaxial stress-strain relationship

$$\sigma_{11} = E \epsilon_{11} \quad (3.7)$$

The similarity between (3.6) and (3.7) is expressed more specifically in the correspondence principle (Flügge, 1967; Christensen, 1971) which states that a solution to a viscoelastic problem can be obtained by replacing the elastic moduli in the elastic solution by the  $s$

multiplied transform of the corresponding viscoelastic relaxation function. The resulting functions are the Laplace transforms of the solution to the viscoelastic problem.

The solution in the time domain can be obtained using the inverse transforms of a function. This is given by

$$f(t) = L^{-1}[\bar{f}(s)] = \frac{1}{2\pi i} \int_{a-i\infty}^{a+i\infty} \bar{f}(s) e^{st} ds \quad (3.8)$$

The inverse Laplace transform of several common functions can be obtained from a table of Laplace transforms and a partial fraction expansion of  $\bar{f}(s)$ . The residue theorem (or integration along a contour in the complex  $s$ -plane) can be used when  $\bar{f}(s)$  is expressed as a quotient of polynomials in which the polynomial in the denominator is of a higher order than that in the numerator (Wylie, 1960; p. 711-716). The above methods have some disadvantages in numerical analysis. An approximate numerical method to evaluate the inverse Laplace transform is discussed later in this chapter.

### 3.1.2 Complex Modulus Representation

It is sometimes desirable to express the constitutive equations as a function of frequency rather than time. Conversion from the time domain to the frequency domain

and vice versa is accomplished using the Fourier transform

$$\bar{f}(\omega) = \int_{-\infty}^{+\infty} f(t) e^{-i\omega t} dt \quad (3.9)$$

and the inverse Fourier transform

$$f(t) = \frac{1}{2\pi} \int_{-\infty}^{+\infty} \bar{f}(\omega) e^{i\omega t} d\omega \quad (3.9a)$$

According to Christensen (1971), the Fourier transform of the relaxation function for deviatoric stress is

$$\bar{s}_{ij}(\omega) = \int_{-\infty}^{+\infty} \left[ \int_{-\infty}^t G_1(t-\tau) \frac{d \epsilon_{ij}(\tau)}{d\tau} d\tau \right] e^{-i\omega t} dt \quad (3.10)$$

If  $\epsilon_{ij}(\tau) = 0$  for  $t < 0$ , and  $\lambda = (t-\tau)$ , then

$$\bar{s}_{ij}(\omega) = \left[ \int_0^{\infty} \frac{d \epsilon_{ij}(\tau)}{d\tau} e^{-i\omega\tau} d\tau \right] \left[ \int_0^{\infty} G_1(\lambda) e^{-i\omega\lambda} d\lambda \right] \quad (3.11)$$

and

$$\int_0^{\infty} \frac{d \epsilon_{ij}(\tau)}{d\tau} e^{-i\omega\tau} d\tau = i\omega \int_0^{\infty} \epsilon_{ij}(\tau) e^{-i\omega\tau} d\tau = i\omega \bar{\epsilon}_{ij}(\omega) \quad (3.12)$$

Decomposing  $\bar{G}(t)$  into two parts

$$G_1(t) = \overset{0}{G}_1 + \hat{G}_1(t) \quad (3.13)$$

where  $\hat{G}_1(t) \rightarrow 0$  as  $t \rightarrow \infty$  and substituting into the second integral of (3.11) yields

$$\int_0^{\infty} G_1(\lambda) e^{-i\omega\lambda} d\lambda = \frac{G_1^0}{i\omega} + \int_0^{\infty} \hat{G}_1(\lambda) e^{-i\omega\lambda} d\lambda \quad (3.14)$$

Equation (3.11) can be rewritten as

$$\begin{aligned} \bar{s}_{ij}(\omega) = \bar{e}_{ij}(\omega) & \left[ G_1^0 + \omega \int_0^{\infty} \hat{G}_1(\lambda) \sin \omega\lambda d\lambda + \right. \\ & \left. i\omega \int_0^{\infty} \hat{G}_1(\lambda) \cos \omega\lambda d\lambda \right] \end{aligned} \quad (3.15)$$

or

$$\bar{s}_{ij}(\omega) = G_1^*(i\omega) \bar{e}_{ij}(\omega) \quad (3.16)$$

after some modification where  $G_1^*(i\omega)$  is the complex deviatoric modulus with real and imaginary parts given by

$$G_1'(\omega) = G_1^0 + \omega \int_0^{\infty} \hat{G}_1(\lambda) \sin \omega\lambda d\lambda \quad (3.17)$$

and

$$G_2''(\omega) = \omega \int_0^{\infty} \hat{G}_1(\lambda) \cos \omega\lambda d\lambda \quad (3.18)$$

Similar expressions can be derived from the Fourier transform of the dilatational stress-strain relations yielding



$$\bar{\sigma}_{kk}(\omega) = G_2^*(i\omega) \bar{\epsilon}_{kk}(\omega) \quad (3.19)$$

whereby the complex dilatational modulus has as the real and the imaginary part

$$G_2'(\omega) = G_2^0 + \omega \int_0^\infty \hat{G}_2(\lambda) \sin \omega \lambda d\lambda \quad (3.20)$$

and

$$G_2''(\omega) = \omega \int_0^\infty \hat{G}_2(\lambda) \cos \omega \lambda d\lambda \quad (3.21)$$

Equations (3.17), (3.18) and (3.20), (3.21) convert the relaxations functions from the time domain to the frequency domain. Since they have the form of a Fourier sine or cosine transform they can be inverted to yield (Christensen, 1971)

$$G_\alpha(t) = \frac{2}{\pi} \int_0^\infty \frac{G_\alpha'(\omega)}{\omega} \sin \omega t d\omega \quad (3.22)$$

$$\hat{G}_\alpha(t) = \frac{2}{\pi} \int_0^\infty \frac{G_\alpha''(\omega)}{\omega} \cos \omega t d\omega \quad (3.23)$$

and  $\alpha = 1, 2$

Equations (3.22) and (3.23) provide a means of obtaining the relaxation functions from dynamic experiments.

### 3.2 Analysis of a Relaxation Experiment

The experimental procedure discussed in this section is based on a method developed by Hughes and Segerlind (1972), who used the procedure to measure the elastic modulus and Poisson's ratio of biological materials under the assumption of time independence. The procedure involves the compression of two cylindrical cores of material. One sample is compressed axially while free to deform in the transverse direction. The second sample is compressed inside a rigid die which prevents lateral deformation (Figure 3.1).

This procedure can also be used to obtain the time dependent material properties of apple flesh. The proof of this follows.

Equations (3.2) and (3.3) are rewritten here in a simple manner whereby the Laplace transform is indicated by a bar

$$\bar{s}_{ij} = s \bar{G}_1 \bar{e}_{ij} \quad (3.24)$$

$$\bar{\sigma}_{kk} = s \bar{G}_2 \bar{\epsilon}_{kk} \quad (3.25)$$

and from (2.3) and (2.4)

$$\bar{s}_{ij} = \bar{\sigma}_{ij} - \frac{1}{2} \delta_{ij} \bar{\sigma}_{kk} \quad (3.26)$$

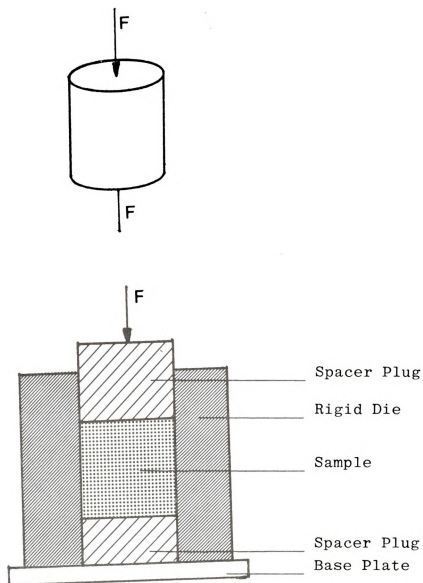


Figure 3.1. Uniaxial Compression and Constrained Compression of Cylindrical Samples

$$\bar{e}_{ij} = \bar{\epsilon}_{ij} - \frac{1}{3} \delta_{ij} \bar{\epsilon}_{kk} \quad (3.27)$$

When a simple uniaxial compression exists in the direction of  $\sigma_{11}$ , the boundary conditions are

$$\bar{\sigma}_{22} = \bar{\sigma}_{33} = 0 \quad (3.28)$$

Combining (3.24), (3.26), (3.27) and (3.28) yields

$$\bar{\sigma}_{11} - \frac{1}{3} \bar{\sigma}_{11} = s \bar{G}_1 \left[ \frac{2}{3} \bar{\epsilon}_{11} - \frac{1}{3} (\bar{\epsilon}_{22} + \bar{\epsilon}_{33}) \right] \quad (3.29)$$

and inserting (3.28) in (3.25) gives

$$\bar{\sigma}_{11} = s \bar{G}_2 (\bar{\epsilon}_{11} + \bar{\epsilon}_{22} + \bar{\epsilon}_{33}) \quad (3.29a)$$

Elimination of  $\bar{\epsilon}_{22}$  and  $\bar{\epsilon}_{33}$  from (3.29) and (3.29a) gives an expression for the uniaxial relaxation function

$$\bar{\sigma}_{11} = s \bar{E} \bar{\epsilon}_{11} \quad (3.30)$$

whereby

$$\bar{E} = \frac{3 \bar{G}_1 \bar{G}_2}{\bar{G}_1 + 2\bar{G}_2} \quad (3.31)$$

If a sample is compressed in a rigid die with no transverse deformation possible then

$$\varepsilon_{22} = \varepsilon_{33} = 0 \quad (3.32)$$

Combining (3.24), (3.25), (3.27) and (3.32), and (3.25) and (3.32) yields

$$\bar{\sigma}_{11} - \frac{1}{3}(\bar{\sigma}_{11} + \bar{\sigma}_{22} + \bar{\sigma}_{33}) = s \bar{G}_1 (\bar{\varepsilon}_{11} - \frac{1}{3} \bar{\varepsilon}_{11}) \quad (3.33)$$

and

$$\bar{\sigma}_{11} + \bar{\sigma}_{22} + \bar{\sigma}_{33} = s \bar{G}_2 \bar{\varepsilon}_{11} \quad (3.34)$$

The last two equations provide an expression for a "constrained" relaxation function,  $\bar{X}(s)$

$$\bar{\sigma}_{11} = s \bar{X} \bar{\varepsilon}_{11} \quad (3.35)$$

with

$$\bar{X} = (2\bar{G}_1 + \bar{G}_2)/3 \quad (3.36)$$

The functions  $E(t)$  and  $X(t)$  can be experimentally determined and the Laplace transform numerically calculated.

The Laplace transform of the deviatoric and dilatational relaxation functions are also needed in this analysis.

Starting with (3.36)

$$\bar{G}_2 = 3 \bar{X} - 2 \bar{G}_1 \quad (3.37)$$

and substituting  $\bar{G}_2$  in (3.31) yields the quadratic equation in  $\bar{G}_1$

$$\bar{G}_1^2 - \bar{G}_1 \left( \frac{\bar{E}}{2} + \frac{3}{2} \bar{X} \right) + \bar{X} \bar{E} = 0 \quad (3.38)$$

One root of the quadratic equation is

$$\bar{G}_1 = \frac{\left( \frac{\bar{E}}{2} + \frac{3}{2} \bar{X} \right) + \left[ \left( \frac{\bar{E}}{2} + \frac{3}{2} \bar{X} \right)^2 - 4 \bar{X} \bar{E} \right]^{\frac{1}{2}}}{2} \quad (3.39)$$

Numerical calculations have shown that only the positive sign in front of the square root gives true values for the relaxation function  $G_1(t)$ . The root with the negative sign is deleted.

Hughes and Segerlind (1972) derived an equation for the elastic Poisson's ratio. Using the correspondence principle, this equation can be rewritten for the viscoelastic case as

$$\bar{\nu} = \frac{1}{4s} \left[ \frac{\bar{E}}{\bar{X}} - 1 + \left\{ \left( \frac{\bar{E}}{\bar{X}} - 1 \right)^2 - 8 \left( \frac{\bar{E}}{\bar{X}} - 1 \right) \right\}^{\frac{1}{2}} \right] \quad (3.40)$$

### 3.2.1 Experimental Determination of the Relaxation Functions $E(t)$ and $X(t)$

The relaxation functions can be expressed as a sum of exponential terms of the form

$$E(t) = \sum_{j=0}^n E_j e^{-\alpha_j t} \quad (3.42)$$

The shape of experimental constrained relaxation functions indicated that (3.42) also can be used to obtain an equation for these functions. Moreover, it can be shown from (3.36) that if the dilatational and deviatoric relaxation functions have the form of an exponential series, then the constrained relaxation function is of the same form.

Consider a state of simple uniaxial compression with non-zero stress and strain components  $\sigma_{11}(t)$  and  $\epsilon_{11}(t)$ . Take the strain as specified in terms of a unit step function  $u(t)$  and the strain amplitude  $\epsilon_0$ .

$$\epsilon_{11}(t) = \epsilon_0 u(t) \quad (3.43)$$

then the convolution integral

$$\sigma_{11}(t) = \int_0^t E(t-\tau) \frac{d[\epsilon_0 u(\tau)]}{d\tau} d\tau \quad (3.44)$$

becomes

$$\sigma_{11}(t) = E(t) \epsilon_0 \quad (3.45)$$

Equation (3.45) suggests that  $E(t)$  can be obtained by measuring the force on a specimen as a function of time when the specimen is subjected to an instantaneous strain  $\epsilon_0$  at time  $t=0$ . An 'instantaneous' deformation, however, is physically impossible. Moreover, it would also

require special recording equipment for the force signal, a feature not commonly available on testing machines.

A ramp-step function as shown in Figure 3.2 is more easily applied. Chen and Fridley (1972) have derived the equations of the force on a specimen subjected to this type of deformation

$$F(t) = \frac{a A}{L_0} \sum_{i=1}^n \frac{E_i}{\alpha_i} (1 - e^{-\alpha_i t}) \quad \text{for } 0 \leq t \leq t_1 \quad (3.46)$$

and

$$F(t) = \frac{a A}{L_0} \sum_{i=1}^n \frac{E_i}{\alpha_i} (1 - e^{-\alpha_i t_1}) e^{-\alpha_i (t - t_1)} \quad \text{for } t > t_1 \quad (3.47)$$

where  $a$  is the slope of the ramp deformation function,  $A$  is the cross-sectional area of the specimen and  $t_1$  is the time after which the deformation is held constant.

Figure 3.3 gives an example of a response curve of a specimen subjected to the deformation in Figure 3.2. After the substitution  $t' = t - t_1$ , equation (3.47) can be rewritten as

$$F(t') = \sum_{i=1}^n C_i e^{-\alpha_i t'} \quad t' > 0 \quad (3.48)$$

where

$$C_i = \frac{a A}{L_0} \frac{E_i}{\alpha_i} (1 - e^{-\alpha_i t_1}) \quad (3.49)$$



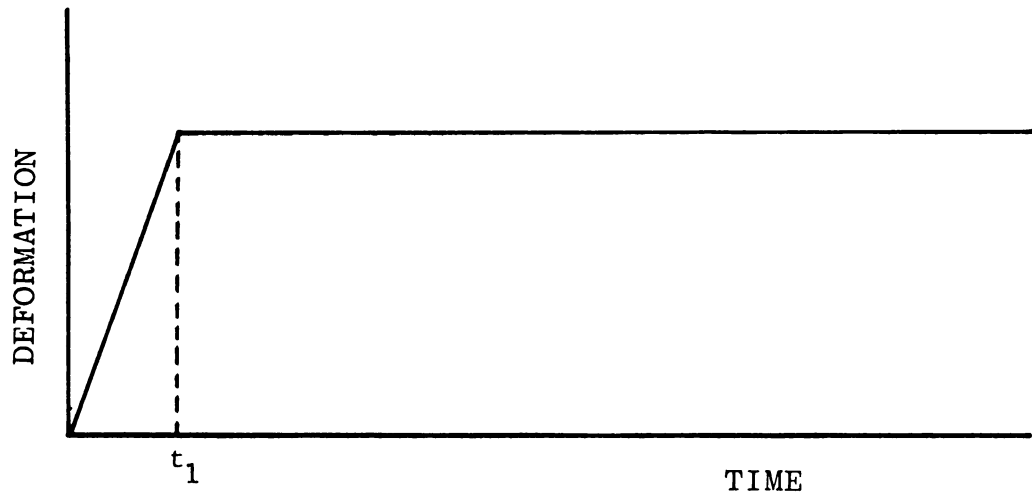


Figure 3.2. Ramp-Step Deformation Function

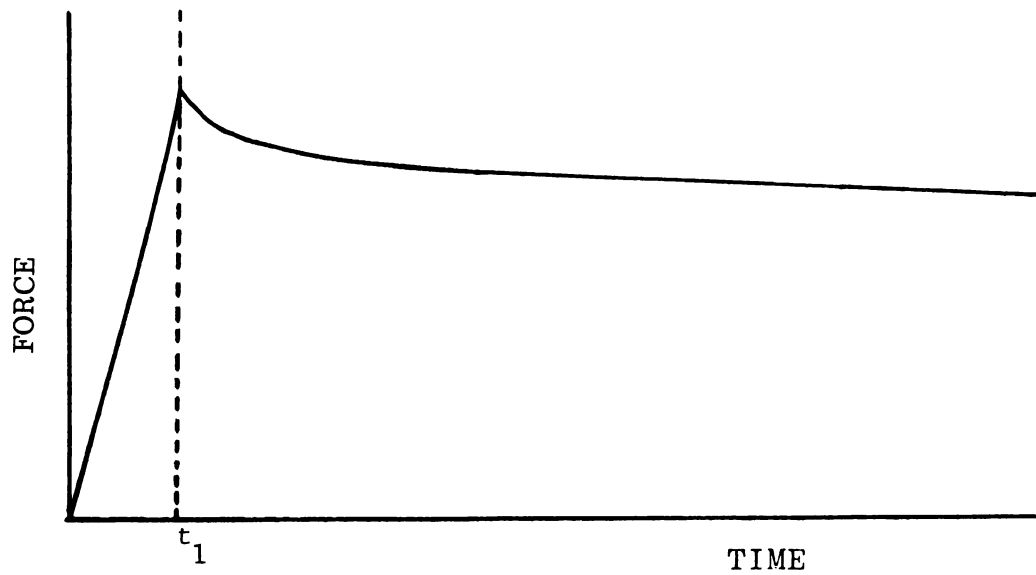


Figure 3.3. Force on a Specimen Subjected to a Ramp-Step Deformation Function

Similar equations can be written for the force acting on a laterally constrained specimen subjected to an axial ramp-step deformation function.

$$F^*(t') = \sum_{i=1}^n C_i^* e^{-\alpha_i^* t'} \quad t' > 0 \quad (3.50)$$

with

$$C_i^* = \frac{a A}{L_0} \frac{X_i}{\alpha_i^*} (1 - e^{-\alpha_i^* t_1}) \quad (3.51)$$

The determination of the coefficients  $C_i$  and  $C_i^*$  and the exponents  $\alpha_i$  and  $\alpha_i^*$  from the experimental values of the force for  $t > t_1$  leads directly to the determination of the uniaxial and constrained relaxation function.

Difficulties arise in trying to fit an exponential series through experimental data. First, the exact number of terms is an unknown. Furthermore, Lanczos (1956, p. 272-280) has shown in a numerical example that a perfectly satisfactory representation of the same data can be obtained by an exponential series with different number of terms. He attributes this fact to the extraordinary sensitivity of the exponents and coefficients to small changes of the data. The only remedy to obtain the "true" model would be an increase of the accuracy of the data to limits which are beyond the possibilities of most measuring devices. Hence, the limitation of the relaxation method for experimental determination of the relaxation function is that the exponential series obtained

is only adequate for the time range of the data used. Extrapolations of the function beyond that time range most likely do not accurately describe the physical phenomenon. Considering the above problem, it is possible that dynamic experiments or a combination of dynamic and relaxation experiments may lead to a more general relaxation function.

A non-linear least squares method is used here to determine the number of terms as well as the coefficients and exponents of the exponential series model. The final selection of a model is based on the following criteria:

- (i) The model results in the smallest estimated variance of observation errors;
- (ii) All the exponents and coefficients have a positive value.

A non-linear least squares statistics program is described by Beck and Arnold (1974). The parameters (i.e. coefficients and exponents) are estimated in an iterative manner according to

$$\underline{b}^{(k+1)} = \underline{b}^{(k)} + (\underline{Z}^{(k)T} \underline{W} \underline{Z}^{(k)})^{-1} \underline{Z}^{(k)T} \underline{W} (\underline{Y} - \underline{\eta}^{(k)}) \quad (3.52)$$

where:  $\underline{b}^{(k)}$  = vector of estimated parameters

$$\underline{Z}^{(k)} = \text{sensitivity matrix : } \underline{Z} = (\underline{\nabla}_{\underline{\beta}} \underline{\eta})^T$$

$\underline{W}$  = weighting matrix. In this application the diagonal terms are set equal to 1, the off-diagonal terms are equal to zero

$\underline{Y}$  = observation vector. Contains the measured values of the force.

$\underline{\eta}^{(k)}$  = model vector. Contains the predicted values of the force using the estimated parameters after the  $k^{\text{th}}$  iteration.

$k$  = number of iterations.

This iterative estimation procedure needs initial or starting values for the parameters. These starting values are obtained through a curve fitting procedure based on the method of successive residuals and described by Chen and Fridley (1972).

The described technique for obtaining the coefficients and exponents of the most generalized Maxwell model is contained in a computer program, GENMAX.

### 3.2.2 Numerical Interconversions of the Relaxation Functions: Approximate Laplace Transform Inversion

The relaxation functions for simple uniaxial compression and constrained compression were discussed in the previous section. The deviatoric and dilatational relaxation functions and the viscoelastic Poisson's ratio

can now be calculated using the expressions (3.39), (3.37) and (3.39a). However, these expressions are the Laplace transforms of the desired functions and an inverse Laplace transformation has to be performed. A numerical inversion procedure must be used to obtain the inverse Laplace transform.

Numerical inversion of the Laplace transform has been described by Lanczos (1956), Papoulis (1957), Cost (1964), Bellman *et al.* (1966), Cost and Becker (1970) and others. The procedure as described here is adopted from Miller and Guy (1966) and uses an orthogonal polynomial series expansion. The Laplace transform  $\bar{f}(s)$  of a function  $f(t)$  is defined by

$$\bar{f}(s) = \int_0^{\infty} f(t) e^{-st} dt \quad (3.54)$$

Assume that  $\bar{f}(s)$  is known at discrete points along the real  $s$ -axis. After the substitution

$$x = 2 e^{-\delta t} - 1 \quad (3.55)$$

where  $\delta$  is a real positive number, a new function is defined over the interval  $(-1 \leq x \leq 1)$

$$g(x) = f(t) = f\left(-\frac{1}{\delta} \ln[(1+x)/2]\right) \quad (3.56)$$

With this substitution, (3.54) becomes

$$\bar{f}(s) = \frac{1}{2\delta} \int_{-1}^{+1} \left[ \left(1 + \frac{x}{2}\right)^{\frac{s}{\delta}-1} \right] g(x) dx \quad (3.57)$$

Jacobi Polynomials  $P_n^{(0,\beta)}(x)$  form a set of orthogonal polynomials in the interval  $[-1 \leq x \leq 1]$ . The expansion of  $g(x)$  over the interval  $[-1, 1]$  in terms of a series of Jacobi polynomials can then be written as

$$g(x) = \sum_{n=0}^{\infty} C_n P_n^{(0,\beta)}(x) \quad (3.58)$$

where  $\beta > 0$ . The major task is to evaluate the coefficients  $C_n$ , which can be done by inserting (3.58) into (3.57) and substituting

$$s = (\beta + 1 + k) \delta \quad (3.59)$$

After integration and algebraic simplification, Miller and Guy (1966) obtained the expression

$$\delta \bar{f}[(\beta+1+k)\delta] = \sum_{m=0}^k \frac{k(k-1) \dots [k-(m-1)]}{(k+\beta+1)(k+\beta+2) \dots (k+\beta+1+m)} C_m \quad (3.60)$$

This result is true for  $k = 0, 1, 2 \dots$  and by successively allowing  $k = 0, 1, \dots$  the following system of equations is generated

$$\begin{aligned}
\delta \bar{f}[(\beta+1)\delta] &= \frac{C_0}{\beta+1} \\
\delta \bar{f}[(\beta+2)\delta] &= \frac{C_0}{(\beta+2)} + \frac{C_1}{(\beta+2)(\beta+3)} \\
\delta \bar{f}[(\beta+3)\delta] &= \frac{C_0}{\beta+3} + \frac{2C_1}{(\beta+3)(\beta+4)} + \frac{2C_2}{(\beta+3)(\beta+4)(\beta+5)}
\end{aligned} \tag{3.61}$$

The coefficient  $C_0$  is obtained by setting  $k = 0$  and from the knowledge of  $\bar{f}(s)$  at  $s = (\beta+1)\delta$ . The coefficient  $C_1$  is found from setting  $k = 1$  and from the knowledge of  $C_0$  and the value of  $\bar{f}(s)$  at  $s = (\beta+2)\delta$ .

When  $N$  coefficients are calculated, the function  $g(x)$  may be approximated by this finite number  $N$  of terms in (3.58). The approximation of  $f(t)$  is

$$f(t) \approx \sum_{n=0}^N C_n P_n^{(0, \beta)} [2e^{-\delta t} - 1] \tag{3.62}$$

The Jacobi polynomials in (3.62) are evaluated using the recurrence formula (Szegő, 1959)

$$\begin{aligned}
2n(n+\beta)(2n+\beta-2)P_n^{(0, \beta)}(x) = \\
(2n+\beta-1)\{(2n+\beta)(2n+\beta-2)x-\beta^2\}P_{n-1}^{(0, \beta)}(x) \\
- 2(n-1)(n+\beta-1)(2n+\beta)P_{n-2}^{(0, \beta)}(x) \quad n = 2, 3, 4 \dots
\end{aligned}$$

$$P_0^{(0, \beta)}(x) = 1$$

$$P_1^{(0,\beta)}(x) = \frac{1}{2}(\beta+2)x - \frac{1}{2}\beta \quad (3.63)$$

Equations (3.61)-(3.63) were programmed for a digital computer solution. The programs were checked using functions whose inverse is known. These programs were combined with a computer program RELAX which calculates the values of the bulk and shear relaxation functions (equations (3.37), (3.39) and (2.5), (2.6)) and of the viscoelastic Poisson's ratio (equation (3.40)) at different values of time. The input to the program consists of the coefficients and exponents of the uniaxial relaxation function  $E(t)$  and the constrained relaxation function  $X(t)$ .

### 3.2.3 Accuracy of the Method

The experimental procedure described above was simulated on a digital computer to evaluate its accuracy. Hypothetical bulk and shear relaxation functions were assumed.

$$B(t) = G_2(t)/3 = 800 e^{-.2t} + 50 e^{-2t} \quad (3.64)$$

$$G(t) = G_1(t)/2 = 450 e^{-.1t} + 100 e^{-5t} \quad (3.65)$$

The uniaxial relaxation functions and the constrained relaxation function were found using equations (3.31)





and (3.36)

$$E(t) = 1136.444e^{-.11574 t} + 7.604e^{-1.90753 t} + 213.211e^{-4.84951 t} \quad (3.66)$$

$$X(t) = 600 e^{-.1t} + 800 e^{-.2t} + 50 e^{-2t} + 133.333 e^{-5t} \quad (3.67)$$

A relaxation force versus time was then calculated for both uniaxial and constrained relaxation.

The following parameters were used ((3.49) and (3.51))

$$a = 1$$

$$L_0 = .75$$

$$A = .5$$

$$t_1 = .06$$

An error term ER was introduced with zero mean and standard deviation SD such that

$$F'(t) = F(t) + ER(0,SD) \quad (3.68)$$

Values of  $F'(t)$  at discrete time points and for different values of SD were used as input to the parameter estimation package GENMAX. It was found that the coefficients and exponents of the three-term model (3.66) could be obtained only when there was zero input error. The four-term model

posed some problems which were assumed to be due to the almost equal values of the exponents .1 and .2 of the first two terms in (3.67). The presence of errors no longer allowed determination of the exact values of the parameters. A two-term model seemed adequate to describe the force as a function of time for the time period considered. A summary of the estimated variances of observations errors is given in Table 3.1.

The estimated coefficients and exponents were then used in the program RELAX for numerical evaluation of the bulk and shear relaxation functions. These calculated values were compared with the theoretical values and the variances and maximum values of the errors are also summarized in Table 3.1 for the different errors of the force. The absolute value of the errors in the relaxation functions generally increased as the variance of the error in the applied force increased. The maximum errors, however, were relatively small. For example, the largest error variance in the force value produced an error for the bulk relaxation function of about two percent of the value of this function.

The two-term approximation of the force curve resulted in accurate values of the bulk and shear relaxation functions only for the time period in which data points for the force were available. Calculation of values of bulk and shear relaxation functions beyond that period resulted in meaningless values.

Table 3.1. Influence of measurement errors on the values of the Bulk and Shear relaxation functions (simulated values according to equations 3.64-3.67).

Input error variance	OUTPUT GENMAX			OUTPUT RELAX		
	Free Compression		Constrained Compression	Bulk Relaxation		Shear Relaxation
	No. of Terms	Variance		Variance	Max. Deviation	
0	3	0	0	.0029	.1340	.0219
0	3	0	0	.0125	.3750	.0018
0	2	.00045	0	.0729	.8383	.0092
0	2	.00045	.00001	.1232	1.6761	.0992
.0004	2	.00045	.00042	.0158	.5158	.0637
.0016	2	.00157	.00150	.1973	1.9534	.0315
.0036	2	.00418	.0042	.7616	2.6817	.1219
.0064	2	.00510	.00515	.0611	.5662	.0616
.01	2	.01061	.01075	.3256	1.1937	.0699
.0144	2	.01372	.01373	.1516	.7091	.1842
.04	2	.04645	.02834	3.2017	8.4324	.6062
.0676	2	.06447	.07443	6.1663	5.8616	1.000
.09	2	.09207	.08339	4.5525	6.1216	.8259
.1024	2	.08716	.08135	16.9421	16.1637	3.0627
						1.9305
						7.267

### 3.2.4 Summary of the Procedure

The following is a summary of the steps involved in the proposed procedure for determination of relaxation functions:

- i) Measurement of the force relaxation curve of a uniaxial compressed specimen and of a laterally constrained specimen under axial compression.
- ii) Estimation of the coefficients and exponents of a generalized Maxwell model (i.e, exponential series) that adequately describe the experimental force curves.
- iii) Using the correspondence principle, find the Laplace transforms of the shear and bulk relaxation function. Transformation to the time domain is performed through numerical inversion of the Laplace transform.

It was shown in an example that errors in the force data as well as the approximative nature of the inverse Laplace transform method lead to errors of the bulk and shear relaxation function. However, the results can be considered satisfactory for relatively small errors of the force data. The method does not allow extrapolation of the bulk and shear relaxation functions beyond the time period for which experimental force values were available.

### 3.3 Determination of Dynamic Properties

The complex modulus representation of the constitutive equations as given by equations (3.16) and (3.19) can serve as a basis for the derivation of an experimental technique for determination of the complex deviatoric modulus  $G_1^*(i\omega)$  and complex dilatational modulus  $G_2^*(i\omega)$ . The derivation is similar to the one for the relaxation functions. A complex uniaxial modulus  $E^*(i\omega)$  and a complex restrained modulus  $X^*(i\omega)$  are introduced. Their relation to deviatoric and dilatational moduli is expressed by the equations

$$E^*(i\omega) = \frac{3G_1^*(i\omega) G_2^*(i\omega)}{G_1^*(i\omega) + 2G_2^*(i\omega)} \quad (3.70)$$

and

$$X^*(i\omega) = [2G_1^*(i\omega) + 2G_2^*(i\omega)]/3 \quad (3.71)$$

from which the following equations are derived

$$G_1^*(i\omega) = \frac{1}{2} \left[ \frac{E^*(i\omega)}{2} + \frac{3X^*(i\omega)}{2} \right] + \frac{1}{2} \left\{ \left[ \frac{E^*(i\omega)}{2} + \frac{3X^*(i\omega)}{2} \right]^2 - 4X^*(i\omega) E^*(i\omega) \right\}^{\frac{1}{2}} \quad (3.72)$$

$$G_2^*(i\omega) = 3X^*(i\omega) - 2G_1^*(i\omega) \quad (3.73)$$

The complex form of Poisson's ratio is

$$v^*(i\omega) = \frac{\frac{E^*(i\omega)}{X^*(i\omega)} - 1 + \left\{ \left[ \frac{E^*(i\omega)}{X^*(i\omega)} - 1 \right]^2 - 8 \left[ \frac{E^*(i\omega)}{X^*(i\omega)} - 1 \right] \right\}^{\frac{1}{2}}}{4} \quad (3.74)$$

The complex moduli  $E^*(i\omega)$  and  $X^*(i\omega)$  can be experimentally determined from the amplitude ratio and phase angle between stress and strain of a specimen subjected to a sinusoidal displacement. Simple axial sinusoidal displacement is used for  $E^*(i\omega)$ , while sinusoidal compression of an axially constrained specimen is used for  $X^*(i\omega)$ .

$$E^*(i\omega) = \frac{\sigma_{11}}{\epsilon_{11}}(i\omega) \quad (3.75)$$

and

$$E^*(i\omega) = E'(\omega) + i E''(\omega) \quad (3.76)$$

with

$$\begin{aligned} E'(\omega) &= |E^*(i\omega)| \cos \theta \\ E''(\omega) &= |E^*(i\omega)| \sin \theta \end{aligned} \quad (3.77)$$

The phase angle is  $\theta$  and  $|E^*(i\omega)|$  denotes the magnitude of the complex value, i.e.

$$|E^*(i\omega)| = [E'(\omega)^2 + E''(\omega)^2]^{\frac{1}{2}} \quad (3.78)$$

Similar equations can be written for the constrained complex modulus

$$X^*(i\omega) = \frac{\sigma_{11}}{\epsilon_{11}}(i\omega) \left| \epsilon_{22} = \epsilon_{33} = 0 \right. \quad (3.79)$$

and

$$X^*(i\omega) = X'(\omega) + i X''(\omega) \quad (3.80)$$

with

$$X'(\omega) = |X^*(i\omega)| \cos \phi$$

and

$$X''(\omega) = |X^*(i\omega)| \sin \phi \quad (3.81)$$

Some preliminary experiments suggested that difficulties may arise in the determination of the phase angle  $\phi$  for the constrained tests due to friction of the specimen against the sidewall of the sample holder. It was also found that the phase angle cannot be determined with sufficient accuracy from a "Lissajous" figure on the oscilloscope screen, and that more accurate instrumentation is required. If these difficulties can be overcome, the determination of the complex moduli through the use of (3.22) and (3.23) might result in a more general expression for the relaxation functions than the relaxation experiment described in the previous section.

### 3.4 Closure

The constitutive equations of viscoelastic materials were given and a boundary value problem was formulated



such that it served as the basis for the experimental determination of the stress-strain relations. A constrained modulus function, based on the stress-strain relationship of a sample subjected to axial deformation but with no lateral deformation possible was introduced. Deviatoric and dilatational stress-strain relations were obtained from the simple uniaxial modulus function and the constrained modulus function. A method for determining either relaxation functions or complex moduli was proposed and its limitations and advantages were discussed.

## 4. EXPERIMENTAL PROCEDURE

### 4.1 Apple Selection and Storage

The apples used in the determination of the material properties were of the variety Red Delicious, Miller Spur, grown at the Michigan State University Horticulture Research Center. The apples were selectively harvested for size (diameter larger than 80 mm) and immediately put in controlled atmosphere storage at 0°C. The apples were removed from storage 20 hours before the experiments were conducted and placed at room temperature.

### 4.2 Sample Preparation

Cylindrical samples with a diameter of 19.05 mm were cut by driving a corkborer into the apple parallel to the stem calyx axis. The samples were then placed in a hole in a plexiglass plate of 19.05 mm thickness and the ends were cut parallel to the plate using a thin sectioning machine, as shown in Figure 4.1. The final length of the specimen was measured to a tenth of a millimeter. The samples were coated with a silicone spray to prevent excessive moisture loss during the relaxation tests.

Four cylindrical samples were cut from each apple. Two of these were used for the determination of the



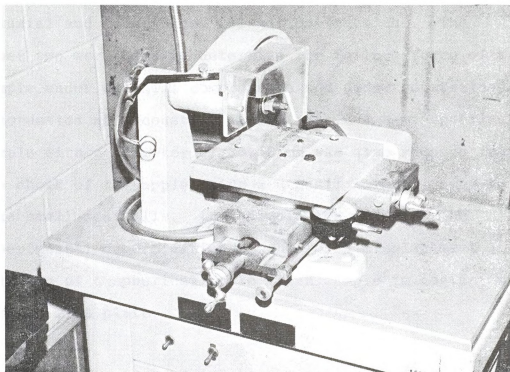


Figure 4.1. Sample Cutting Machine

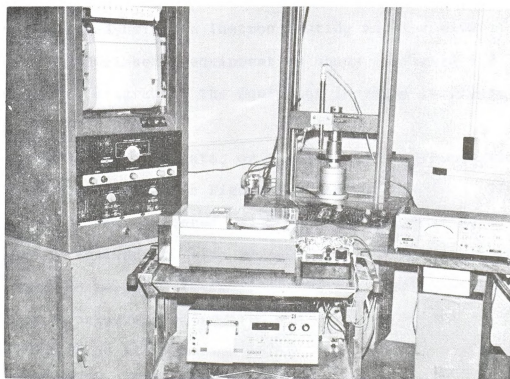


Figure 4.2. Force and Deformation Measuring and Recording Equipment



uniaxial and constrained relaxation functions. The other two were used to determine the failure force of a sample under uniaxial compression and under constrained compression at a constant strain rate. A semi-spherical sample with a diameter of 35.56 mm was also removed from the cheek of the apple using a utensil normally used to make small meatballs. This sample was used for the experimental determination of the force-displacement relation of a spherical apple flesh sample in contact with a rigid flat plate.

#### 4.3 Relaxation Tests

Relaxation tests on the free and constrained samples were performed using an Instron testing machine with some added peripheral equipment as shown in Figure 4.2. A schematic diagram of the equipment is given in Figure 4.3.

The deformation rate, or the slope of the ramp-step deformation function in Figure 3.2 was 25.4 mm/min. The deformation was monitored using a linear variable displacement transducer. The crosshead of the testing machine was stopped whenever the deformation was approximately 1.65 mm, corresponding to a strain of .0864 mm/mm.

The force was measured using the strain gage bridge circuit of the Instron load cell and a d.c. bridge amplifier. The amplifier output was fed into a data

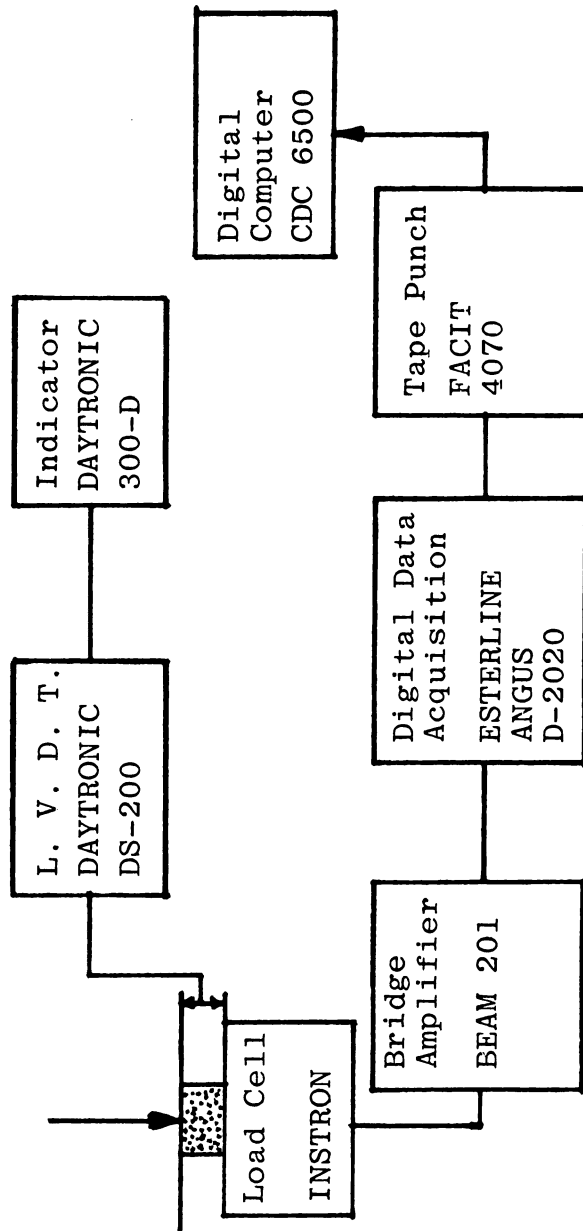


Figure 4.3. Schematic Diagram of Equipment for a Relaxation Test





acquisition system. The force signal was sampled every .4 second and punched on paper tape. The relaxation experiments were conducted for approximately ten minutes. The paper tape output was read on the CDC 6500 computer of the Michigan State University Computer Laboratory. After decoding and correcting occasionally defective recordings, the maximum force value corresponding to  $t' = 0$  in (3.48) and (3.50) was determined. A force vector and time vector were obtained in a form ready for use in the program GENMAX for estimation of the coefficients and exponents in the generalized Maxwell model.

The output of GENMAX was inspected for the nature of the signs of the coefficients and exponents, their variance-covariance matrix and the estimated variance of the input error. A two-term exponential series gave the best results for most samples.

The coefficients and exponents of the Maxwell model for the uniaxial and constrained compression tests were introduced as input to the program RELAX, together with control parameters for the polynomial expansion. Discrete numerical values of bulk and shear relaxation functions and time dependent Poisson's ratio were the final results.

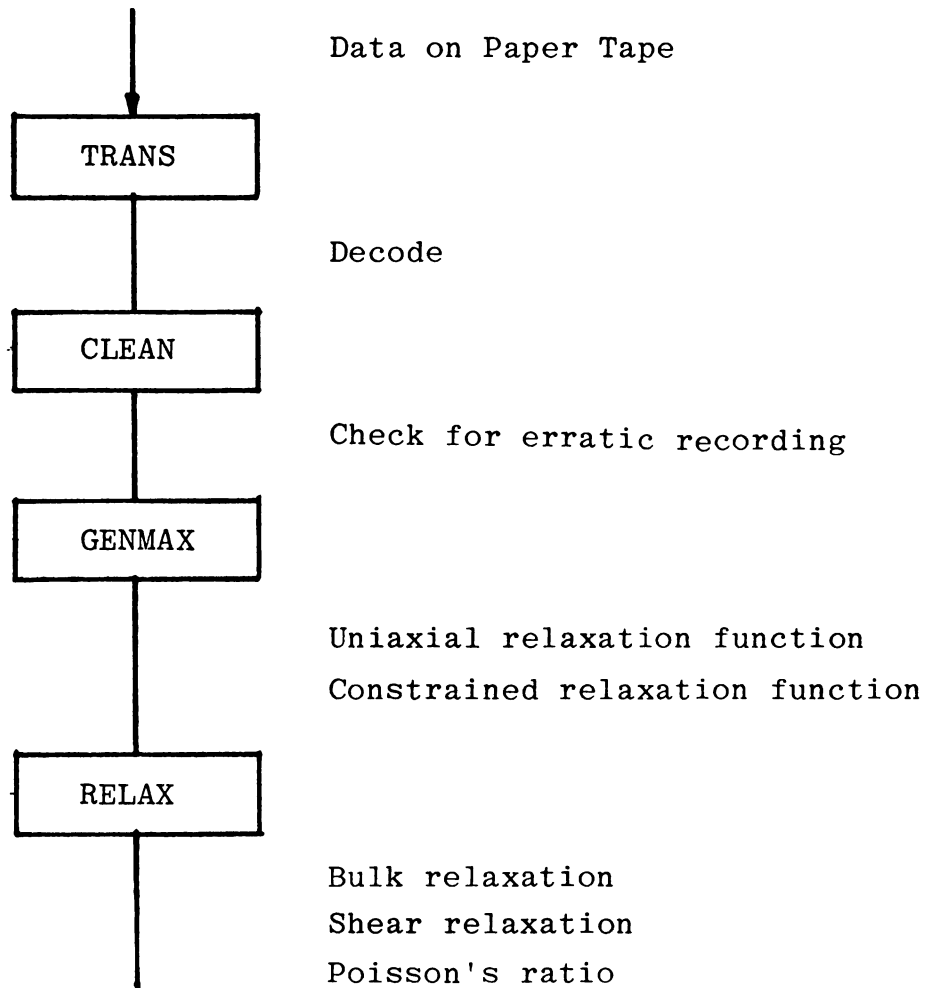


Figure 4.4. Analysis of Relaxation Test Data to Obtain Relaxation Functions and Poisson's Ratio

## 5. EXPERIMENTAL RELAXATION FUNCTIONS

The theoretical developments and experimental techniques described in the previous chapters were used for the determination of relaxation functions of apple flesh. The results of these experiments are first given for a single apple; the average values for a larger sample of apples are shown thereafter.

### 5.1 Relaxation Force Curves

Measured relaxation force values for a uniaxial and a constrained compression are given in Figures 5.1 and 5.2. The forces are shown from the moment the displacement became constant, for  $t' > 0$  in (3.48) and (3.50). The test specimen had a diameter of 19.05 mm and an initial length of 19.1 mm. The deformation was held constant at -1.65 mm and -1.70 mm respectively for the uniaxial compression and the constrained compression. Only every twentieth data point is shown in the graphs. The force is in newtons, the time in minutes. The solid lines represent the exponential series that were used to model the experimental force curves. Both curves were represented by a two-term exponential series.

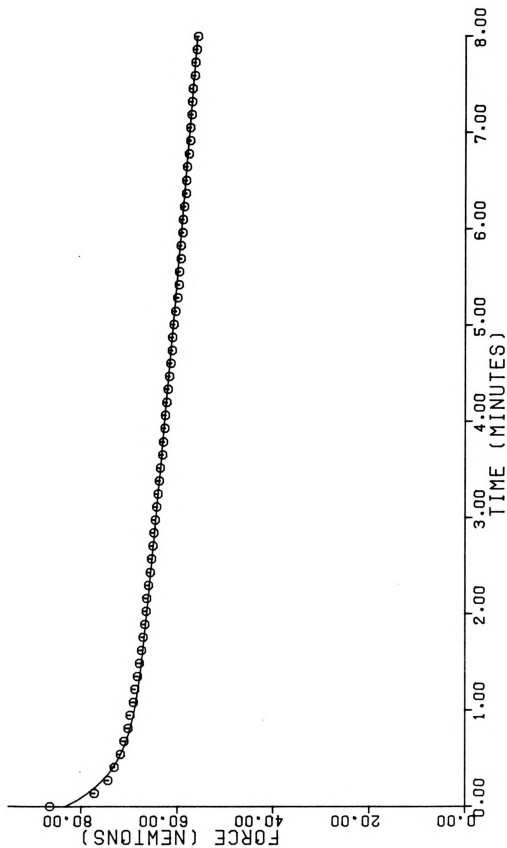


Figure 5.1. Uniaxial Relaxation Force; Model not through First Data Point

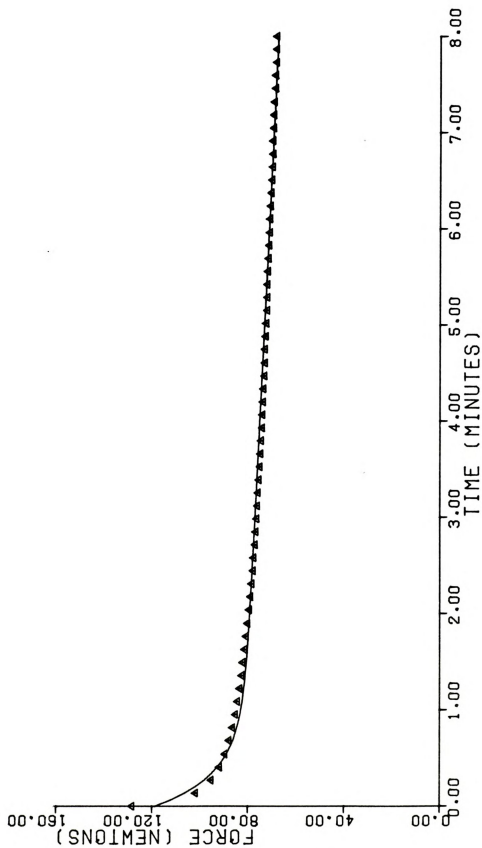


Figure 5.2. Constrained Relaxation Force; Model not through First Data Point

The uniaxial relaxation force model was

$$F(t) = 13.0 e^{-2.965 t'} + 70.24 e^{-.029 t'} \quad (5.1)$$

which resulted in an estimated variance of the observation errors of 0.12092. The variance-covariance matrix of the parameters  $C_i$  and  $\alpha_i$  (equations 3.48 and 5.1) is given in Table 5.1. The model for the constrained relaxation force was

$$F^*(t) = 35.24 e^{-3.10 t'} + 83.44 e^{-.027 t'} \quad (5.2)$$

and the estimated variance of the observation errors was 1.42. The variance-covariance matrix of the parameters in this model is also given in Table 5.1.

Observation of the model and the experimental values in Figures 5.1 and 5.2 indicated that the model showed large deviations from the measured values for small values of time, especially for time  $t' = 0$ . Therefore, the estimation of the coefficients in (3.48) and (3.50) was subjected to the linear restraints

$$F(t'=0) = \sum_{i=1}^n C_i \quad (5.3)$$

and

$$F^*(t'=0) = \sum_{i=1}^n C_i^* \quad (5.4)$$

Table 5.1. Variance-covariance matrices of parameters in a two-term exponential series.

$$F = \sum C_i e^{-\alpha_i t} \quad [\text{Equations (5.1) and (5.2)}]$$

Uniaxial Relaxation Force<sup>(a)</sup>

	$C_1$	$C_2$	$\alpha_1$	$\alpha_2$
$C_1$	.00930	-.00012	-.00202	0
$C_2$		.00052	-.00040	0
$\alpha_1$			.00129	0
$\alpha_2$			0	0

Constrained Relaxation Force<sup>(a)</sup>

	$C_1^*$	$C_2^*$	$\alpha_1^*$	$\alpha_2^*$
$C_1^*$	.11450	-.00248	-.00936	.00001
$C_2^*$		.00907	-.00259	-.00002
$\alpha_1^*$			-.00256	0
$\alpha_2^*$				0

(a) Zero value when zero in the fifth decimal place.

Kmenta (1971) comments that imposing such restraints increases the value of the estimated variance of the observation errors, but a better model can be obtained due to the inclusion of some known values.

The linear restraints were introduced such that

$$C_1 = F(t'=0) - \sum_{i=2}^n C_i \quad (5.3a)$$

and

$$C_1^* = F^*(t'=0) - \sum_{i=2}^n C_i^* \quad (5.4a)$$

The results of forcing the models through the observed force value at time  $t'=0$  are shown in Figures 5.3 and 5.4. The resulting equations were

$$F(t) = 16.06 e^{-4.152 t'} + 70.46 e^{-.029 t'} \quad (5.5)$$

for the uniaxial relaxation, and

$$F^*(t) = 43.91 e^{-4.631 t} + 84.37 e^{-.028 t} \quad (5.6)$$

for the constrained relaxation. In this case the estimated variance of the observation errors were respectively 0.1665 and 1.847. These values were higher than in the previous case as was expected. The variance-covariance matrices of the three parameters in these models are given in Table 5.2.



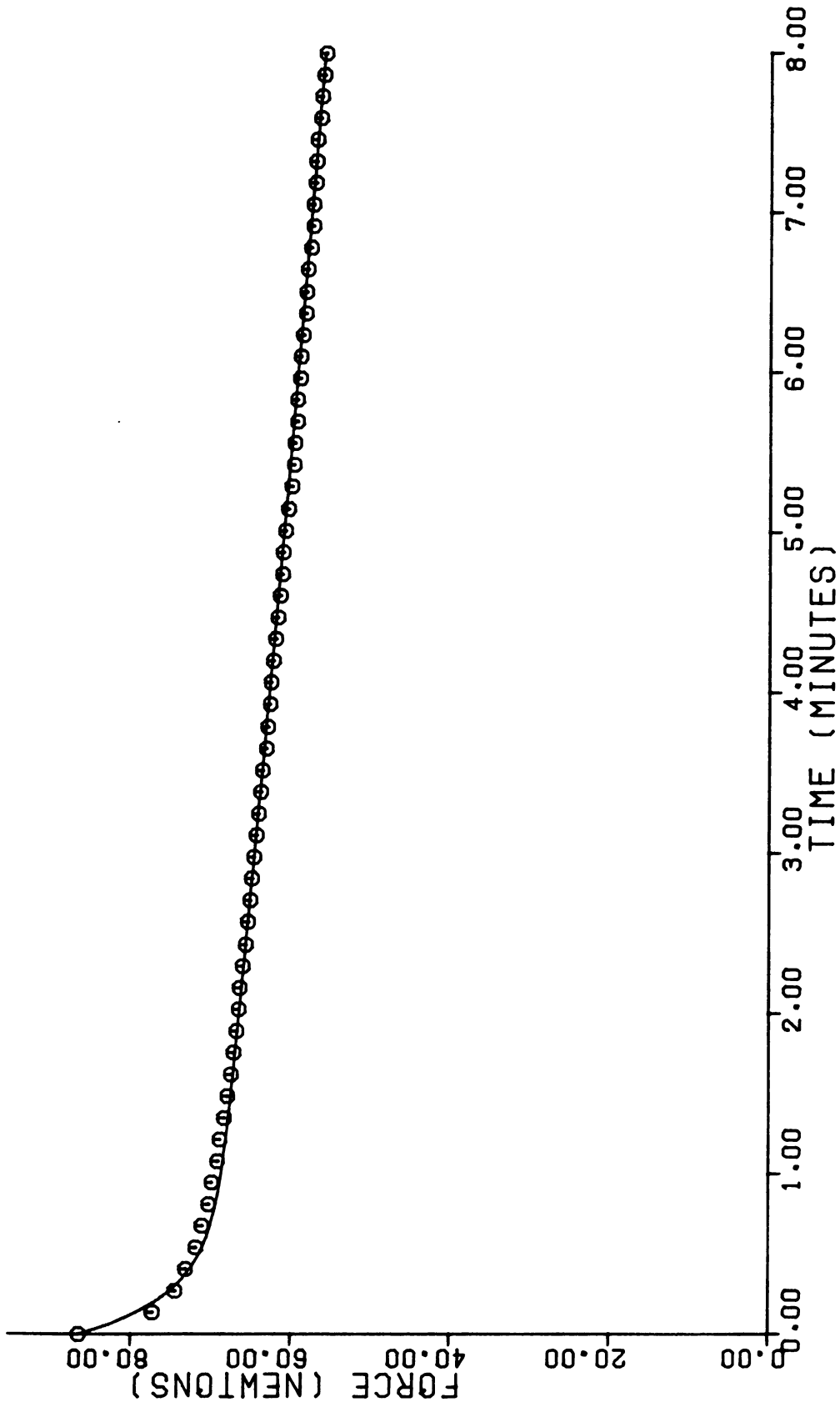


Figure 5.3. Uniaxial Relaxation Force; Model through First Data Point

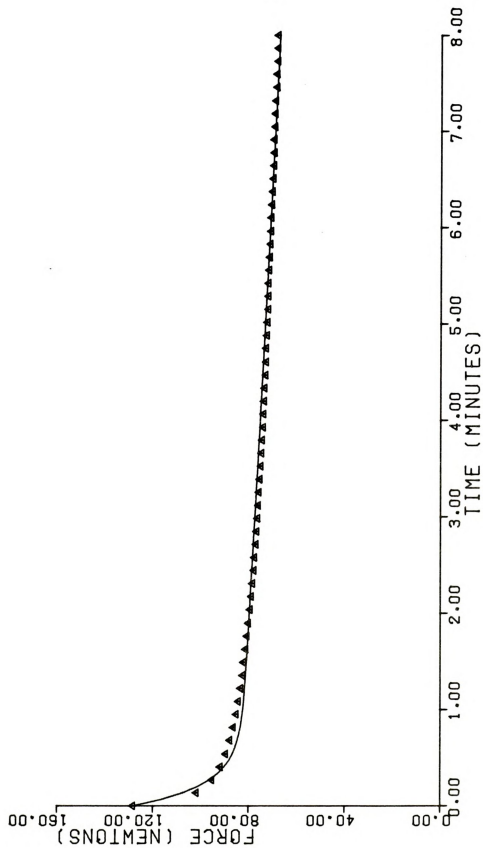


Figure 5.4. Constrained Relaxation Force; Model through First Data Point

Table 5.2. Variance-covariance matrix of parameters in a two-term exponential series subjected to the linear restraint  $C_1 = F(t'=0) - C_2$

[Equations (5.5) and (5.6)]

Uniaxial Relaxation Force<sup>(a)</sup>

	$C_2$	$\alpha_1$	$\alpha_2$
$C_2$	.0006	-.00042	0
$\alpha_1$		.00154	0
$\alpha_2$			0

Constrained Relaxation Force<sup>(a)</sup>

	$C_2^*$	$\alpha_1^*$	$\alpha_2^*$
$C_2^*$	.00927	-.00260	-.00002
$\alpha_1^*$		.00331	.00001
$\alpha_2^*$			0

(a) Zero value assumed when zero in the fifth decimal place.

## 5.2 Relaxation Functions

The uniaxial and constrained relaxation functions,  $E(t)$  and  $X(t)$ , were determined from the relaxation force curves using equations (3.49) and (3.51), and (5.5) and (5.6). The uniaxial relaxation function

$$E(t) = .744 e^{-4.152 t} + 2.863 e^{-.029 t} \quad (5.7)$$

is shown in Figure 5.5. Figure 5.6 represents the constrained relaxation function

$$X(t) = 2.011 e^{-4.630 t} + 3.325 e^{-.028 t} \quad (5.8)$$

The dimensions of the relaxation functions  $E(t)$  and  $X(t)$  are in megapascals (MPa) or  $10^6 \text{ N/m}^2$ , while  $t$  is time in minutes.

Discrete values of the bulk and shear relaxation functions and Poisson's ratio were calculated using the numerical procedure described in Section 3.2.2. The results are displayed in Figures 5.7, 5.8 and 5.9. It can be seen that while all these material properties are time dependent, the bulk relaxation function exhibited the largest changes with time.



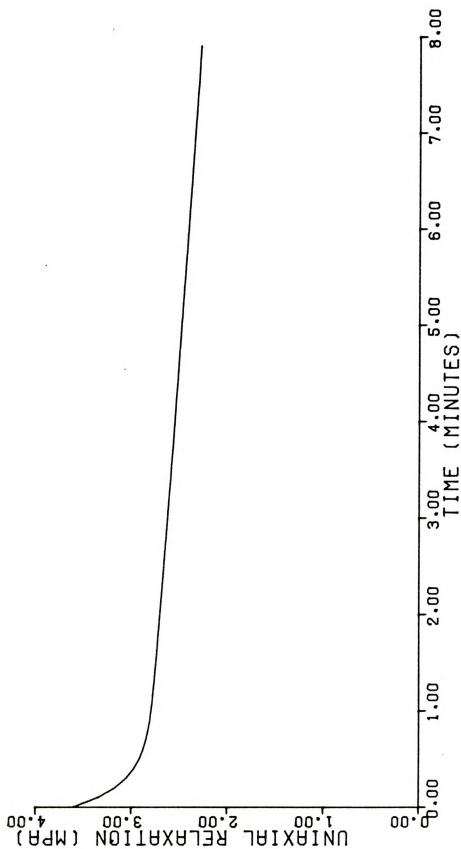


Figure 5.5. Uniaxial Relaxation Function

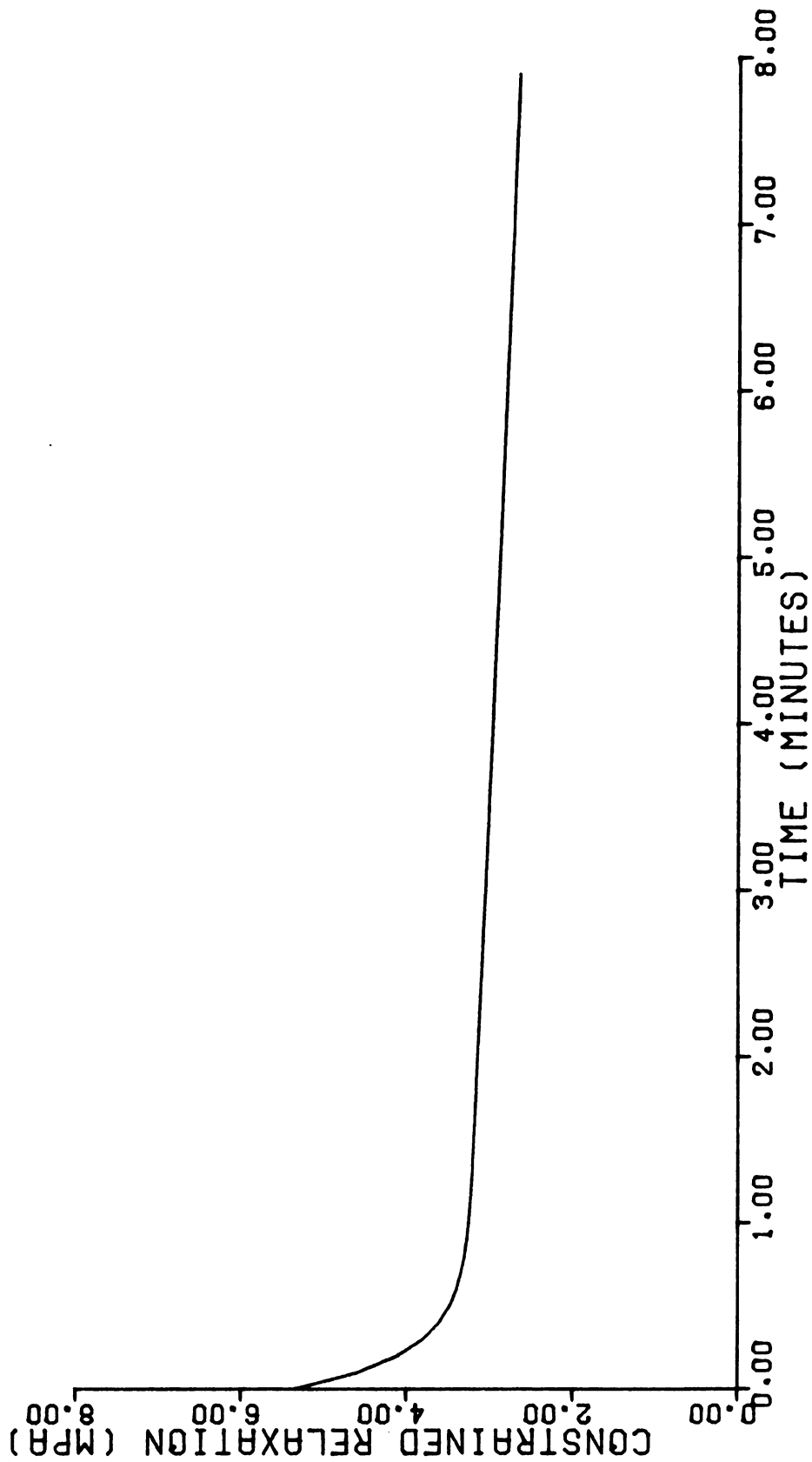


Figure 5.6. Constrained Relaxation Function





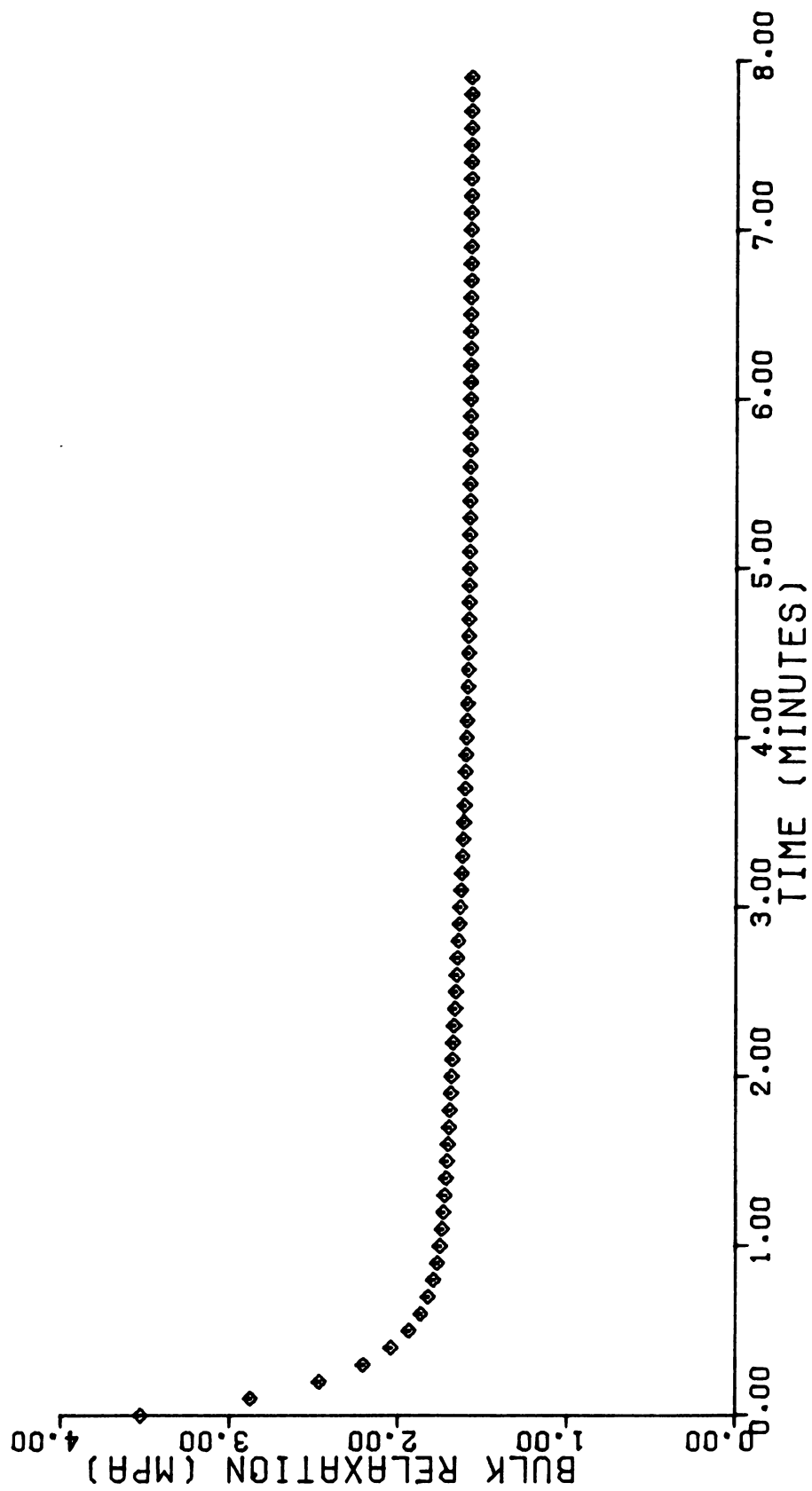


Figure 5.7. Bulk Relaxation Function

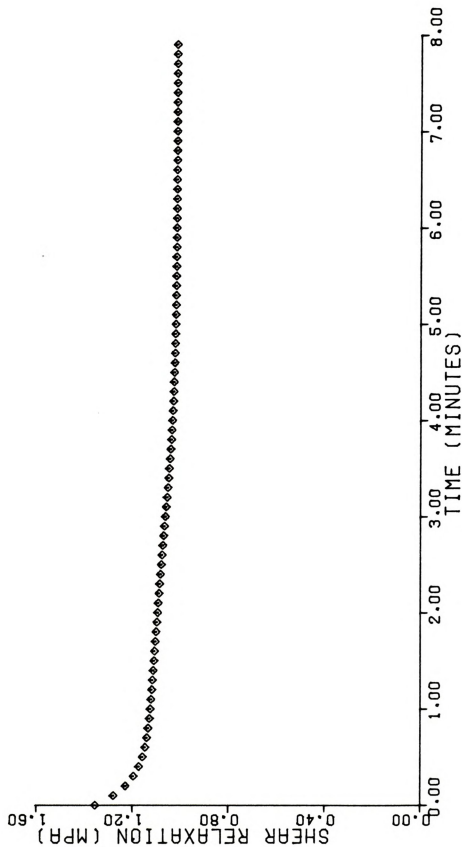


Figure 5.8. Shear Relaxation Function

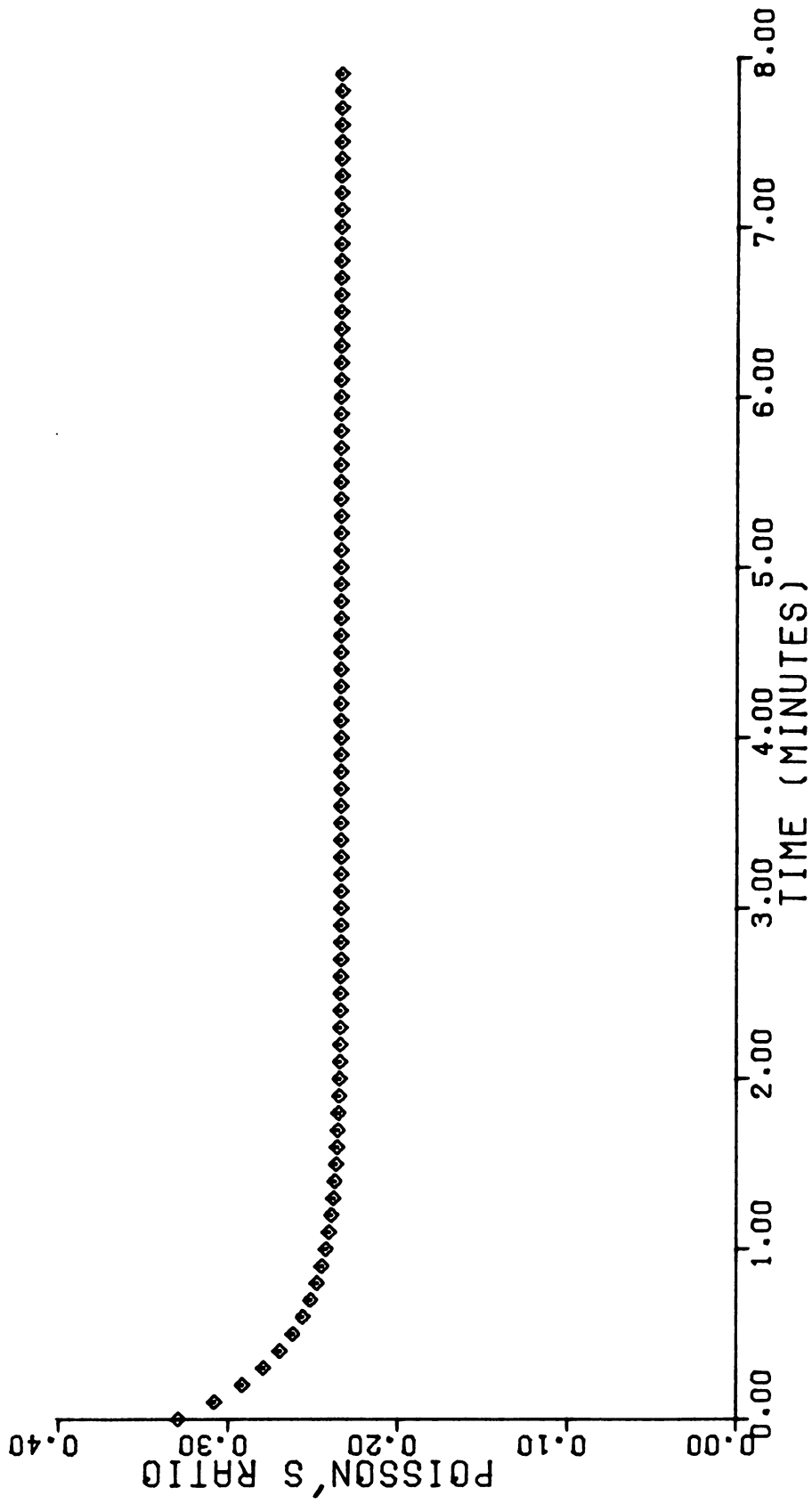


Figure 5.9. Time Dependent Poisson's Ratio

### 5.3 Average Values of Relaxation Functions

The uniaxial and constrained relaxation functions and discrete values of the bulk and shear relaxation functions and Poisson's ratio for 24 apples are given in Appendix A. They are summarized in Table 5.3. The tests on these apples were run within less than three weeks from the time of harvest. In Figures 5.10 through 5.14, the average values and standard deviations of the respective relaxation functions are given for different time values. It can be noted that the bulk relaxation function decreased very rapidly during the initial time periods. The shear relaxation functions and Poisson's ratio also decreased with time, but their decrease was less rapid than for the bulk relaxation function. These properties also varied among apples. The standard deviations of the values of the relaxation functions at a single time were as large as ten percent of the average value. They were generally larger at the small time values.

Table 5.3. Average values and standard deviations of the relaxation functions of 24 Red Delicious apples

Time (min)	UNIAXIAL RELAXATION		CONSTRAINED RELAXATION		POISSON'S RATIO	
	Mean (MPa)	Standard Deviation	Mean (MPa)	Standard Deviation	Mean	Standard Deviation
.0	3.44	.395	5.22	.674	.33	.034
.031	3.37	.384	5.01	.593	.33	.034
.062	3.30	.374	4.83	.530	.32	.034
.125	3.19	.357	4.52	.446	.31	.033
.250	3.02	.333	4.09	.377	.30	.033
.50	2.82	.306	3.67	.354	.29	.033
1.0	2.66	.288	3.41	.356	.28	.035
2.0	2.55	.279	3.26	.363	.28	.040
4.0	2.40	.265	3.05	.381	.27	.045
8.0	2.12	.249	2.68	.422	.27	.048
Time (min)	SHEAR RELAXATION		BULK RELAXATION			
	Mean (MPa)	Standard Deviation	Mean (MPa)	Standard Deviation		
0	1.29	.171	3.49	.678		
.031	1.27	.167	3.31	.594		
.062	1.25	.165	3.16	.526		
.125	1.22	.159	2.90	.432		
.250	1.16	.151	2.55	.344		
.50	1.10	.140	2.21	.306		
1.0	1.04	.130	2.02	.308		
2.0	1.00	.124	1.92	.321		
4.0	.95	.117	1.79	.346		
8.0	.93	.115	1.76	.356		

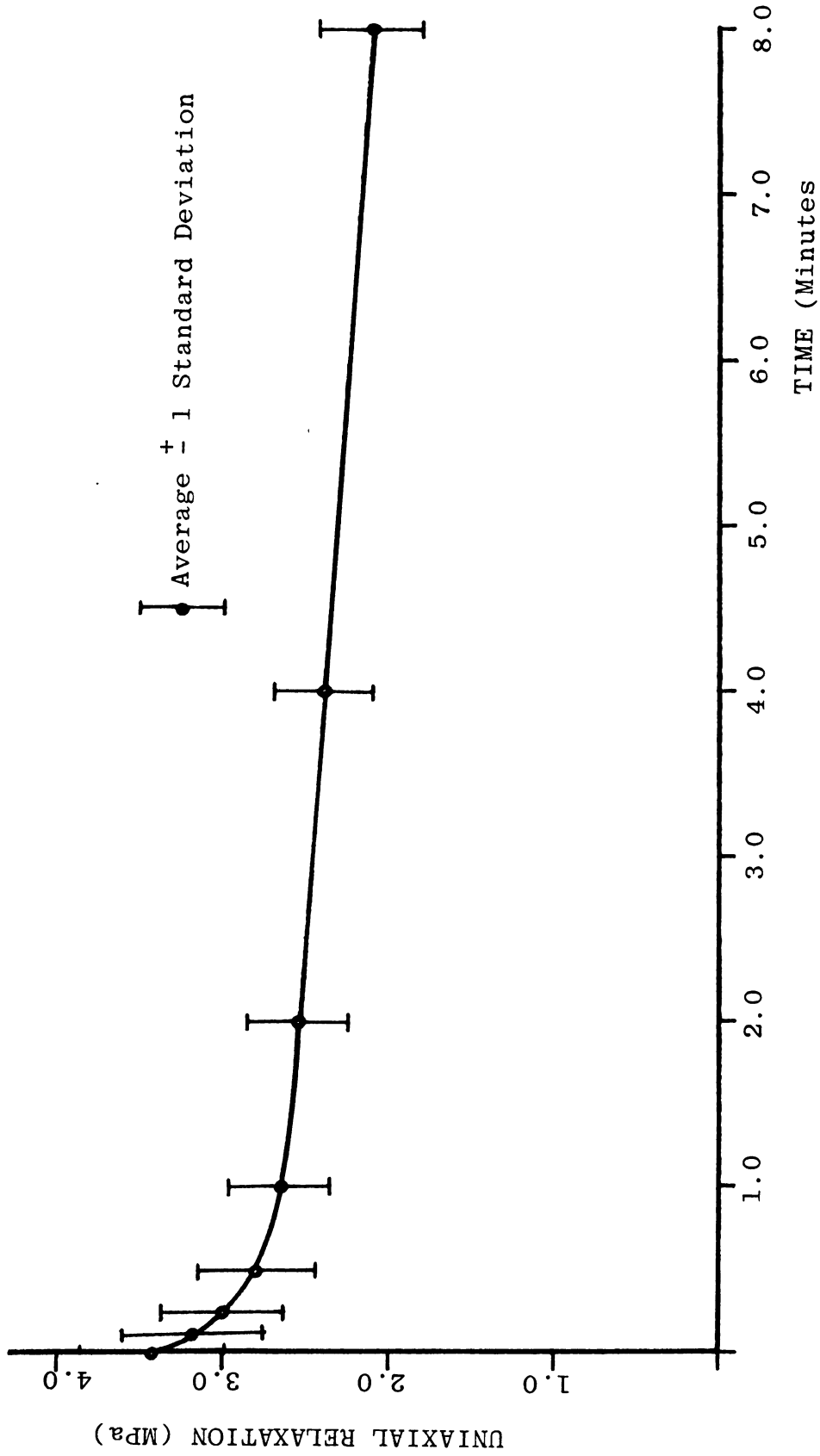


Figure 5.10. Average and Standard Deviation of Uniaxial Relaxation Function of 24 Red Delicious Apples

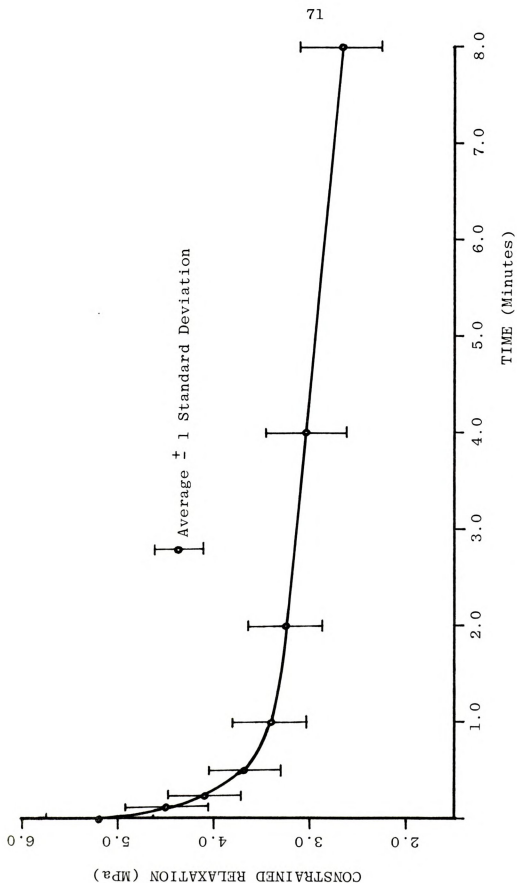


Figure 5.11. Average and Standard Deviation of the Constrained Relaxation Function of 24 Red Delicious Apples

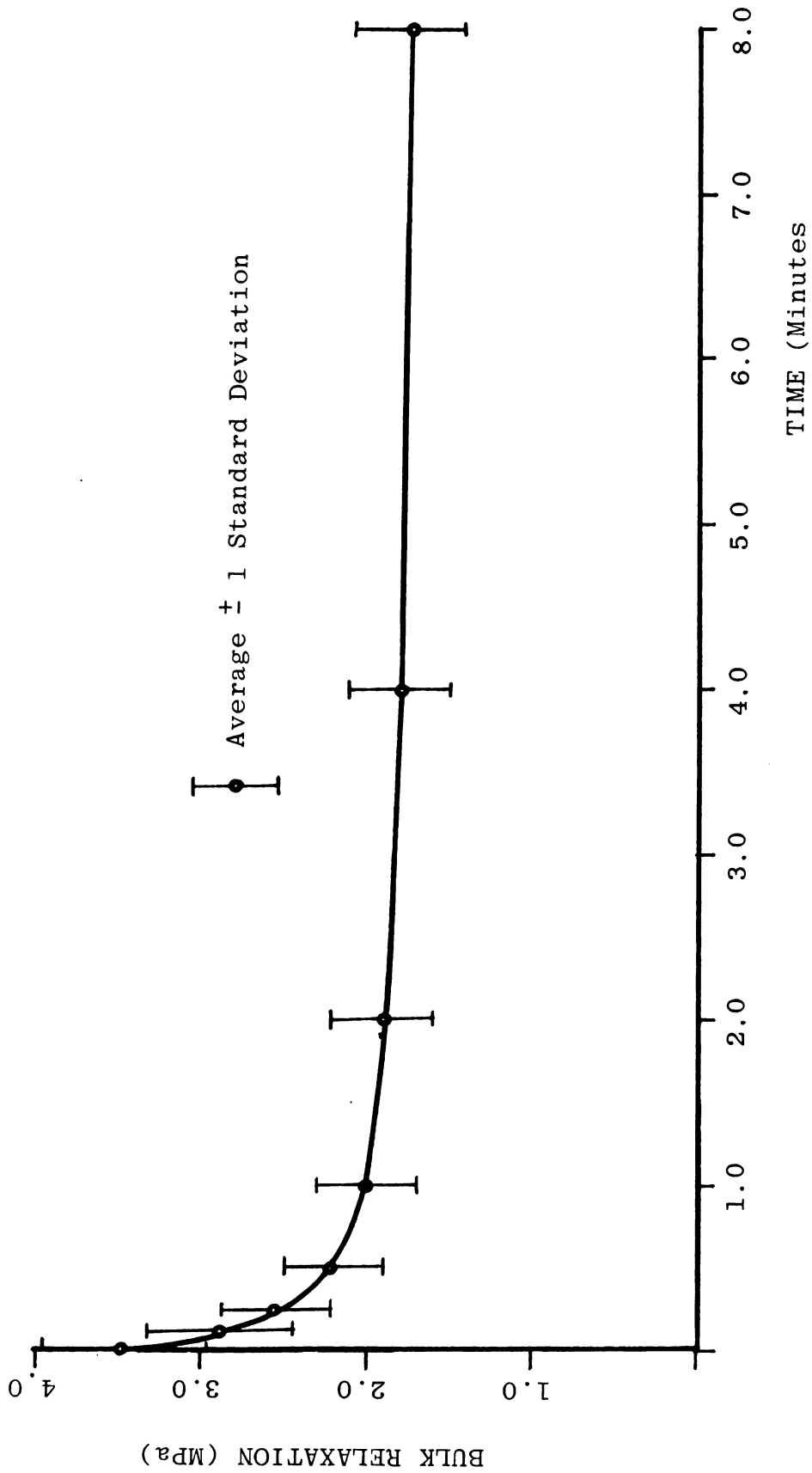


Figure 5.12. Average and Standard Deviation of the Bulk Relaxation Function of 24 Red Delicious Apples



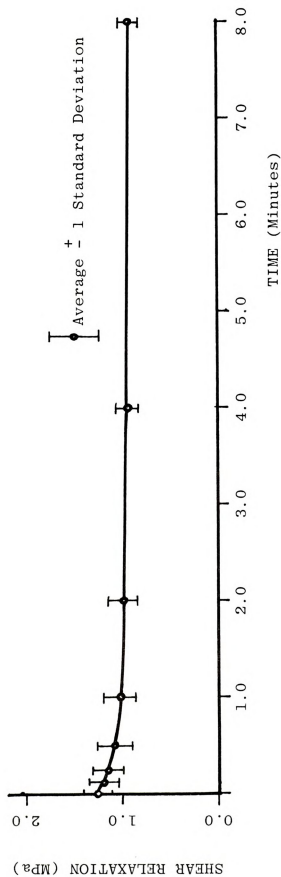


Figure 5.13. Average and Standard Deviation of the Shear Relaxation Function of 24 Red Delicious Apples

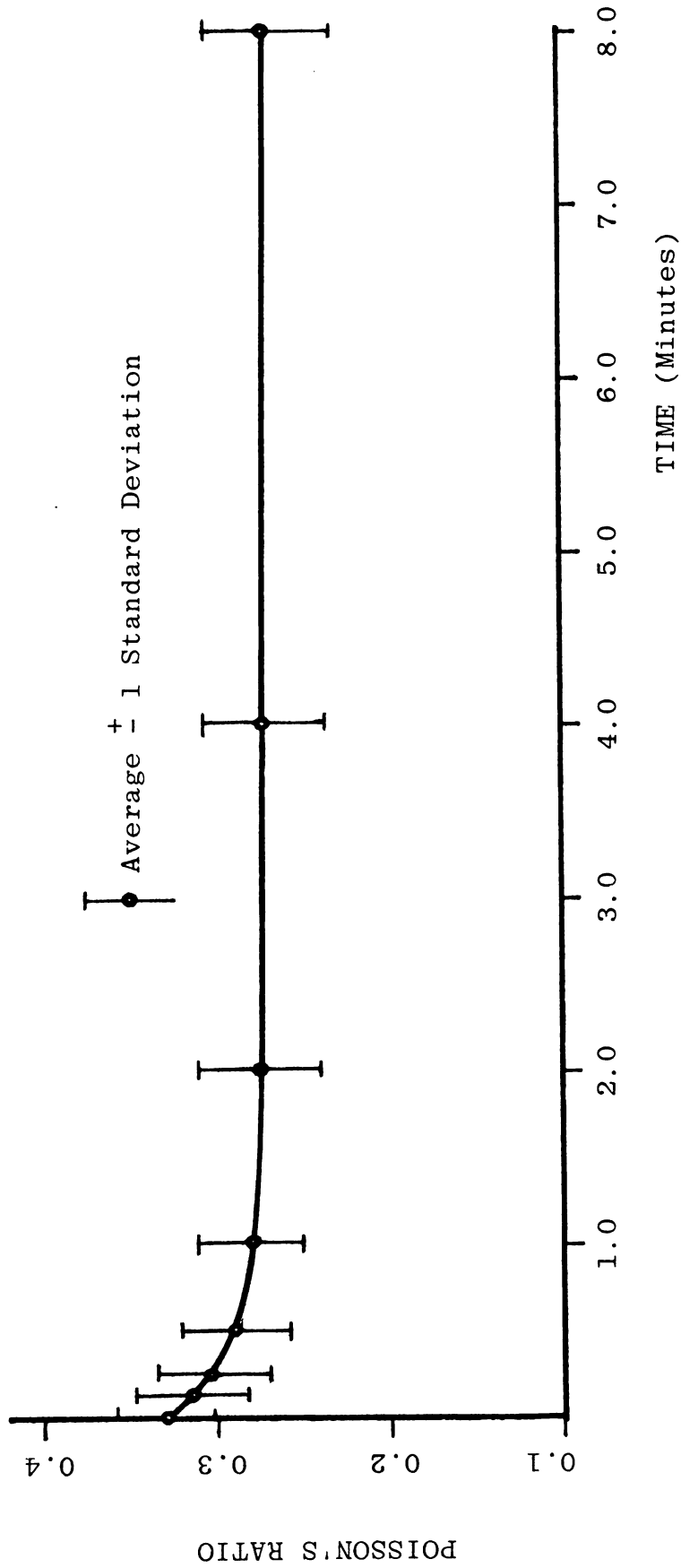


Figure 5.14. Average and Standard Deviation of the Poisson's Ratio of 24 Red Delicious Apples



## 6. FINITE ELEMENT FORMULATION IN VISCOELASTICITY

A method for determining the viscoelastic constitutive relations of biological material was presented in the previous section. These constitutive equations are essential for the analysis of the behavior of these materials under different loading conditions.

A finite element method for solving these viscoelastic boundary value problems is now presented. Its application will be illustrated in a following section.

Finite element methods have already been used by several authors in solving viscoelastic boundary value problems (for example, Taylor *et al.*, 1968; Herrmann and Peterson, 1968; Heer and Chen, 1969; Malone and Connor, 1971; Carpenter, 1972). The following derivations are similar to those by Taylor *et al.* (1968) and Heer and Chen (1969).

### 6.1 Viscoelastic Boundary Value Problem: Variational Theorem

A viscoelastic quasi-static boundary value problem is governed by the following relations which have to be satisfied, and which are similar to the elastic boundary value relations (Christensen, 1971):

(i) Equilibrium equations

$$\sigma_{ij,j} + F_i = 0 \quad i, j = 1, 2, 3 \quad (6.1)$$

where a comma denotes a differentiation and  $F_i$  is a body force vector.

(ii) Constitutive equations

$$\sigma_{ij} = \int_0^t G_{ijkl}(t-\tau) \frac{\partial \epsilon_{kl}}{\partial \tau}(\tau) d\tau \quad (6.2)$$

where

$$\begin{aligned} G_{ijkl} = & \frac{1}{3} [G_2(t) - G_1(t)] \delta_{ij} \delta_{kl} \\ & + \frac{1}{2} G_1(t) [\delta_{ik} \delta_{jl} + \delta_{il} \delta_{jk}] \end{aligned} \quad (6.3)$$

Using convolution notation (6.2) can be written as

$$\sigma_{ij} = G_{ijkl} * \epsilon_{kl} \quad (6.4)$$

(iii) Strain displacement relations

$$\epsilon_{ij} = \frac{1}{2} (u_{i,j} + u_{j,i}) \quad (6.5)$$

(iv) Prescribed boundary values

$$\sigma_{ij} n_j = S_i \text{ on } B_\sigma \quad (6.6)$$

and

$$u_i = \Delta_i \quad \text{on } B_u$$

$B_\sigma$  is the part of the boundary on which the tractions  $S_i$  are prescribed and  $B_u$  is that part on which the displacements  $\Delta_i$  are prescribed.  $n_j$  denotes the components of the unit normal vector to the boundary.

Let  $I$  be a functional defined as (Christensen, 1971)

$$I = \int_V [\frac{1}{2} G_{ijkl} * \epsilon_{ij} * \epsilon_{kl} - F_i * u_i] dV - \int_{B_\sigma} (S_i * u_i) da \quad (6.7)$$

where it is assumed that the displacement boundary conditions are satisfied.  $V$  is the total volume of the solid. It can be shown that the first variation  $\delta I$  of  $I$  due to a displacement variation vanishes when the equilibrium equations and the boundary conditions are satisfied. In other words, the solution of the boundary value problem stated in (6.1), (6.2), (6.5) and (6.6) can be obtained by finding the stationary value of the functional  $I$  in (6.7). The finite element method can be used as a numerical technique based on the minimization of this functional.

## 6.2 Axisymmetric Viscoelastic Solids

In the case of axial symmetry (no displacement or displacement gradients in the  $\theta$  direction), Figure 6.1, the strain displacement relations are (Sokolnikoff, 1956)

$$\begin{aligned}\epsilon_{rr} &= \epsilon_{11} = \frac{\partial u_r}{\partial r} \\ \epsilon_{zz} &= \epsilon_{22} = \frac{\partial u_z}{\partial z} \\ \epsilon_{\theta\theta} &= \epsilon_{33} = \frac{u_r}{r} \\ \epsilon_{rz} &= \epsilon_{12} = \frac{1}{2} \left( \frac{\partial u_r}{\partial z} + \frac{\partial u_z}{\partial r} \right)\end{aligned}\quad (6.8)$$

Combining (6.2) and (6.3) the constitutive equations are

$$\begin{aligned}\sigma_{11} &= \sigma_{rr} = \int_0^t G_{11kl}(t-\tau) \frac{d\epsilon_{kl}}{d\tau} d\tau \\ &= \int_0^t \left[ \frac{1}{3}(G_2 - G_1) \frac{d}{d\tau} (\epsilon_{rr} + \epsilon_{zz} + \epsilon_{\theta\theta}) + \right. \\ &\quad \left. G_1 \frac{d\epsilon_{rr}}{d\tau} \right] d\tau\end{aligned}$$

or

$$\sigma_{rr} = \frac{1}{3}[(G_2 - G_1) + 3G_1] * \epsilon_{rr} + \frac{1}{3}(G_2 - G_1) * (\epsilon_{zz} + \epsilon_{\theta\theta}) \quad (6.9)$$





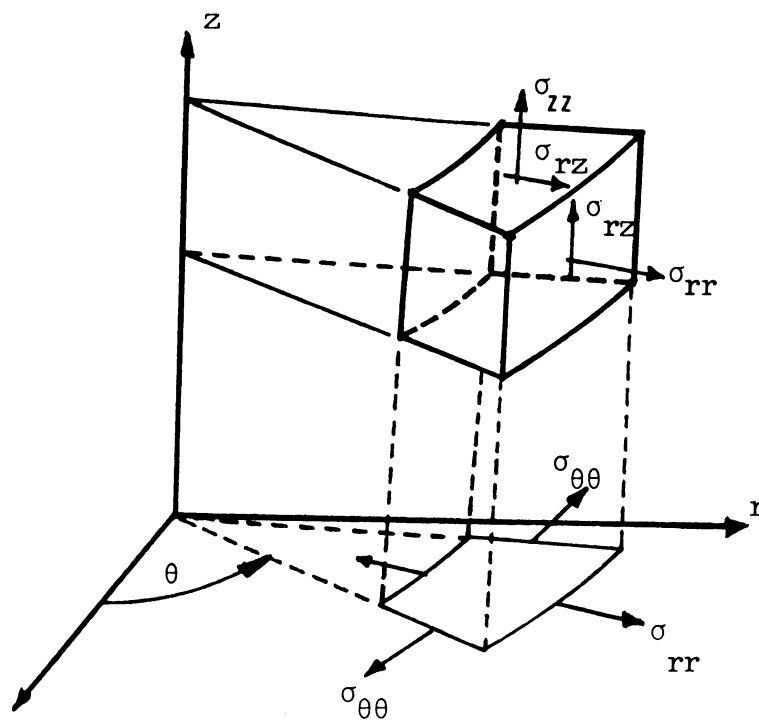


Figure 6.1. Stresses in Axially Symmetric Problems

Equation (6.9) can be rewritten as

$$\sigma_{rr} = A_{11} * \epsilon_{rr} + A_{12} * \epsilon_{zz} + A_{13} * \epsilon_{\theta\theta} \quad (6.10)$$

Similar expressions can be derived for the other stress components  $\sigma_{zz}$ ,  $\sigma_{\theta\theta}$ ,  $\sigma_{rz}$ . At this moment, it is convenient to simplify the notation by setting (Figure 6.1)

$$\sigma_1 = \sigma_{rr}, \quad \sigma_2 = \sigma_{zz}, \quad \sigma_3 = \sigma_{\theta\theta}, \quad \sigma_4 = \sigma_{rz}$$

and

$$\epsilon_1 = \epsilon_{rr}, \quad \epsilon_2 = \epsilon_{zz}, \quad \epsilon_3 = \epsilon_{\theta\theta}, \quad \epsilon_4 = \epsilon_{rz} \quad (6.11)$$

The stress-strain relations can then be expressed as

$$\sigma_K = A_{KM} * \epsilon_M \quad K, M = 1, 2, 3, 4 \quad (6.12)$$

where

$$A_{KM} = A_{MK}$$

and

$$\begin{aligned} A_{11} &= A_{22} = A_{33} = \frac{1}{3}(G_2 + 2G_1) = B + \frac{4}{3}G \\ A_{12} &= A_{13} = A_{23} = \frac{1}{3}(G_2 - G_1) = B - \frac{2}{3}G \\ A_{44} &= \frac{1}{2}G_1 = G \\ A_{41} &= A_{42} = A_{43} = 0 \end{aligned} \quad (6.13)$$



The axisymmetric expression for the functional (6.7) becomes

$$I = \int_V \left[ \frac{1}{2} A_{KM} * \epsilon_M * \epsilon_K - F_\alpha * u_\alpha \right] dV \\ - \int_{B_\sigma} (S_\alpha * u_\alpha) da \quad (6.14)$$

where  $K, M = 1, 2, 3, 4$

and  $\alpha = 1, 2$

### 6.3 Discretization of a Region: Finite Element Formulation

#### 6.3.1 Nodal Displacements

The volume and surface integrals in (6.14) can be expressed as a sum of integrals over a set of subregions

$$I = \sum_{e=1}^p \frac{1}{2} \int_V^e (\epsilon_K^e * A_{KM} * \epsilon_M^e) dV \\ - \sum_{e=1}^p \int_V^e (u_\alpha^e * F_\alpha^e) dV - \sum_{e=1}^p \int_{B_\sigma^e} (u_\alpha^e * S_\alpha^e) da \quad (6.15)$$

where the superscripts  $e$  indicate the subregions.

The displacements in each subregion or element are approximated by algebraic polynomials relating them to displacements of nodal points of that element (Zienkiewicz, 1971)



$$\text{or } \{u^e\} = [N^e]\{U\} \quad (6.16)$$

$[N^e]$  is the matrix of shape functions relating displacements in the element  $\{u^e\}$  to the nodal displacements  $\{U\}$ .

An example of an axisymmetric element is given in Figure 6.2, and the nodal displacements are indicated.

The strain vector is obtained by appropriate space differentiation of (6.16)

$$\{\epsilon^e\} = [B^e]\{U\} \quad (6.17)$$

Substitution of (6.16) and (6.17) into (6.15) and the use of matrix notation instead of indicial notation yields

$$\begin{aligned} I = & \sum_{e=1}^p \frac{1}{2} \int_V (\{U\}^T [B]^T * [A] * [B] \{U\}) dV \\ & - \sum_{e=1}^p \int_V (\{U\}^T [N]^T * \{F\}) dV \\ & - \sum_{e=1}^p \int_{B_\sigma} (\{U\}^T [N]^T * \{S\}) da \end{aligned} \quad (6.18)$$

where  $[B]^T$  is the transpose of matrix  $[B]$  and the element superscripts are deleted for clarity. The order of integration can be changed. The integration over space is performed first, then the convolution. Hence,



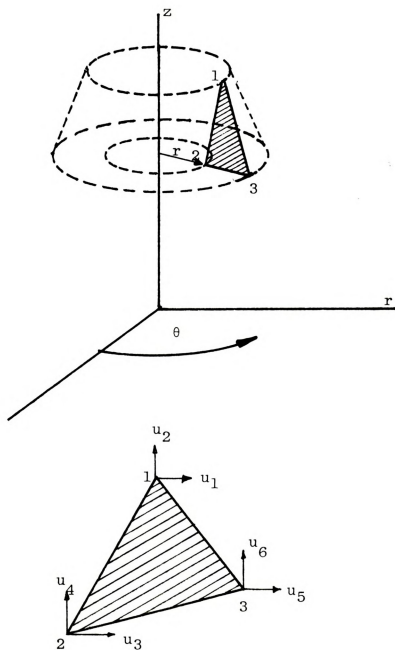


Figure 6.2. Triangular Axisymmetric Element and Nodal Displacements



1. The first part of the paper is devoted to the study of the asymptotic behavior of the solutions of the system of equations (1) as  $\epsilon \rightarrow 0$ . It is shown that the solutions of the system (1) converge to the solutions of the system (2) in the sense of the  $L^2$ -norm.

$$\begin{aligned}
I = & \sum_{e=1}^p \frac{1}{2} \{U\}^T * \left[ \int_V [B]^T [A][B] dV \right] * \{U\} \\
& - \sum_{e=1}^p \{U\}^T * \left[ \int_V [N]^T \{F\} dV \right] \\
& - \sum_{e=1}^p \{U\}^T * \left[ \int_{B_\sigma} [N]^T \{S\} da \right] \quad (6.19)
\end{aligned}$$

This functional can be written in a simpler form as

$$I = \frac{1}{2} \{U\}^T * [K] * \{U\} - \{U\}^T * \{R\} \quad (6.20)$$

The stiffness matrix is

$$[K] = \sum_{e=1}^p [k^e] = \sum_{e=1}^p \int_V [B^e]^T [A][B^e] dV \quad (6.21)$$

The force vector is

$$\begin{aligned}
\{R\} = \sum_{e=1}^p \{r^e\} &= \sum_{e=1}^p \left( \int_V [N^e]^T F^e dV + \right. \\
&\left. \int_{B_e} [N^e]^T \{S^e\} da \right) \quad (6.22)
\end{aligned}$$

It should be noted that the displacement vector  $\{U\}$  now contains all the nodal displacements of a region and  $\{R\}$  is the vector of all the nodal forces.

Taking the first variation of (6.20) and setting it equal to zero yields



$$\delta I = \delta \{U\}^T * [K] * \{U\} - \delta \{U\}^T * \{R\} = 0$$

or

$$[K] * \{U\} - \{R\} = 0 \quad (6.23)$$

Equation (6.23) resembles the finite element equations of elasticity where the displacements are also the unknowns. However, the explicit form of (6.23) contains a time integral

$$\int_{\tau=0}^t [K(t-\tau)] d\{U(\tau)\} = \{R(t)\} \quad (6.24)$$

These integral equations can be solved numerically by the use of time increments (Gupta, 1974). Rewriting the integral in (6.24) as a summation over time steps results in

$$\sum_{m=1}^n [K(t_n - t_m)] \{\Delta U(t_m)\} = \{R(t_n)\} \quad (6.25)$$

where  $\{\Delta U(t_m)\}$  is a vector of displacement increments from time  $t_m$  to  $t_{m+1}$ , approximated as a displacement at the beginning of the time increment.

The last displacement increment can now be found from the previous displacement increments and a possible initial step displacement  $\{U_0\}$  at time  $t=0$ . This is done by reordering the terms in the summation in (6.25)

$$\begin{aligned}
[K(t_n - t_n)]\{\Delta U(t_n)\} &= \{R(t_n)\} - \\
\sum_{m=1}^{n-1} [K(t_n - t_m)]\{\Delta U(t_m)\} &- [K(t_n)]\{U_o\} \quad (6.26)
\end{aligned}$$

Hence the equation for the first few time steps are

$$\begin{aligned}
[K(o)]\{U_o\} &= \{R(t_o)\} \\
[K(o)]\{\Delta U(t_1)\} &= \{R(t_1)\} - [K(t_1)]\{U_o\} \\
[K(o)]\{\Delta U(t_3)\} &= \{R(t_2)\} - [K(t_1)]\{\Delta U(t_1)\} \\
&- [K(t_2)]\{U_o\} \quad (6.27)
\end{aligned}$$

A disadvantage of this method is that the number of terms on the right-hand side in (6.27) increases with an increasing number of time steps. If the stiffness matrix for each time interval is stored, an enormous amount of computer storage space is required. An alternate method is to rebuild these stiffness matrices each time they are used. This procedure, however, rapidly increases the required computer time, and, therefore, the cost. The latter method was used in the computer programs written for this study. Another approach is the use of logarithmic time increments which can be organized such that only one stiffness matrix has to be stored at each moment (Gupta, 1974). More simplifications could be made in the case of

exponential series representation of relaxation functions (Taylor *et al.*, 1968; Heer and Chen, 1969).

### 6.3.2 Element Stresses

The stress in each element can be derived from the nodal displacements by substituting (6.17) into (6.12)

$$\{\sigma^e\} = [A] * [B^e]\{U^e\}$$

or

$$\{\sigma^e\} = [A][B^e] * \{U^e\} \quad (6.25)$$

Writing (6.25) as a convolution integral, and dropping the superscript notation gives

$$\{\sigma(t)\} = \int_0^t [A(t-\tau)][B] d\{U(\tau)\} \quad (6.26)$$

Replacing the integral by a summation over discrete time steps yields the stress as a function of the displacement increments

$$\begin{aligned} \{\sigma(t_n)\} &= [A(t_n)][B]\{U_o\} + \\ &\sum_{m=1}^n [A(t_n - t_m)][B]\{\Delta U(t_m)\} \end{aligned} \quad (6.27)$$

Note that the calculations performed in (6.27) have to be repeated for each element.

## 7. NUMERICAL ANALYSIS OF MECHANICAL BEHAVIOR OF APPLES UNDER LOADS

A finite element method for the solution of visco-elastic boundary value problems was presented in the previous section. Existing finite element programs for two-dimensional elasticity were modified to accommodate the viscoelastic problems related to the loading of apples. The modification included a change to axially symmetric triangular elements, allocation of computer storage for the displacement increments calculated during each time step and the recalculation of the force vector on the right-hand side of the equation (6.27) after each time step. The finite element method was used with the previously discussed constitutive equations to analyze the behavior of apples under different loading conditions.

The behavior of a spherical specimen in contact with a rigid flat plate was studied. It was used as a model for the behavior of an apple in contact with a rigid wall or floor.

An analysis of the compression of a simple cylindrical sample was performed in order to evaluate the accuracy of the procedure. Comparisons were made between the numerical results and analytical solutions for simple problems.

### 7.1 Division into Elements

The finite element grids of a cylindrical and a spherical sample are shown in Figures 7.1 and 7.2. The cylindrical sample had a 9.025 mm radius and a length of 19.1 mm. The radius of the spherical sample was 17.8 mm. Each triangle represents a ring-shaped element as was shown in Figure 6.2. The region in Figure 7.2 represents a half sphere, in which the other half was omitted because of symmetry with respect to the  $r-\theta$  plane. The element size of the spherical sample was varied such that a very fine grid was obtained in the vicinity of the applied contact loads. This fine grid was necessary to obtain accurate results.

The division of the regions into elements was done with an automatic grid generating program which also labeled the nodes for minimum computer memory requirements relative to the storage of the stiffness matrix  $[K]$  in (6.23). There were 42 elements with 32 nodes in the cylindrical sample and 370 elements with 215 nodes in the spherical sample.

### 7.2 Special Techniques for the Solution of Contact Problems

The solution of the viscoelastic contact problems using finite elements required special care in the determination at each time step of those nodes that make



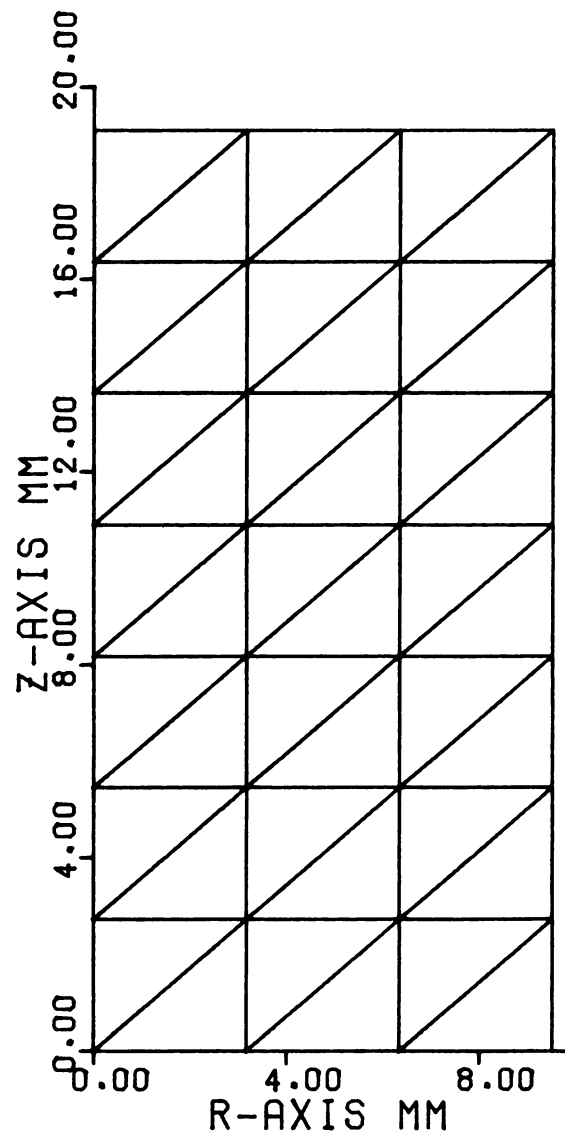


Figure 7.1. Finite Element Grid for a Cylindrical Specimen



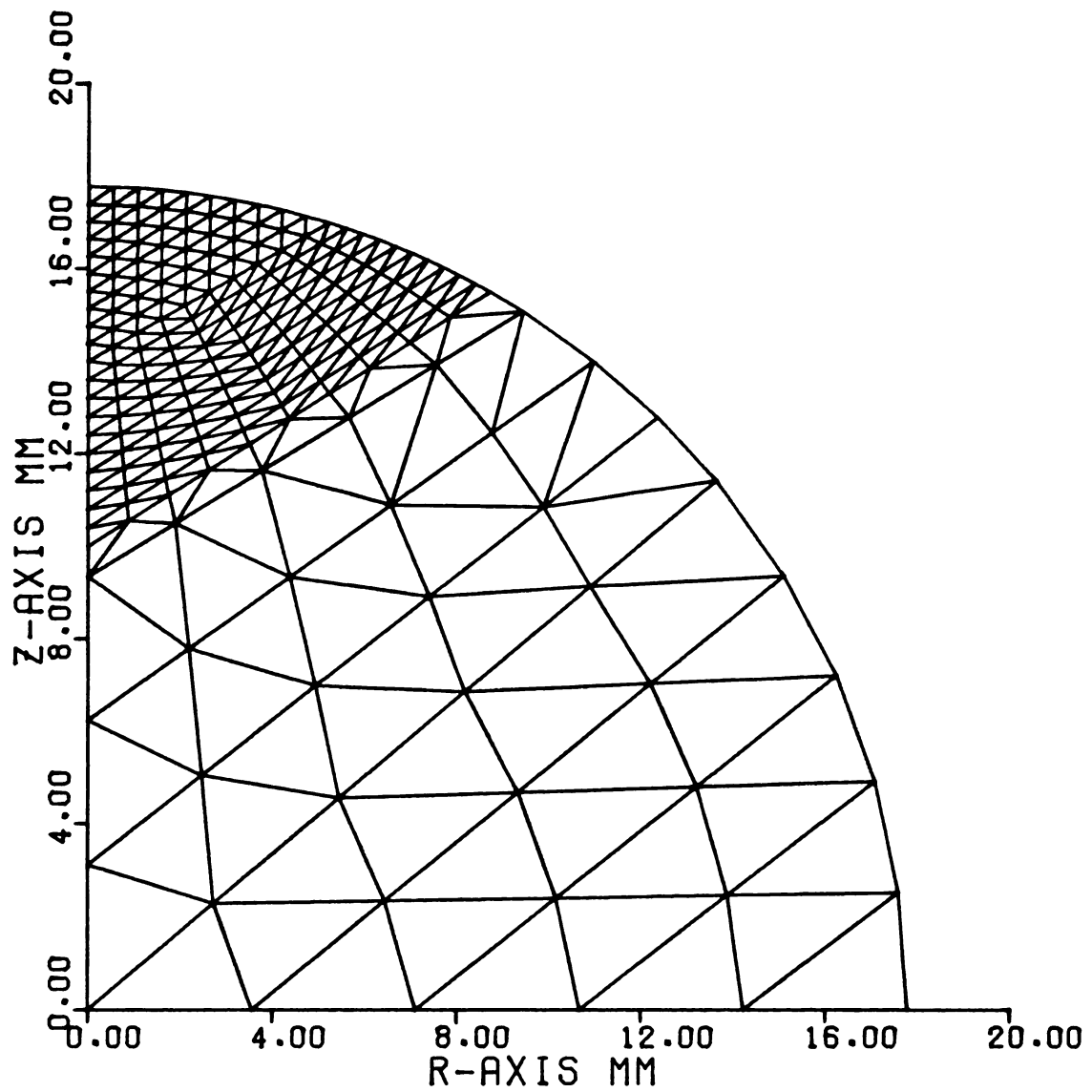


Figure 7.2. Finite Element Grid for a Spherical Specimen



contact with the flat plate after each time step. The force between the sphere and the plate was assumed in the z-direction. A special subroutine was written to monitor the displacement of boundary nodes and, if necessary, to impose nodal displacements to make them compatible with the flat plate displacement. Nodes in contact with a flat plate are illustrated in Figure 7.3.

The calculation of the resultant contact force between the flat plate and the specimen also required the knowledge of the nodes in contact with the flat plate. They determined over which elements the stress had to be integrated to obtain the resultant contact force. Integration was done by multiplying the element stress in the z-direction with the projection in the r- $\theta$  plane of the outside surface area of these boundary elements.

The formulation of the finite element method in terms of nodal displacements assumes that nodal forces and/or some nodal displacements can be specified, after which all the other nodal displacements can be calculated. This formulation creates some special problems when analyzing the behavior of a spherical sample under a constant force (creep) loading. The actual distribution of the force over the contact area depends on the size of the contact area, but this in turn depends on the axial displacement. Hence, no nodal contact forces can be accurately specified since the axial displacement is the unknown of the problem. The formulation of a constant force loading was solved by



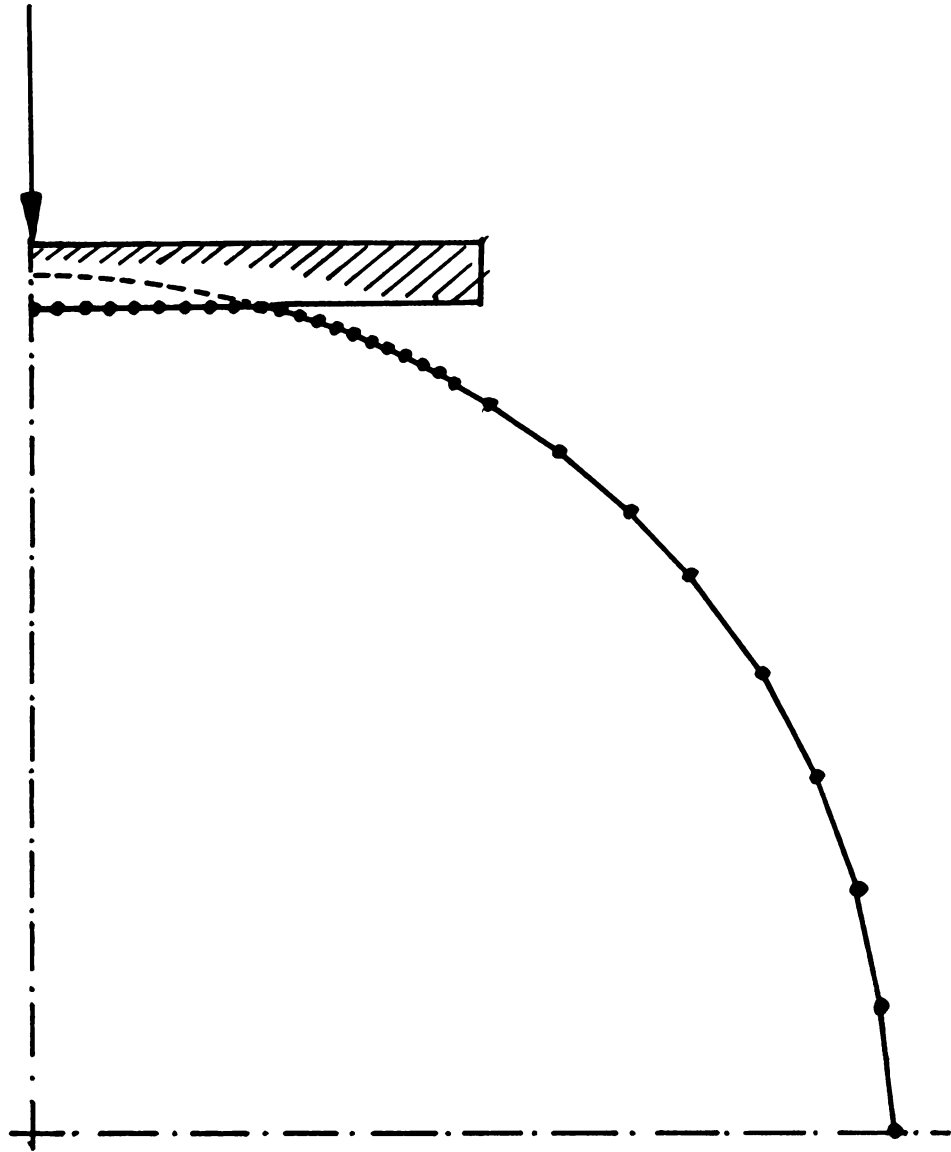


Figure 7.3. Spherical Sample in Contact with Rigid Flat Plate: Prescribed Displacement of the Contact Nodes





assuming an axial displacement, and calculating the contact force for this displacement. If this contact force was not equal to the specified creep load, the specified displacements were corrected and the contact force was recalculated. This iterative procedure is illustrated in Figure 7.4.  $F_c$  is the constant creep load,  $U_1$  is the initially assumed displacement. The displacement  $U_1$  requires a force  $F_1$  which is larger than the creep force. Multiplying  $U_1$  by  $F_c/F_1$  results in a displacement  $U_2$  which requires a force  $F_2$ . This iteration is continued until a displacement is obtained which requires a force very close to the constant creep load.

### 7.3 Material Properties

Most of the numerical analyses in this chapter were done for apple material having the following experimentally determined relaxation functions in the zero to two minute time region

$$E(t) = .888 e^{-15.897t} + 2.731 e^{-.106t} \quad (7.1)$$

$$X(t) = 1.386 e^{-19.303t} + 3.549 e^{-.119t} \quad (7.2)$$

These relaxation functions are shown in Figures 7.5 and 7.6. The values of bulk and shear relaxation functions, which were used in the finite element analysis, are given in Figures 7.7 and 7.8 respectively. In some examples



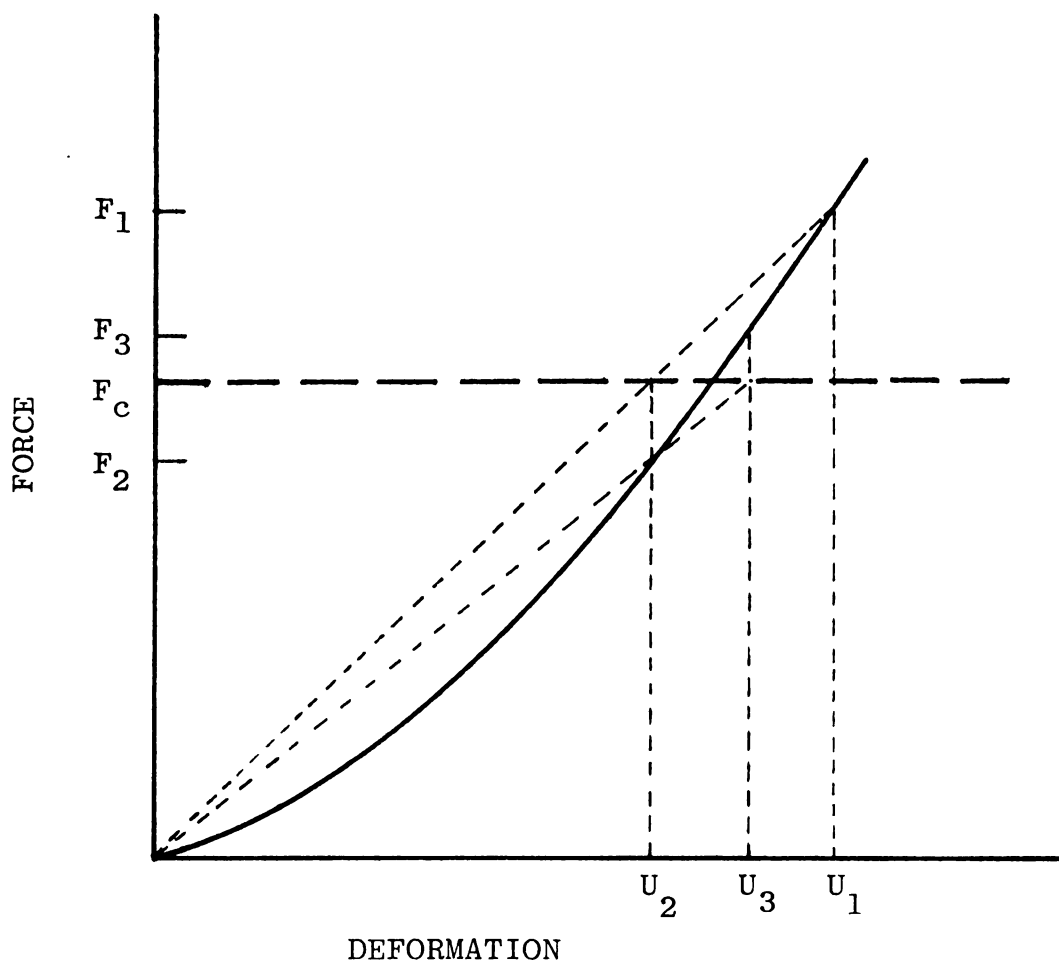


Figure 7.4. Iterative Procedure for Determining the Deformation under a Constant Load



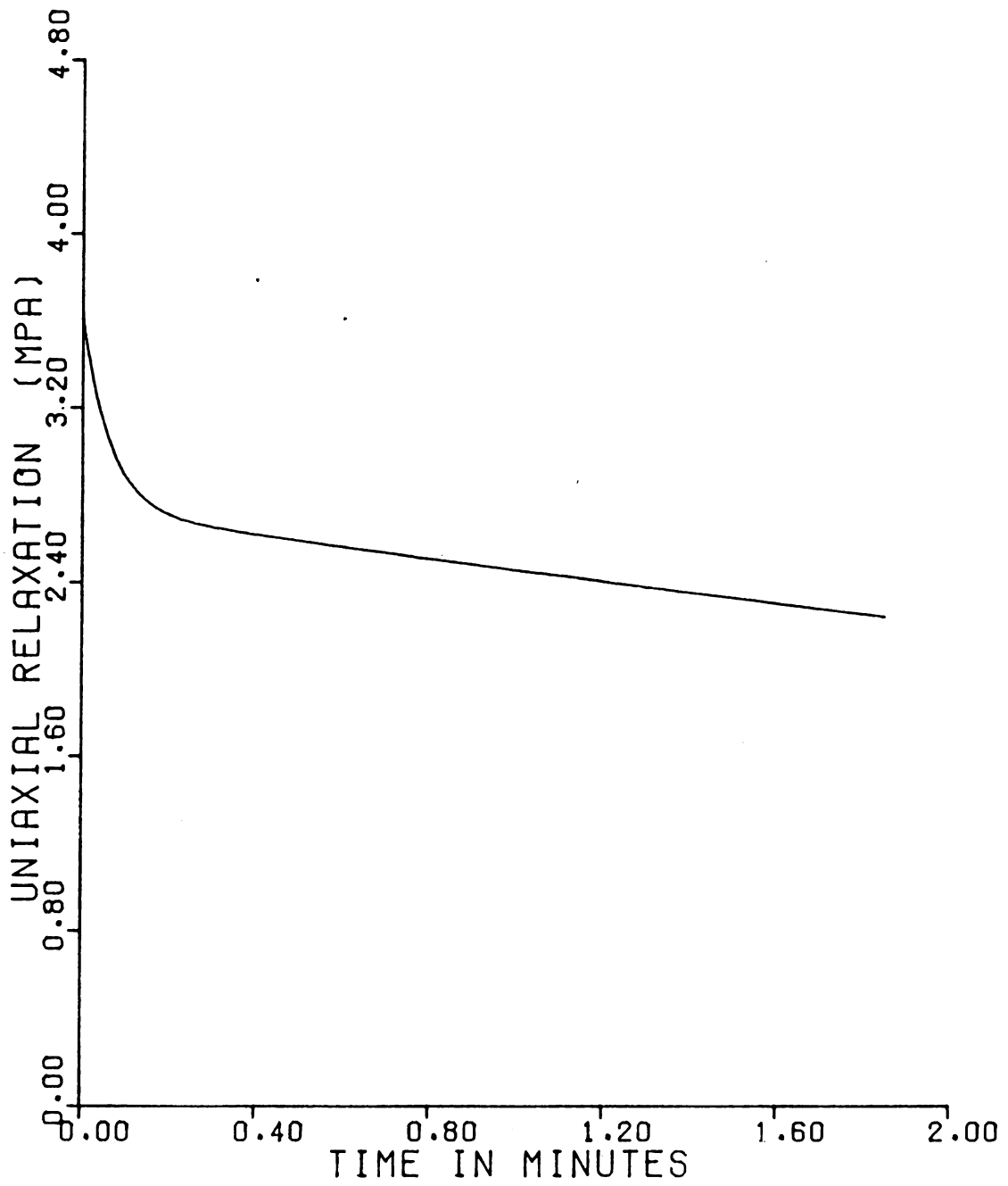


Figure 7.5. Uniaxial Relaxation Function for Sample I



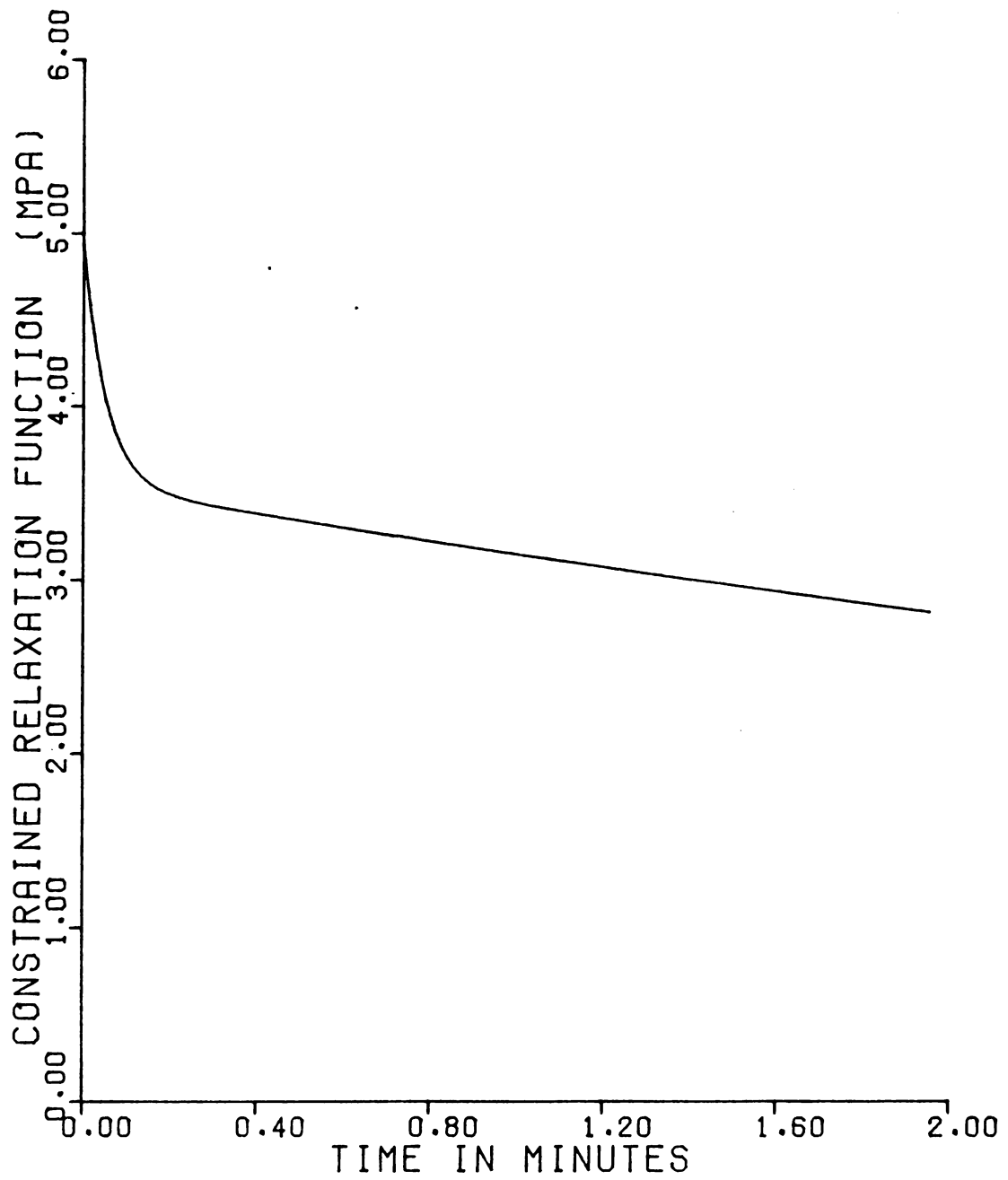


Figure 7.6. Constrained Relaxation Function for Sample I





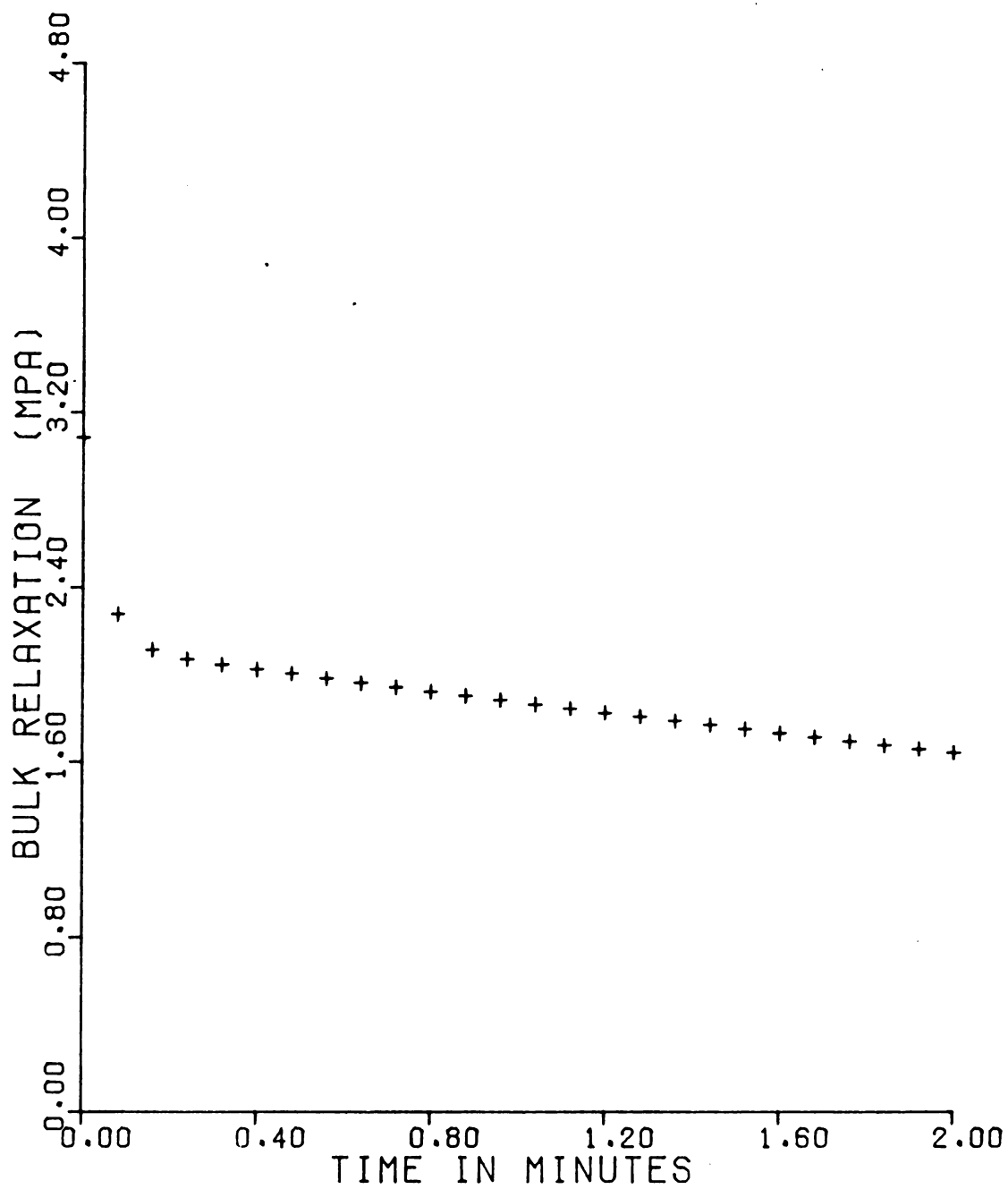


Figure 7.7. Bulk Relaxation Function for Sample I



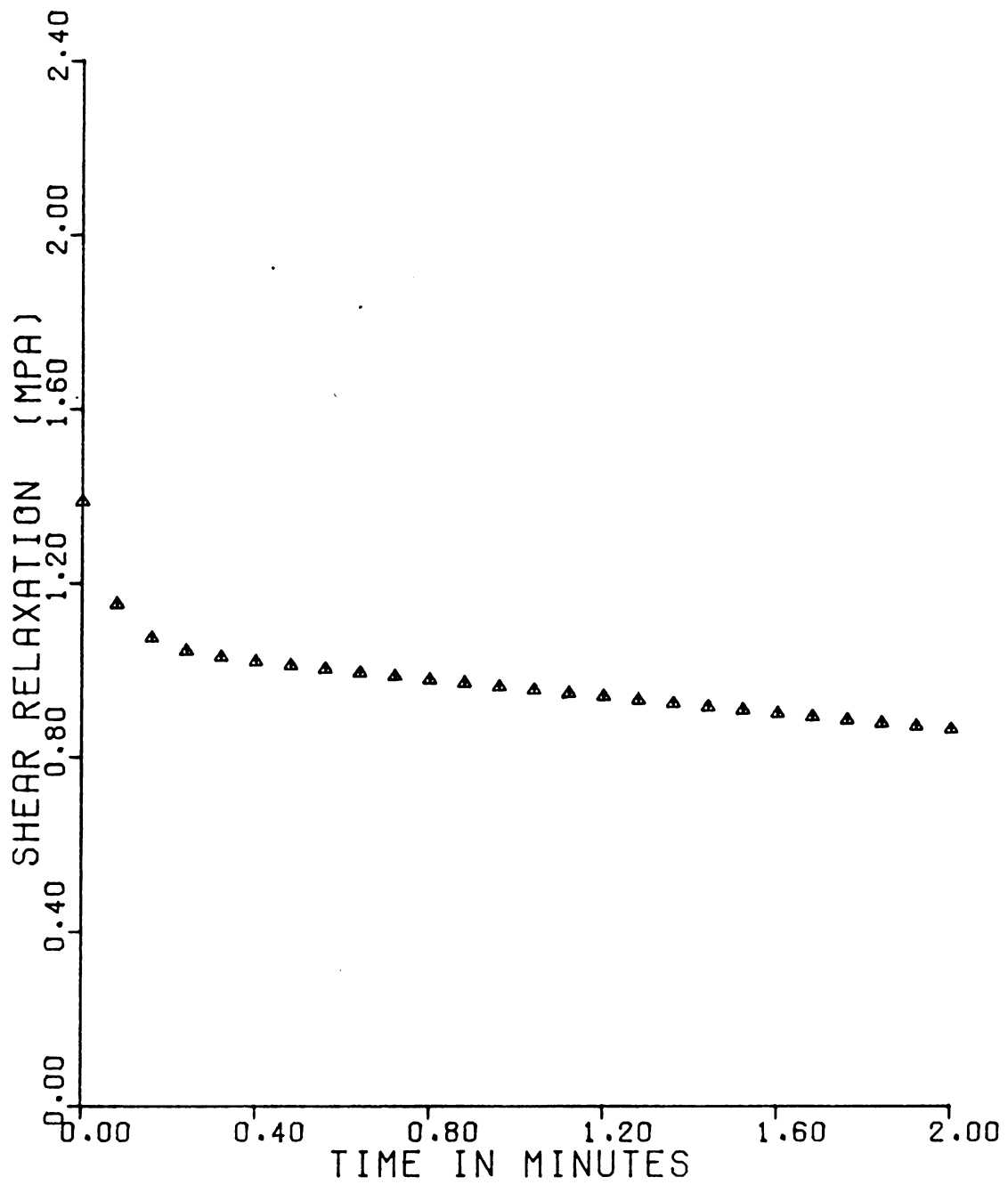


Figure 7.8. Shear Relaxation Function for Sample I



specimens were used whose material properties are expressed by the relaxation functions

$$E(t) = 1.018 e^{-17.561t} + 3.092 e^{-.096t} \quad (7.3)$$

and

$$X(t) = 1.964 e^{-22.127t} + 3.886 e^{-.129t} \quad (7.4)$$

The latter sample is referred to as Sample II, while the former will be designated as Sample I.

#### 7.4 Specimen Subjected to a Constant Deformation Rate

The finite element models of both the cylindrical and the spherical specimen were subjected to a deformation rate of -2.54 mm/min in the z-direction (axial compression). The required compressive force on the cylindrical sample to obtain this deformation rate was analytically found from (3.46) and (7.1)

$$F(t) = 978.61 - 2.12 e^{-15.897t} - 976.61 e^{-.106t} \quad (7.3)$$

where the force is in newtons.

This force versus time function was plotted in Figure 7.9 for comparison with the force values obtained from the finite element analysis. Excellent agreement between the analytical and the numerical technique was observed, except at time  $t=0$  where a non-zero force value was



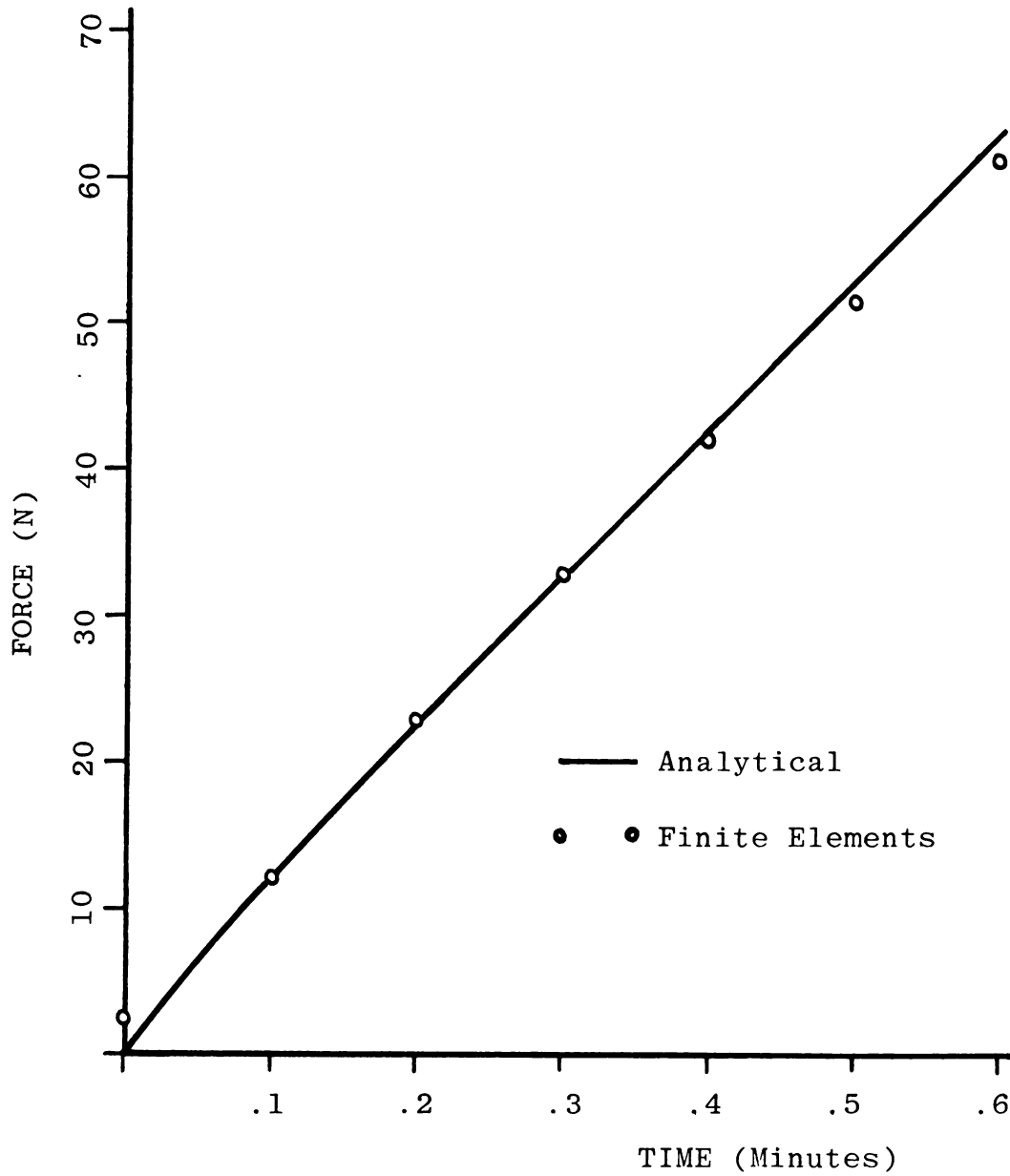


Figure 7.9. Comparison of Analytical and Numerical Force Versus Time Curves of a Cylindrical Specimen Under Constant Deformation Rate of 2.54 mm/min





obtained, an error inherent in the summation over time in equation (6.27).

The calculated force versus time curve was also compared with experimentally obtained force-time curves of cylindrical samples subjected to a deformation rate of 2.54 mm/min. Figure 7.10 shows two experimental curves and a calculated curve. The variation in response among samples of the same apple can readily be observed. The calculated value does not exactly coincide with either of the two experimental curves. In most cases the calculated values are slightly lower than the measured ones. This can also be seen in the results for a different apple (Sample II) represented in Figure 7.11.

Comparison of experimental and calculated force-time curves for several samples taken from different apples indicated that the slope of the calculated curves was in general smaller than the slope of the measured values. The slope of these force-time curves at this deformation rate depends on the value of the relaxation functions for very small values of time. It was already discussed in Section 3.2.1 that relaxation experiments do not always result in very good values of the relaxation functions for small time values, and that dynamic experiments would be necessary. However, the relaxation functions determined from the relaxation experiments would be sufficient for smaller deformation rates.



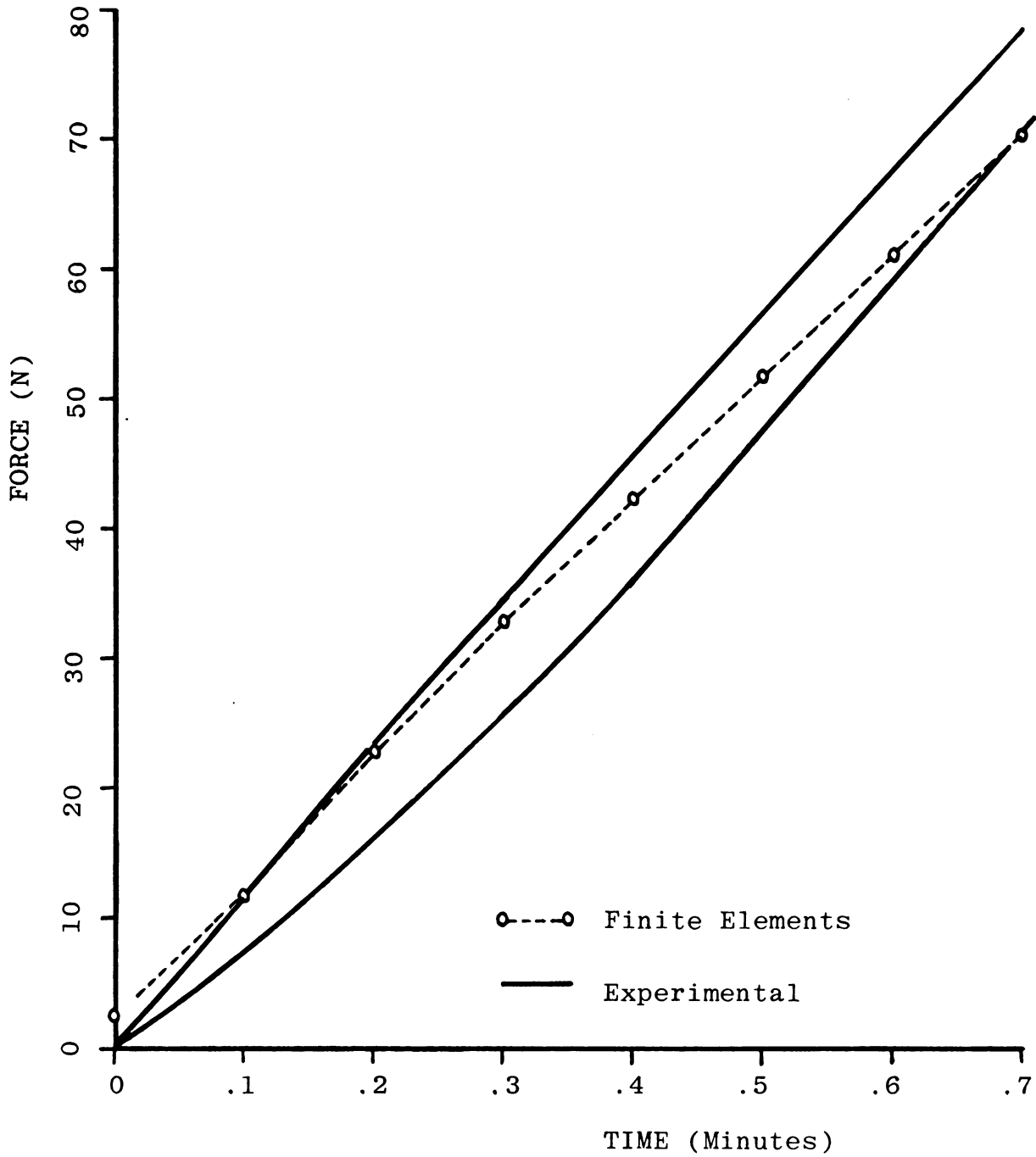


Figure 7.10. Experimental and Calculated Force-Time Curves of a Cylindrical Specimen, Sample I. Deformation Rate = 2.54 mm/min



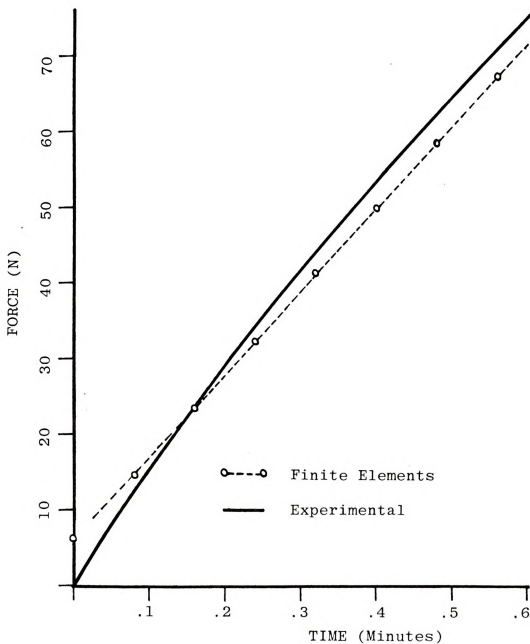


Figure 7.11. Experimental and Calculated Force-Time Curves of a Cylindrical Specimen, Sample II. Deformation Rate = 2.54 mm/min



The compressive force on a spherical sample subjected to a constant axial deformation rate of 2.54 mm/min is illustrated in Figure 7.12 and Figure 7.13. The calculated values in both cases are higher than the measured values. This difference was believed to be caused by differences in the radius of curvature between the experimental sample and the model in Figure 7.2. The calculated force-deformation relation for a 15.1 mm radius sphere given in Figure 7.12 illustrates this effect of the radius of curvature. Slight irregularities in the specimen boundary at the contact point were very difficult to eliminate during the sample preparation. Unfortunately, it was seldom possible to obtain more than one spherical sample from one apple after the cylindrical samples were removed.

The comparison of the calculated and experimental force deformation or force-time curves in this section has shown that the numerical technique can be used to simulate the mechanical behavior of the fruit. It is also clear that the experimental relaxation functions have to be applied with caution and do not always give close agreement between calculated and measured force values for rapidly changing loading conditions. This indicates the need for dynamic experiments if dynamic loadings are to be studied.





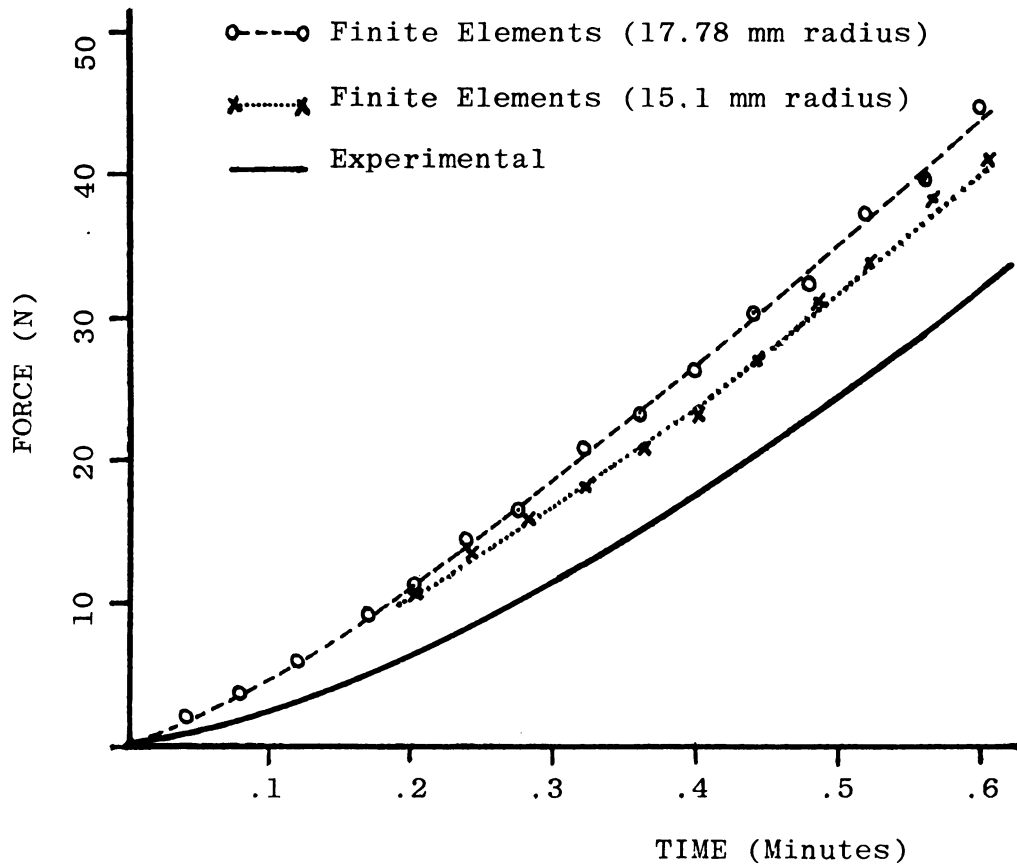


Figure 7.12. Experimental and Calculated Force-Time Curves of a Spherical Specimen, Sample I. Deformation Rate = 2.54 mm/min



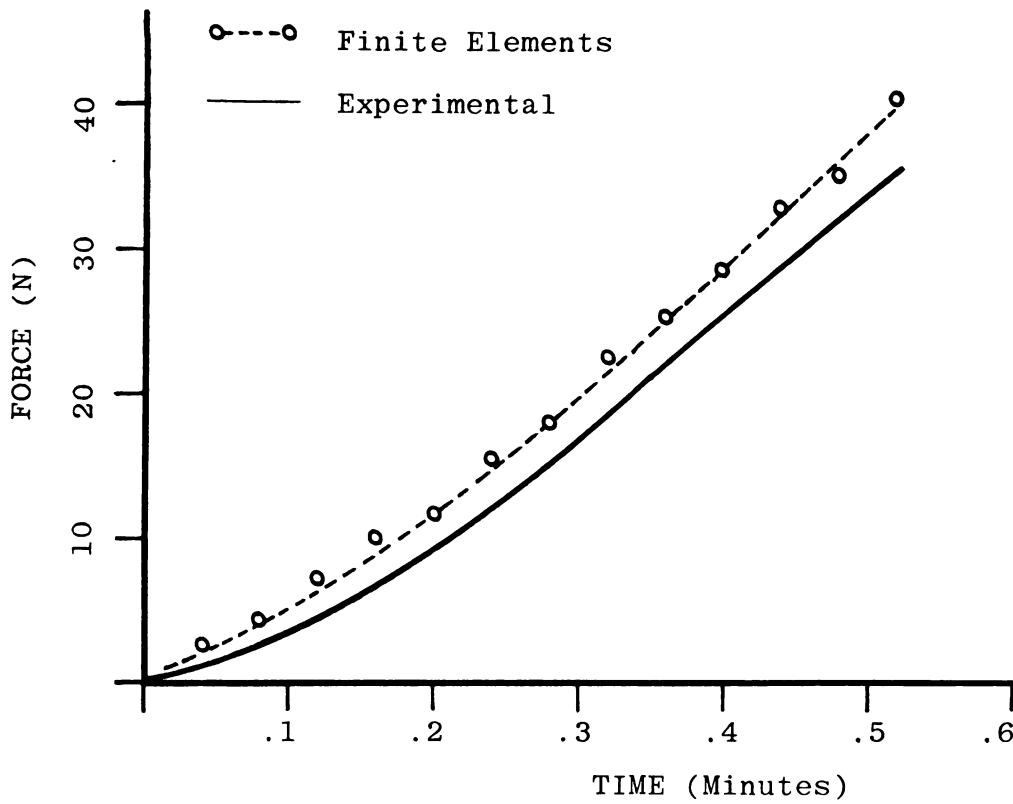


Figure 7.13. Experimental and Calculated Force-Time Curves of a Spherical Specimen, Sample II. Deformation Rate = 2.54 mm/min



## 7.5 Behavior of Fruit under a Constant Load

The experiments and calculations up to this point were performed assuming a fixed displacement. In the following, the displacement of a specimen is analyzed as it evolves in time under the influence of a constant load.

### 7.5.1 Creep Behavior of a Cylindrical Specimen

A creep compliance  $D(t)$  can be defined to express viscoelastic strain of a one-dimensional specimen as a function of stress (Christensen, 1971)

$$\varepsilon_{11}(t) = \int_0^t D(t-\tau) \frac{d\sigma_{11}(\tau)}{d\tau} d\tau \quad (7.5)$$

This creep compliance can be related to the uniaxial relaxation function via their respective Laplace transforms

$$\bar{D}(s) = \frac{1}{s^2 \bar{E}(s)} \quad (7.6)$$

Combining (7.6) with the uniaxial relaxation function of (7.1) yields the creep compliance

$$D(t) = .365 + .0387t - .0883 e^{-12.02t} \quad (7.7)$$

which is shown in Figure 7.14. The units of  $D(t)$  are  $(\text{megapascal})^{-1}$ .



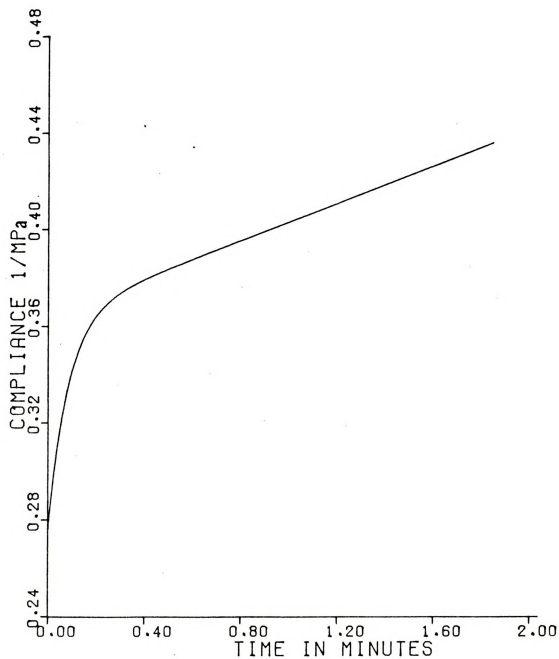


Figure 7.14. Uniaxial Compliance (Sample I)





Equations (7.7) and (7.5) were used to calculate the change in length of a cylindrical specimen subjected to a constant compressive load of 80 N, applied at time  $t=0$ . The deformation of the specimen is shown in Figure 7.15 as a function of time.

The nodal loads could have been specified for this particular specimen. The iterative procedure described in Section 7.2, however, was used to demonstrate its applicability. The calculated force had to be within plus or minus 2.5 percent of the creep load to terminate the iteration. The results shown in Figure 7.15 indicate the validity of the technique.

#### 7.5.2 Creep Behavior of a Spherical Specimen

The deformation of and the stress distribution in a spherical body composed of apple parenchyma and subjected to a constant flat plate load of 50 N was calculated. The evolution of the axial deformation, calculated using the iterative finite element procedure, is depicted in Figure 7.16. The creep deformation rate became very small after only 0.5 minute.

Isostress curves were interpolated from nodal stress values which were obtained from the element stress values through a "consistent stress analysis" technique (Oden and Brauchli, 1971). The isostress lines at time  $t=0$ , or the instant of loading, are shown in Figures 7.17 through 7.20.



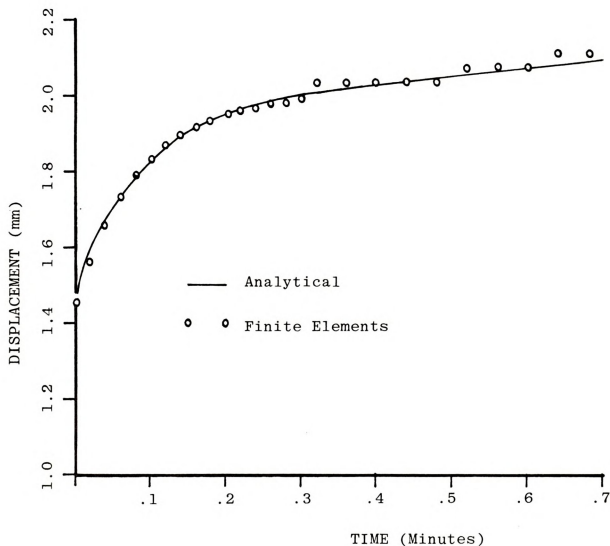
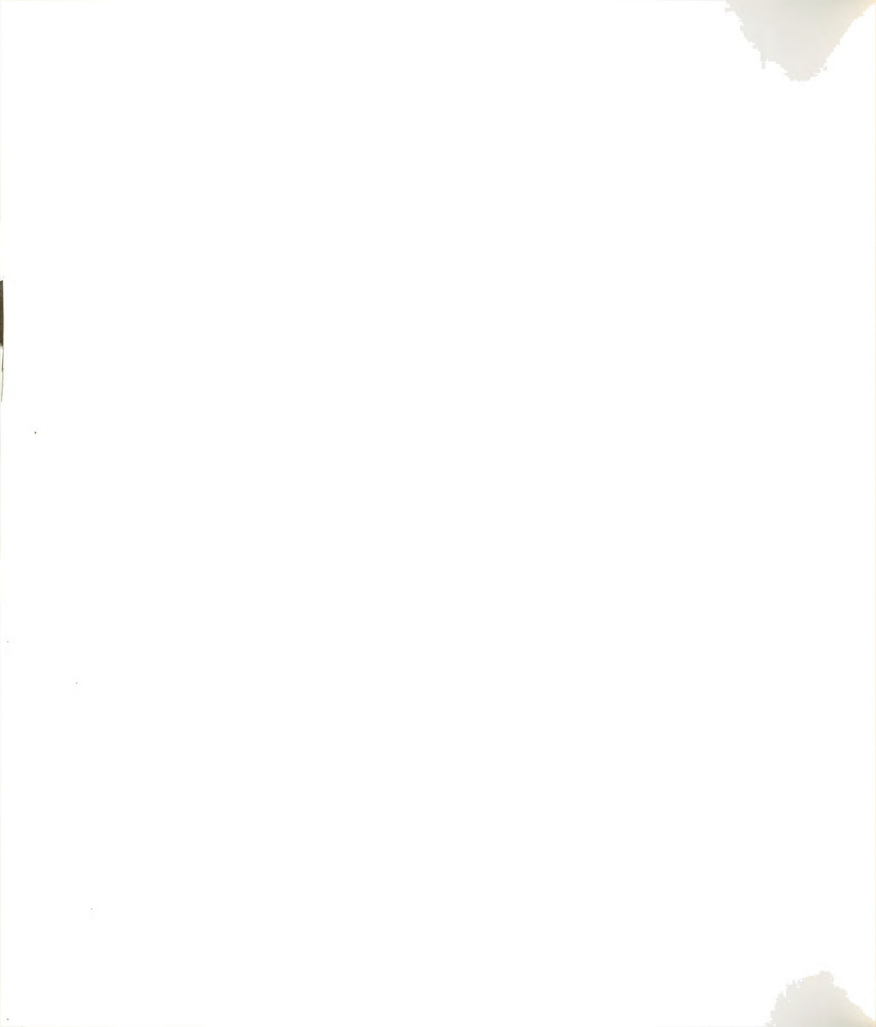


Figure 7.15. Creep Response of a Cylindrical Specimen of 19.1 mm Length Subjected to a Constant Compressive Force of 80 N



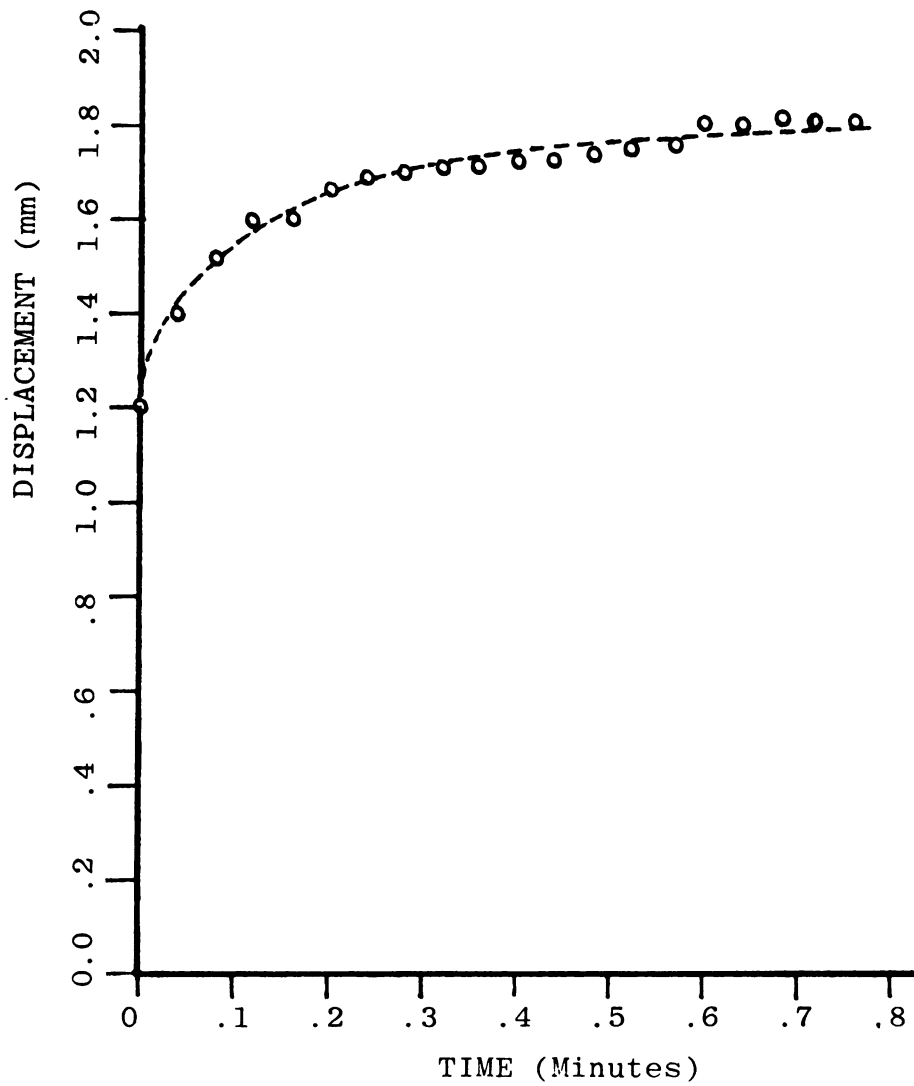


Figure 7.16. Calculated Creep Response of a Sphere With a 17.8 mm Radius Under Flat Plate Compressive Load of 50 N



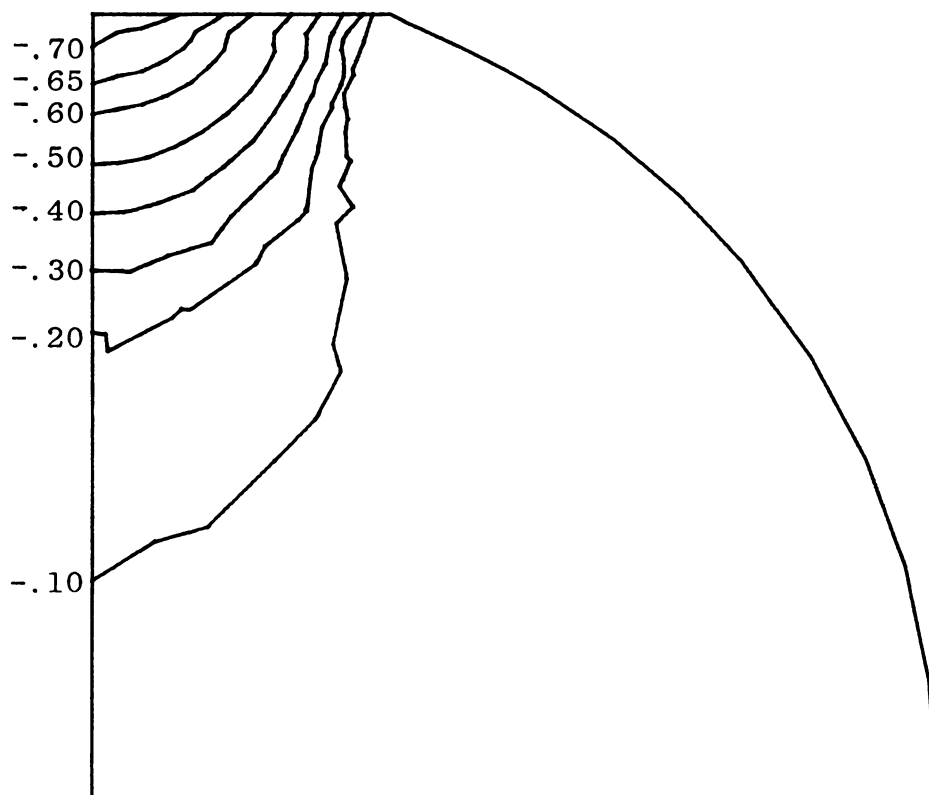


Figure 7.17. Lines of Constant Stress in the z-Direction at Time  $t=0$





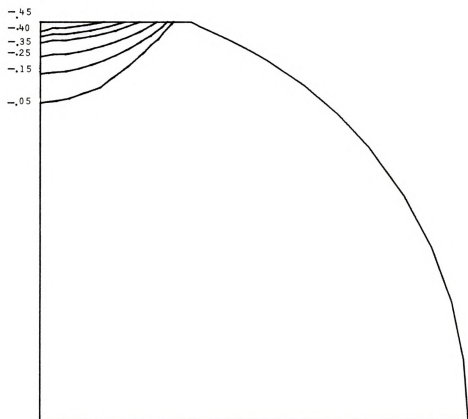


Figure 7.18. Lines of Constant Maximum Principal Stress at Time  $t=0$

1

2

3

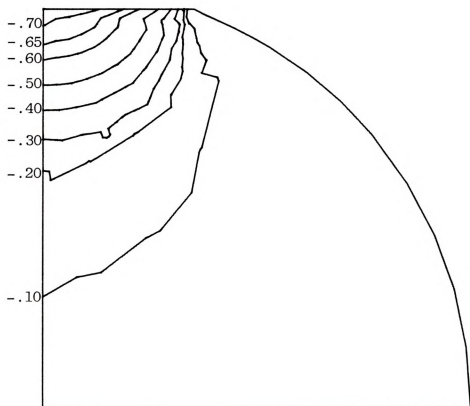


Figure 7.19. Lines of Constant Minimum Principal Stress at Time  $t=0$

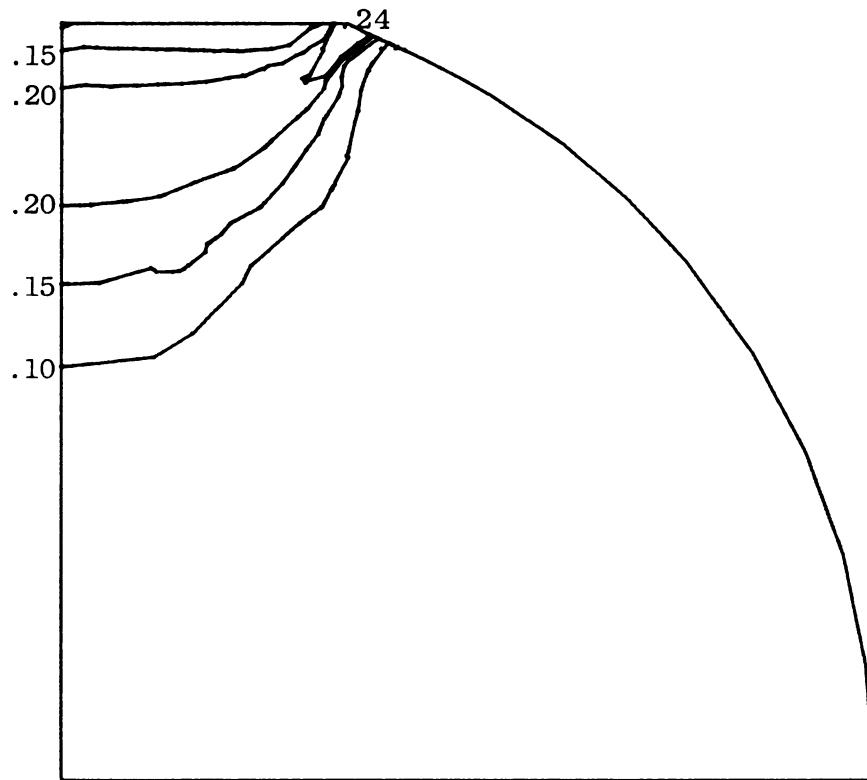


Figure 7.20. Lines of Constant Maximum Shear Stress  
at Time  $t=0$



In Figures 7.21 through 7.24 those lines were repeated at time  $t = 0.76$  minutes. The stresses in the  $z$ -direction and the principal stresses appeared largest near the initial point of contact and decreased with increasing distance from the contact point. The shear stress, however, had a maximum near the contact point farthest from the axis of symmetry. The maximum value of the shear stress at that point was .476 MPa at  $t = 0$  and decreased to .2 MPa at  $t = .76$  minute. The decrease with time of the maximum compressive stress and maximum shear stress is illustrated in Figure 7.25.

Closer observation of the principal stress values also showed that there existed a tensile stress at the circular boundary of the surface of contact with a maximum value of 1.02 MPa at time  $t = 0$  and decreasing to 0.57 MPa at  $t = .76$  min. The tensile stress acted in the axial direction. Some of the stresses in spherical bodies in elastic contact were discussed by Timoshenko and Goodier (1971). They indicated the existence of a radial tensile stress at the circular boundary of the surface of contact, but the magnitude of this tensile stress was smaller in comparison with the compressive stresses at the center of contact. The location of the maximum shear stress and the maximum tensile stress is indicated in Figure 7.26, which also shows the deformed grid at time  $t = 0.76$  min.

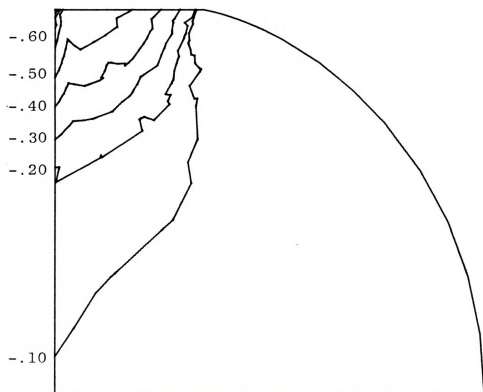


Figure 7.21. Lines of Constant Stress in the  
z-Direction at Time  $t = 0.76$  min





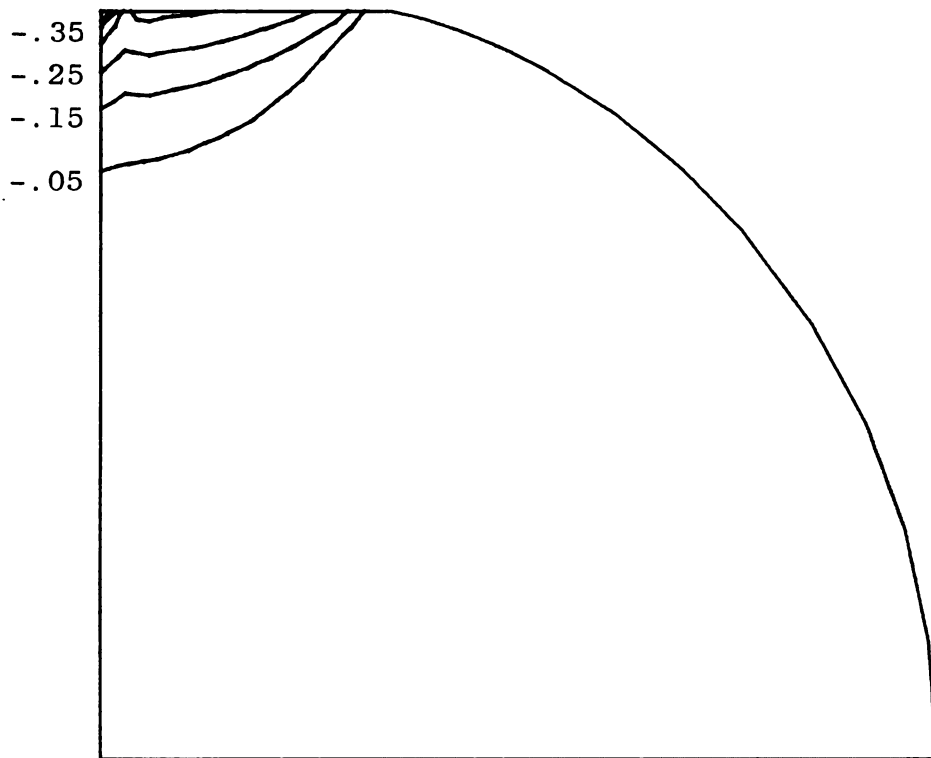


Figure 7.22. Lines of Constant Maximum Principal Stress at Time  $t = 0.76$  min



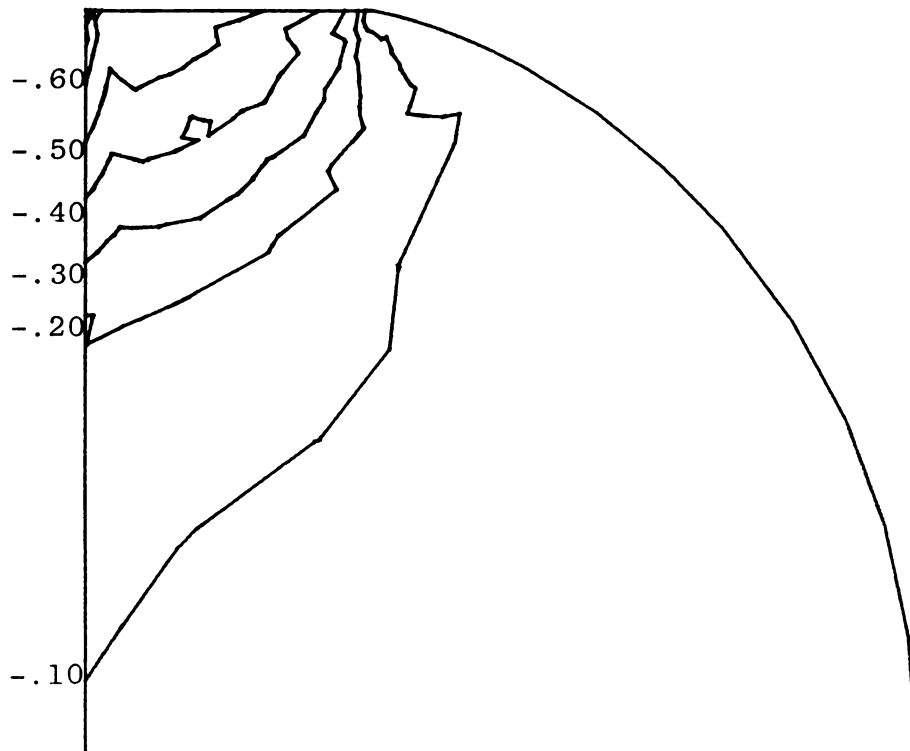


Figure 7.23. Lines of Constant Minimum Principal Stress at Time  $t = 0.76$  min

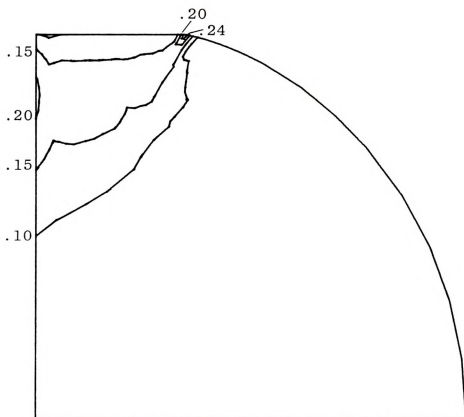


Figure 7.24. Lines of Constant Maximum Shear Stress  
at Time  $t = 0.76$  min

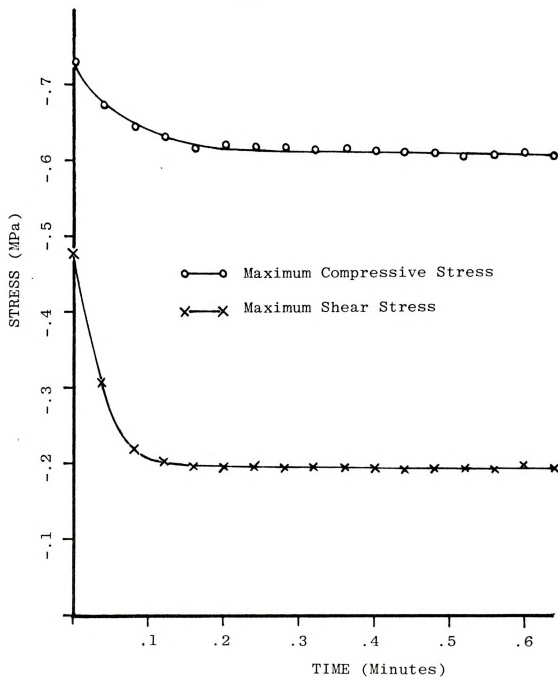


Figure 7.25. Maximum Compressive and Shear Stress in a Spherical Sample Under a 50 N Creep Load (Sample Diameter = 17.8 mm)



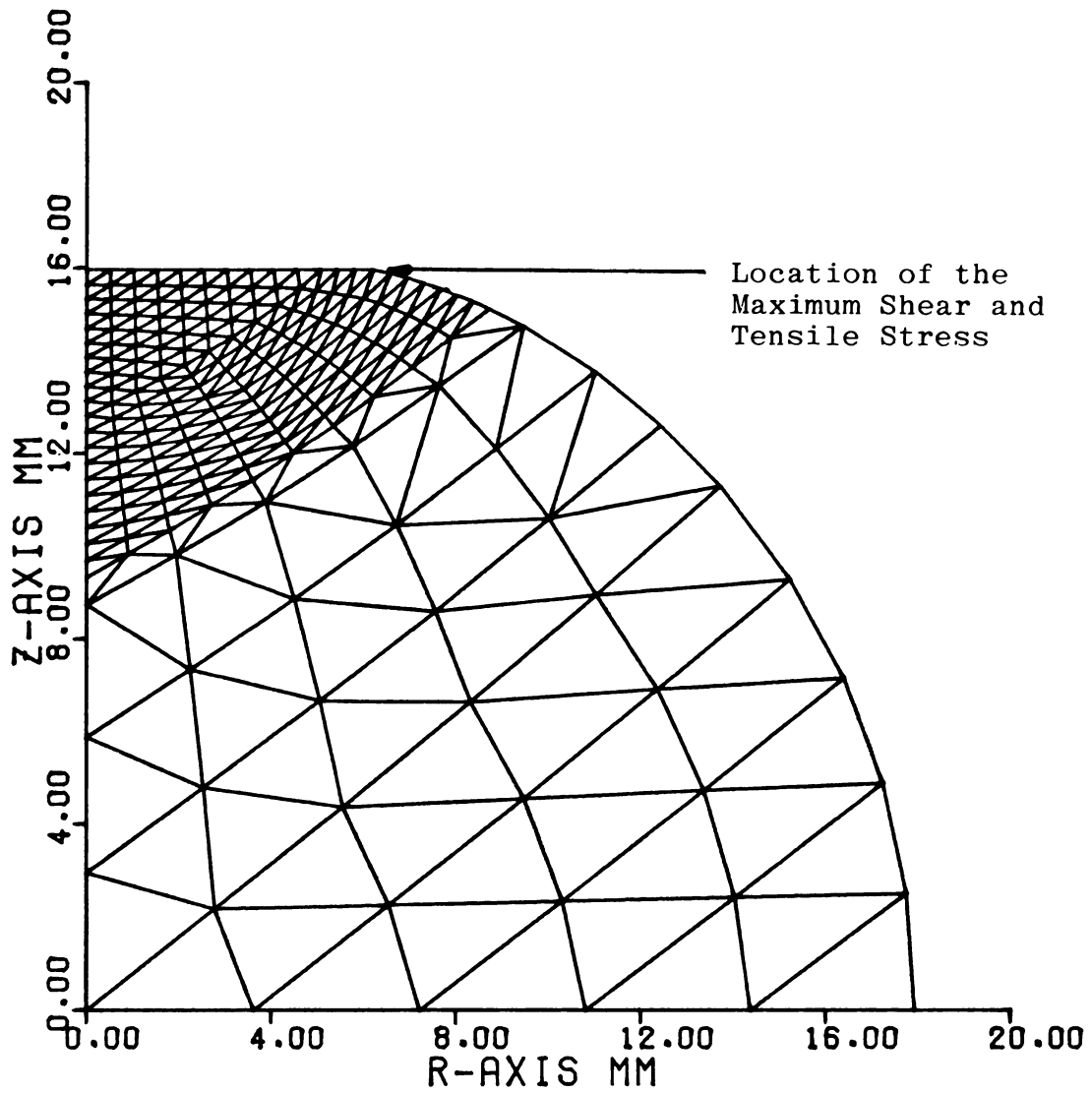


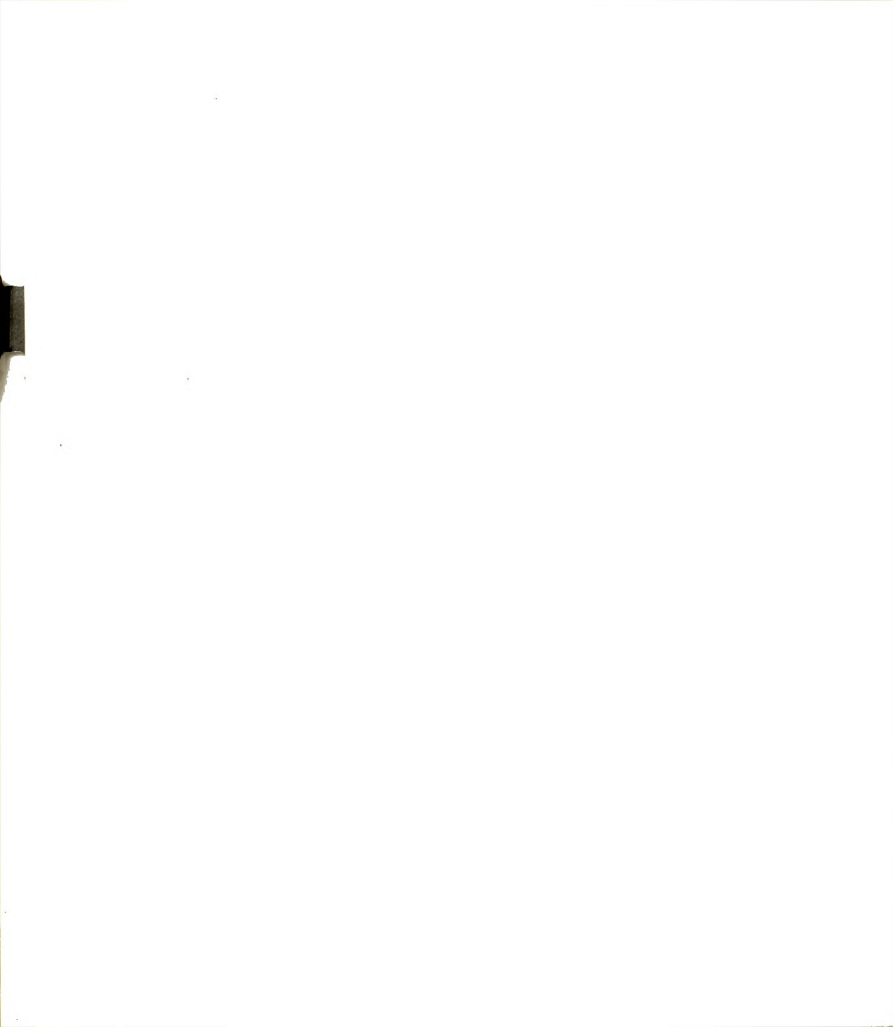
Figure 7.26. Deformed Finite Element Grid of the Spherical Specimen at Time  $t = 0.76$  min





## 7.6 Closure

Experimental loadings of spherical samples up to failure were performed. Inspection of the resulting bruises showed bruise shapes which passed through the point of maximum tensile and shear stress as presented in Figure 7.20. Similar bruise shapes were reported by Horsfield *et al.* (1972). The application of the numerical methods presented in determining the occurrence of a bruise depends on the availability of a criterion to describe the condition of material failure. It follows from the previous section that if a maximum stress is a failure criterion, then bruising would occur at the instant of loading of the apple with the creep load. A discussion on failure criteria is presented in section 9.4.



## 8. SUMMARY AND CONCLUSIONS

A new experimental procedure for the determination of bulk and shear relaxation functions and Poisson's ratio of apple flesh was developed. This procedure utilizes the relaxation properties of free and constrained cylindrical specimens and numerical techniques related to the inverse Laplace transform to obtain numerical values for these viscoelastic properties. The experimentally determined constitutive relations were used in a viscoelastic finite element analysis to calculate the stresses in apples under loads. An iterative method was presented for finding the deformation of a spherical specimen under a constant force.

The following conclusions can be drawn from this study:

- 1) The bulk and shear relaxation functions and Poisson's ratio of apple flesh are time dependent properties.
- 2) There is a large variation in the magnitude of the relaxation functions between apples.
- 3) Apples subjected to constant creep loads



experience maximum stresses at the initial application of the force.

- 4) Maximum shear and tensile stresses exist at the circular boundary of the contact surface during a flat plate loading.



## 9. FURTHER DEVELOPMENTS AND SUGGESTIONS FOR FUTURE RESEARCH

The research reported in this dissertation was part of an ongoing regional research project related to the harvesting and handling of fruits and vegetables (NE-93). Michigan's contribution to this project is the development of failure criteria for apple and potato flesh. This dissertation was the first step in this study and focused on the definition of the material properties of apples and the determination of the stress components within the apple when it is subjected to static loads. Some of the important areas related to apple bruising which must still be investigated are discussed in the following sections.

### 9.1 Change of Material Properties During Ripening

A method has been presented within this dissertation for the determination of viscoelastic constitutive equations of apple parenchyma. These constitutive relations were used in a numerical technique for the solution of viscoelastic boundary value problem and the analysis of stress in fruit under loading. The underlying assumption in these calculations was that the





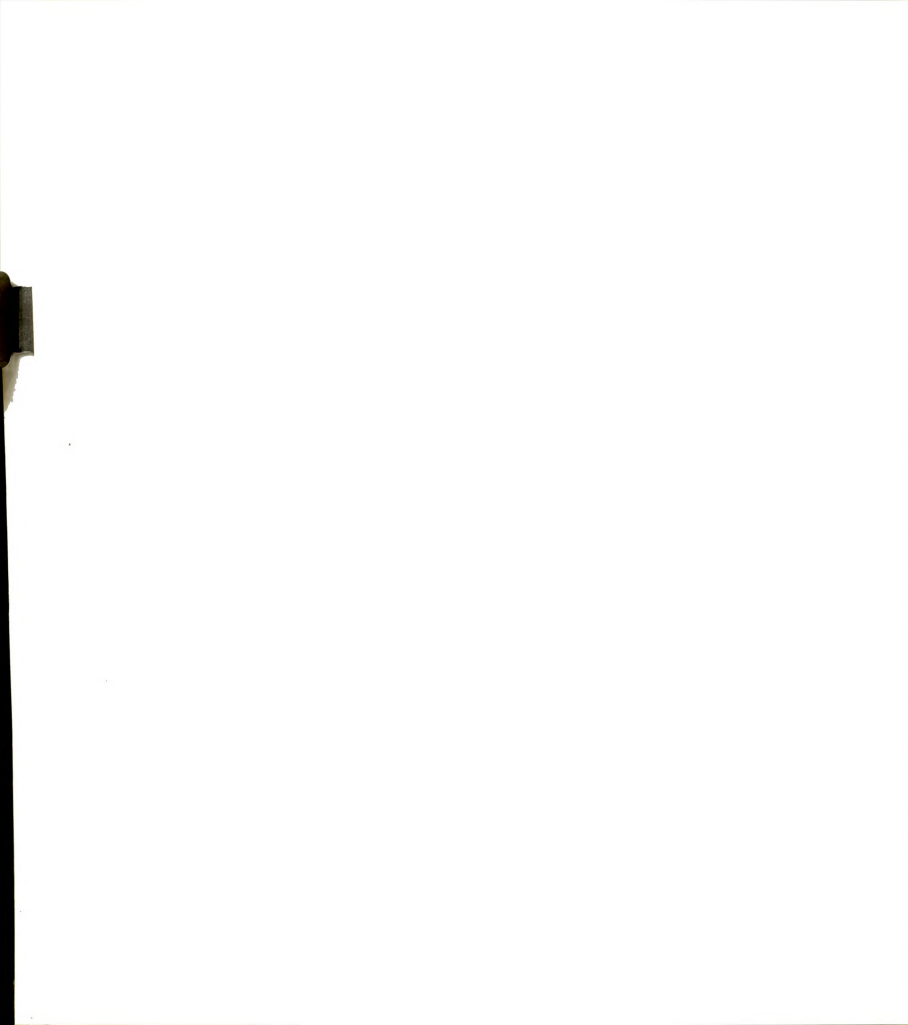
material structure is not altered during the time period of the experiment. It seems logical that for the study of long time fruit behavior this assumption has to be modified.

Water loss during storage and the chemical changes due to ripening can have a great effect on the material properties. These factors are very difficult to incorporate into the described analytical technique merely because ripening itself is a phenomenon that is difficult to quantify. The hypothesis is made here that a ripeness index ( $\Psi$ ) can be established. This ripeness index could be based on either starch content, sugar content, pectin content (itself a component of the structural strength of the fruit), or simply on the time in storage under steady state conditions.

The relaxation functions in Section 5 have to be determined for different values of the ripeness index  $\Psi$ .  $G_{\alpha}(t)$  denotes the value of the relaxation function at the reference value of the ripeness index  $\Psi$ . If the ripeness index changes then the relaxation function for that ripeness index can be designated as  $g_{\alpha}(t, \Psi)$ . Thus,

$$g_{\alpha}(t, \Psi_0) = G_{\alpha}(t) \quad \alpha = 1, 2 \quad (9.1)$$

The equation (9.1) is similar to the one used by Christensen (1971) to express temperature dependence



of mechanical properties. Considerable simplification can be achieved if a unique shift function  $\chi(\Psi)$  can be found for which

$$g_{\alpha}(t, \Psi) = G_{\alpha}(\xi) \quad (9.2)$$

and

$$\xi = t \chi(\Psi) \quad (9.3)$$

This shift function allows the superposition of time and ripeness in the same way time and temperature can be superimposed for thermorheological simple materials (Ferry, 1970; Hammerle and Mohsenin, 1970). The use of the reduced variable  $\xi$  means that the behavior of material in long-term storage can be analyzed with the same ease with which the mechanical behavior was studied in the previous section.

## 9.2 The Effect of the Skin

The presence of the skin was neglected in the models used in this study. Rumsey and Fridley (1974) found that the presence of an elastic skin produced no significant change of the internal stress distribution of the parenchyma. Gustafson (1974), however, showed that the restraint created by the skin can cause increased stresses in the body if the turgor pressure is accounted for. The effect of the skin properties on the stresses



in the apple parenchyma demands more investigation.

### 9.3 Dynamic Mechanical Properties

It was mentioned in section 7.4 that the values of the relaxation functions for small values of time are important for the study of material behavior under rapidly changing conditions. A theoretical analysis for the determination of dynamic material properties was presented in section 3.3. An improved experimental technique should be developed for the measurement of the complex moduli.

### 9.4 Development of a Failure Criterion

Combination of the stress analysis techniques with a criterion for material failure is required to determine under which state of external loading apples start to bruise. Work of Miles and Rehkugler (1971) towards the development of a failure criterion has been mentioned in section 2.3. Theirs and some other work on yield criteria of polymers is analyzed here and some suggestions for further development are proposed.

Figure 9.1 is a plot of the principal stresses  $\sigma_1$  and  $\sigma_2$  at failure from data given by Miles and Rehkugler (1971). This failure locus has more characteristics of the yield locus of maximum distortional energy theory than of the locus associated with the maximum shear stress



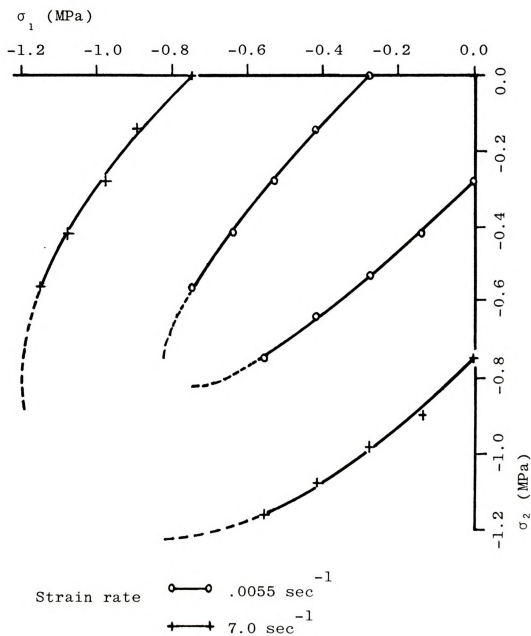


Figure 9.1. Failure Locus of Parenchyma of Northern Spy Apples at Two Strain Rates (Calculated From Data by Miles and Rehkgler, 1971)



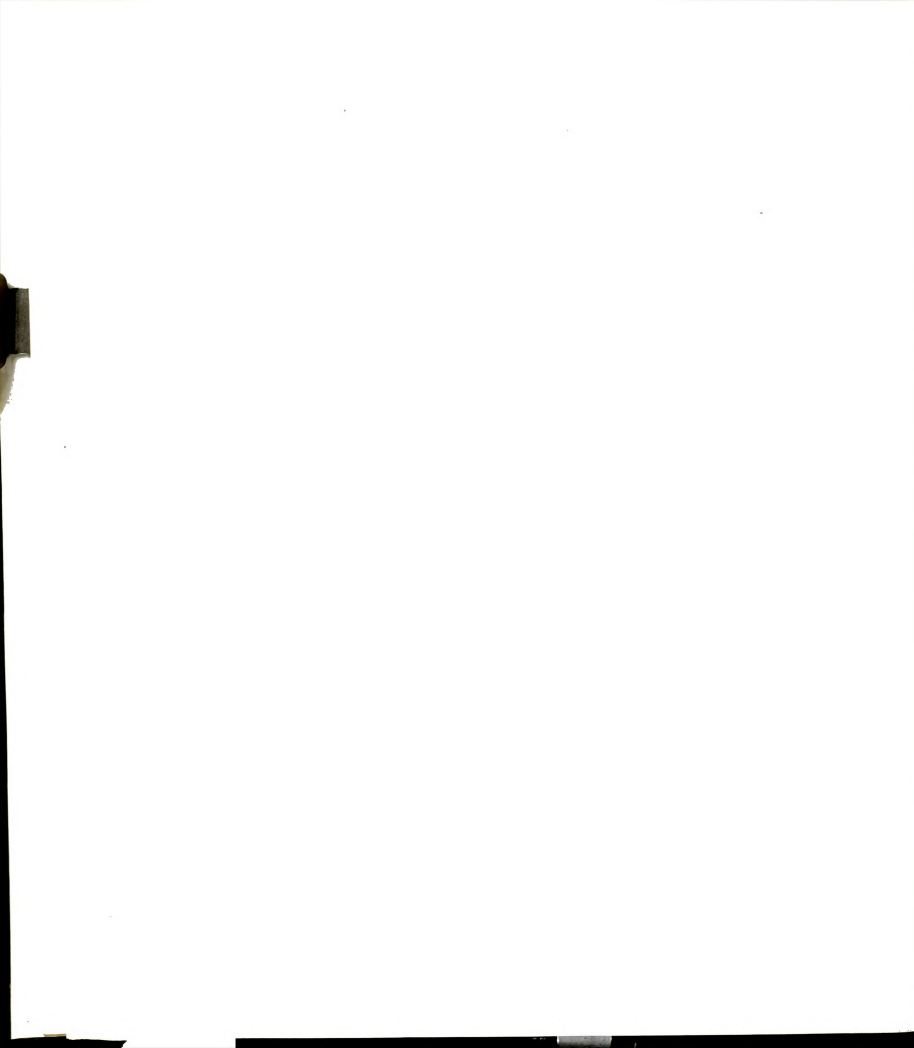


theory (Mendelson, 1968). Moreover, data on compressive failure strength at higher hydrostatic pressures are needed to complete the compressive part of the failure locus graph.

Yield criteria for polymer materials have been investigated. Mears *et al.* (1969) showed that tensile yield stress of polyethylene and polypropylene increases significantly with increasing hydrostatic pressures. The applied hydrostatic stresses were about ten times higher than the mean normal stress at the yield point. Raghava *et al.* (1973) used thin-walled polymer tubes under different internal pressures and axial tension or compression to study the yield behavior of polycarbonate and polyvinylchloride. They proposed the yield criterion

$$(\sigma_1 - \sigma_2)^2 + (\sigma_2 - \sigma_3)^2 + (\sigma_3 - \sigma_1)^2 + 2(C-T)(\sigma_1 + \sigma_2 + \sigma_3) = 2CT \quad (9.4)$$

where  $\sigma_1$ ,  $\sigma_2$  and  $\sigma_3$  are the principal stresses of the applied stress state while C and T are the absolute values of the compressive and tensile yield strengths respectively. The influence of the hydrostatic pressure is indicated by the term  $(\sigma_1 + \sigma_2 + \sigma_3)$ . When  $C = T$ , the criterion reduces to the maximum distortion energy theory (von Mises criterion). Tensile strength of apple flesh should be investigated in view of the tensile



stresses mentioned in section 7.5. They are required to determine whether equation (9.1) or any variation thereof is applicable in this case.

The changing of material properties during ripening can have an effect on: (i) the failure criterion to be used at different ripeness stages and (ii) the level of distortional energy or shear stress at failure, whichever may be the criterion. It was mentioned in section 4.2 that some cylindrical specimens were loaded to failure. The average axial compressive stress in cylindrical samples at failure was found to be  $-0.49$  MPa at the beginning of the storage period and  $-0.34$  MPa after four months of storage. It is conceivable that bruise development later than the time of application of the creep load may result from these changes.



## BIBLIOGRAPHY



# BIBLIOGRAPHY

- Akyurt, M.  
1969. Constitutive Relations for Plant Materials.  
Ph.D. thesis, Purdue University.
- Apacilla, R.  
1973. Stress Analysis in Agricultural Products Using  
the Finite Element Method. Unpublished  
Technical Problem Research Report, Department  
of Agricultural Engineering, Michigan State  
University.
- Arridge, R. G. L.  
1974. A New Method for Measurement of Bulk Modulus  
of Solid Polymers. Journal of Physics E:  
Scientific Instruments, 7(5):399-401.
- Bashford, L. L. and R. W. Whitney  
1973. A Computer Program for Determining Creep and  
Relaxation Models. American Society of  
Agricultural Engineers, Paper No. 73-302.
- Beck, J. V. and K. J. Arnold  
1974. Parameter Estimation in Engineering and Science.  
Bound Notes, Division of Engineering Research,  
Michigan State University.
- Bellman, R. E., R. E. Kalaba and J. Lockett  
1966. Numerical Inversion of the Laplace Transform.  
American Elsevier, New York.
- Brusewitz, G. H.  
1969. Consideration of Plant Material as an Inter-  
acting Continuum. Ph.D. thesis, Michigan  
State University.
- Carpenter, W. C.  
1972. Viscoelastic Stress Analysis. International  
Journal for Numerical Methods in Engineering,  
4:357-366.
- Chappell, T. W. and D. D. Hamann  
1968. Poisson's Ratio and Young's Modulus for Apple  
Flesh Under Compressive Loading. Trans. of the  
ASAE, 11(5):608-610.





- Chen, P. and R. B. Fridley  
 1972. Analytical Method for Determining Viscoelastic Constants of Agricultural Products. Trans. of the ASAE, 15(6):1103-1106.
- Christensen, R. M.  
 1971. Theory of Viscoelasticity. An Introduction. Academic Press, New York and London.
- Clevenger, J. T. and D. D. Hamann  
 1968. The Behavior of Apple Skin Under Tensile Loading. Trans. of the ASAE, 11(1):34-37.
- Cost, T. L.  
 1964. Approximate Laplace Transform Inversions in Viscoelastic Stress Analysis. AIAA Journal, 2:2157-2166.
- Cost, T. L. and E. B. Becker  
 1970. A Multidata Method of Approximate Laplace Transform Inversion. International Journal for Numerical Methods in Engineering, 2:207-219.
- Davis, D. C. and G. E. Rehkugler  
 1971. A Theoretical and Experimental Analysis of the Apple-Limb Impact Problem. Trans. of the ASAE, 14(2):234-239.
- Ferry, J. D.  
 1970. Viscoelastic Properties of Polymers. Second Edition. John Wiley and Sons, New York.
- Finney, E. E.  
 1963. The Viscoelastic Behavior of the Potato, *Solanum Tuberosum*, Under Quasi-Static Loading. Ph.D. thesis, Michigan State University.
- Fletcher, S. W., N. N. Mohsenin, J. R. Hammerle and L. D. Tukey  
 1965. Mechanical Behavior of Selected Fruits and Vegetables Under Fast Rates of Loading. Trans. of the ASAE, 8(3):324-326, 331.
- Flügge, W.  
 1967. Viscoelasticity. Blaisdell Publishing Company, Waltham (Mass.), Toronto, London.
- Fluck, R. C. and E. M. Ahmed  
 1972. Impact Testing of Fruits and Vegetables. American Society of Agricultural Engineers, Paper No. 72-306.



- Fridley, R. B., H. Goehlich, L. L. Claypool and P. A. Adrian  
1964. Factors Affecting Impact Injury to Mechanically Harvested Fruit. Trans. of the ASAE, 7(4):401-409.
- Fridley, R. B. and P. A. Adrian  
1966. Mechanical Properties of Peaches, Pears, Apricots, and Apples. Trans. of the ASAE, 9(1):135-142.
- Fridley, R. B., R. A. Bradley, L. W. Rumsey and P. A. Adrian  
1968. Some Aspects of Elastic Behavior of Selected Fruits. Trans. of the ASAE, 11(1):46-49.
- Gottenberg, W. G. and R. M. Christensen  
1966. An Experiment for Determination of the Mechanical Property in Shear for a Linear, Isotropic Viscoelastic Solid. International Journal of Engineering Science, 2:45-57.
- Gradowczyk, M. H. and F. Moavenzadeh  
1969. Characterization of Linear Viscoelastic Materials. Trans. of the Society of Rheology, 13(2):173-191.
- Gupta, K. K. and E. Heer  
1974. Viscoelastic Structures, In Structural Mechanics Computer Programs. Edited by W. Pilkey, K. Saczalski and H. Schaeffer, University Press of Virginia, Charlottesville, Virginia.
- Gustafson, R. J.  
1974. Continuum Theory for Gas-Solid-Liquid Media. Unpublished Ph.D. thesis, Michigan State University.
- Hamann, D. D.  
1967. Some Dynamic Mechanical Properties of Apple Fruits and Their Use in the Solution of an Impacting Contact Problem of a Spherical Fruit. Unpublished Ph.D. thesis, Virginia Polytechnic Institute, Blacksburg, Virginia.
- Hamann, D. D.  
1970. Analysis of Stress During Impact of Fruit Considered to be Viscoelastic. Trans. of the ASAE, 13(6):893-899.
- Hammerle, J. R. and N. N. Mohsenin  
1966. Some Dynamic Aspects of Fruit Impacting Hard and Soft Materials. Trans. of the ASAE, 9(4):484-488.



- Hammerle, J. R. and N. N. Mohsenin.  
1970. Tensile Relaxation Modulus of Corn Horny Endosperm as a Function of Time, Temperature and Moisture Content. Trans. of the ASAE, 13(3):372-375.
- Hammerle, J. R. and W. F. McClure  
1971. The Determination of Poisson's Ratio by Compression Tests of Cylindrical Specimens. Journal of Texture Studies, 2:31-49.
- Hammerle, J. R., M. V. N. Rao and D. D. Hamann  
1971. Comparison of Static Creep and Relaxation Rate Sensitive and Frequency Sensitive Loading for Axial Compression. American Society of Agricultural Engineers, Paper No. 71-801.
- Hayes, M. A. and L. W. Morland  
1969. The Response Functions of an Anisotropic Linear Viscoelastic Material. Trans. of the Society of Rheology, 13:231-240.
- Heer, E. and J. C. Chen  
1969. Finite Element Formulation for Linear Thermo-viscoelastic Materials. Technical Report, 32-1381, Jet Propulsion Laboratory, California.
- Herrmann, L. R. and F. E. Peterson  
1968. A Numerical Procedure for Viscoelastic Stress Analysis. Aerojet General Report, Sacramento, California.
- Horsfield, B. L., R. B. Fridley and L. L. Claypool  
1972. Application of Theory of Elasticity to the Design of Fruit Harvesting and Handling Equipment for Minimum Bruising. Trans. of the ASAE, 15:746-750.
- Huff, E. R.  
1967. Tensile Properties of Kennebec Potatoes. Trans. of the ASAE, 10(3):414-419.
- Hughes, H. and L. J. Segerlind  
1972. A Rapid Mechanical Method for Determining Poisson's Ratio in Biological Materials. ASAE Paper 17-310.
- Kmenta, J.  
1971. Elements of Econometrics. The Macmillan Co., New York, New York.



- Knoff, W. F. and I. L. Hopkins  
 1972. An Improved Numerical Interconversion for Creep Compliance and Relaxation Modulus. Technical Report No. 134, Research Sponsored by the Office of Naval Research, Task No. NR 056-377.
- Laird, G. W. and H. B. Kingsbury  
 1973. A Method for Determining Complex Moduli of Viscoelastic Materials. *Experimental Mechanics*, 13(3):126-131.
- Lanczos, C.  
 1956. *Applied Analysis*. Prentice Hall, Englewood Cliffs, New Jersey.
- Malone, D. W. and J. J. Connor  
 1971. Finite Elements and Dynamic Viscoelasticity. *Journal of the Engineering Mechanics Division, Proceedings of the ASCE*, 97(EM4):1145-1158.
- Mears, D. R., K. D. Pae and J. A. Sauer  
 1969. Effects of Hydrostatic Pressure on the Mechanical Behavior of Polyethylene and Polypropylene. *Journal of Applied Physics*, 40(11):4229-4237.
- Mendelson, A.  
 1968. *Plasticity: Theory and Application*. The Macmillan Co., New York, New York.
- Miles, J. A. and G. E. Rehkugler  
 1971. The Development of a Failure Criterion for Apple Flesh. *American Society of Agricultural Engineers, Paper No. 71-330*.
- Miller, Max K. and W. T. Guy, Jr.  
 1966. Numerical Inversion of the Laplace Transform by Use of Jacobi Polynomials. *SIAM Journal of Numerical Analysis*, 3(4):624-635.
- Mohsenin, N. N. and H. Göhlich  
 1962. Techniques for Determination of Mechanical Properties of Fruits and Vegetables Related to Design and Development of Harvesting and Processing Machinery. *Journal of Agricultural Engineering Research*, 7(4):300-315.
- Mohsenin, N. N., H. E. Cooper and L. D. Tukey  
 1963. Engineering Approach to Evaluating Textural Factors in Fruits and Vegetables. *Trans. of the ASAE*, 6(2):85-88.





- Mohsenin, N. N.  
 1970. Physical Properties of Plant and Animal Materials, Volume I, Structure, Physical Characteristics and Mechanical Properties. Gordon and Breach Science Publishers, New York.
- Mohsenin, N. N.  
 1971. Mechanical Properties of Fruits and Vegetables. Review of a Decade of Research, Applications and Future Needs. American Society of Agricultural Engineers, Paper No. 71-849.
- Morrow, C. T.  
 1965. Viscoelasticity in a Selected Agricultural Product. M.S. thesis in Agricultural Engineering, Pennsylvania State University, University Park, Pennsylvania.
- Morrow, C. T. and N. N. Mohsenin  
 1966. Consideration of Selected Agricultural Products as Viscoelastic Materials. Journal of Food Science, 31(5):686-698.
- Morrow, C. T. and N. N. Mohsenin  
 1968. Dynamic Viscoelastic Characterization of Solid Food Materials. Journal of Food Science, 33(6):646-651.
- Morrow, C. T., D. D. Hamann, N. N. Mohsenin and E. E. Finney, Jr.  
 1971. Mechanical Characterization of Red Delicious Apples. American Society of Agricultural Engineers, Paper No. 71-372.
- Nelson, C. W. and N. N. Mohsenin  
 1968. Maximum Allowable Static and Dynamic Loads and Effect of Temperature for Mechanical Injury in Apples. Journal of Agricultural Engineering Research, 13(4):305-317.
- Oden, J. T. and H. J. Brauchli  
 1971. On the Calculation of Consistent Stress Distributions in Finite Element Approximations. International Journal for Numerical Methods in Engineering, 3:317-325.
- Papoulis, A.  
 1957. A New Method of Inversion of the Laplace Transform. Quarterly of Applied Mathematics, 14(4):405-414.



- Parsons, J. S., W. Yates and F. Schloss  
 1969. The Measurement of Dynamic Properties of Materials Using a Transfer Impedance Technique. Naval Ship Research and Development Center, Washington. Report No. 2981.
- Peterson, C. L. and C. W. Hall  
 1973. Consideration of the Russet Burbank Potato as a Thermorheological Simple Material. ASAE Paper No. 73-303.
- Raghava, R., R. M. Caddell and G. S. Y. Yeh  
 1973. The Macroscopic Yield Behavior of Polymers. Journal of Materials Science, 8:225-232.
- Rigbi, Z.  
 1967. The Value of Poisson's Ratio of Viscoelastic Materials in High Speed Testing. Volume VI: Rheology of Solids, Wiley-Interscience, New York.
- Rumsey, T. R. and R. B. Fridley  
 1974. Analysis of Viscoelastic Contact Stresses in Agricultural Products Using a Finite Element Method. ASAE Paper No. 74-3513.
- Sharma, M. G. and N. N. Mohsenin  
 1970. Mechanics of Deformation of a Fruit Subjected to Hydrostatic Pressure. Journal of Agricultural Engineering Research, 15(1):65-74.
- Sokolnikoff, I. S.  
 1956. Mathematical Theory of Elasticity. McGraw-Hill Book Company, New York.
- Szegö, C.  
 1959. Orthogonal Polynomials. American Mathematical Society Colloquium Publications, Volume XIII, Revised Edition, American Mathematical Society, New York.
- Taylor, R. L., K. S. Pister and G. L. Goudreau  
 1968. Thermomechanical Analysis of Viscoelastic Solids. Report Number 68-7, Structural Engineering Laboratory, University of California, Berkeley.
- Theocaris, P. S.  
 1964. Creep and Relaxation Contraction Ratio of Linear Viscoelastic Materials. Journal of Mechanics and Physics of Solids, 12:125-138.



- Timbers, G. E., L. M. Staley and E. L. Watson  
1966. Some Mechanical and Rheological Properties of the Netted Gem Potato. Canadian Journal of Agricultural Engineering, February.
- Timoshenko, S. P. and J. N. Goodier  
1970. Theory of Elasticity. Third Edition. McGraw-Hill Book Company, New York.
- White, R. K. and N. N. Mohsenin  
1967. Apparatus for Determination of Bulk Modulus and Compressibility of Materials. Trans. of the ASAE, 10(5):670-671.
- Wright, F. S. and W. E. Splinter  
1968. Mechanical Behavior of Sweet Potatoes Under Slow Loading and Impact Loading. Trans. of the ASAE, 11(6):765-770.
- Wylie, L. R. Jr.  
1966. Advanced Engineering Mathematics. Third Edition. McGraw-Hill Book Company, New York.
- Zienkiewicz, O. C.  
1971. The Finite Element Method in Engineering Science. McGraw-Hill Book Company, New York.



APPENDIX A

EXPERIMENTAL RELAXATION FUNCTIONS FOR APPLE FLESH

(24 apples, Red Delicious)





## APPENDIX A

## EXPERIMENTAL RELAXATION FUNCTIONS FOR APPLE FLESH

## UNIAXIAL RELAXATION FUNCTION 001

.7760 EXP( -3.33358 \*T)

2.8532 EXP( -.03357 \*T)

## CONSTRAINED RELAXATION FUNCTION 002

1.2415 EXP( -3.82835 \*T)

3.6281 EXP( -.02657 \*T)

TIME (MIN.)	SHEAR MOD (MEGAPASC.)	BULK MOD (MEGAPASC.)	POIS. RATIO
.0	.13980E+01	.33054E+01	.29861E+00
.31000E-01	.13704E+01	.29005E+01	.29595E+00
.62000E-01	.13452E+01	.28078E+01	.29359E+00
.12500E+00	.13007E+01	.26512E+01	.28964E+00
.25000E+00	.12337E+01	.24360E+01	.28440E+00
.50000E+00	.11542E+01	.22245E+01	.28000E+00
.10000E+01	.10889E+01	.21080E+01	.27980E+00
.20000E+01	.10397E+01	.20546E+01	.28311E+00
.40000E+01	.96940E+00	.19752E+01	.28817E+00
.80000E+01	.94978E+00	.19527E+01	.28926E+00

## UNIAXIAL RELAXATION FUNCTION 003

.9438 EXP( -3.47148 \*T)

3.4920 EXP( -.02973 \*T)

## CONSTRAINED RELAXATION FUNCTION 005

1.7949 EXP( -5.85637 \*T)

4.0180 EXP( -.03313 \*T)

TIME (MIN.)	SHEAR MOD (MEGAPASC.)	BULK MOD (MEGAPASC.)	POIS. RATIO
.0	.17190E+01	.35205E+01	.28999E+00
.31000E-01	.16965E+01	.32487E+01	.27801E+00
.62000E-01	.16754E+01	.30243E+01	.26761E+00
.12500E+00	.16365E+01	.26826E+01	.25063E+00
.25000E+00	.15735E+01	.23021E+01	.22937E+00
.50000E+00	.14881E+01	.20640E+01	.21450E+00
.10000E+01	.14055E+01	.20180E+01	.21679E+00
.20000E+01	.13478E+01	.19632E+01	.22078E+00
.40000E+01	.12754E+01	.18255E+01	.21688E+00
.80000E+01	.12536E+01	.17885E+01	.21562E+00



## UNIAXIAL RELAXATION FUNCTION 006

.8126 EXP( -3.50315 \*T)  
2.8765 EXP( -.03152 \*T)

## CONSTRAINED RELAXATION FUNCTION 007

1.2592 EXP( -3.28398 \*T)  
3.7083 EXP( -.02986 \*T)

TIME (MIN.)	SHEAR MOD (MEGAPASC.)	BULK MOD (MEGAPASC.)	POIS. RATIO
.0	.14187E+01	.30757E+01	.30015E+00
.31000E-01	.13862E+01	.29939E+01	.29947E+00
.62000E-01	.13570E+01	.29194E+01	.29881E+00
.12500E+00	.13063E+01	.27880E+01	.29750E+00
.25000E+00	.12328E+01	.25911E+01	.29505E+00
.50000E+00	.11517E+01	.23616E+01	.29112E+00
.10000E+01	.10929E+01	.21890E+01	.28693E+00
.20000E+01	.10512E+01	.20934E+01	.28532E+00
.40000E+01	.98797E+00	.19796E+01	.28647E+00
.80000E+01	.97053E+00	.19477E+01	.28722E+00

## UNIAXIAL RELAXATION FUNCTION 008

.6906 EXP( -2.87651 \*T)  
2.6616 EXP( -.03032 \*T)

## CONSTRAINED RELAXATION FUNCTION 009

1.2021 EXP( -4.32877 \*T)  
3.5872 EXP( -.02705 \*T)

TIME (MIN.)	SHEAR MOD (MEGAPASC.)	BULK MOD (MEGAPASC.)	POIS. RATIO
.0	.12699E+01	.30961E+01	.31950E+00
.31000E-01	.12510E+01	.29674E+01	.31525E+00
.62000E-01	.12331E+01	.28562E+01	.31157E+00
.12500E+00	.12003E+01	.26744E+01	.30560E+00
.25000E+00	.11476E+01	.24402E+01	.29835E+00
.50000E+00	.10770E+01	.22410E+01	.29410E+00
.10000E+01	.10100E+01	.21605E+01	.29733E+00
.20000E+01	.96204E+00	.21162E+01	.30210E+00
.40000E+01	.90332E+00	.20240E+01	.30432E+00
.80000E+01	.88533E+00	.20041E+01	.30458E+00



## UNIAXIAL RELAXATION FUNCTION 014

.9378 EXP( -2.74615 \*T)

2.9911 EXP( -.03062 \*T)

## CONSTRAINED RELAXATION FUNCTION 015

1.7878 EXP( -3.40880 \*T)

3.7663 EXP( -.03088 \*T)

TIME (MIN.)	SHEAR MOD (MEGAPASC.)	BULK MOD (MEGAPASC.)	POIS. RATIO
.0	.14924E+01	.35637E+01	.31626E+00
.31000E-01	.14668E+01	.34155E+01	.31224E+00
.62000E-01	.14431E+01	.32822E+01	.30855E+00
.12500E+00	.14002E+01	.30524E+01	.30202E+00
.25000E+00	.13323E+01	.27236E+01	.29220E+00
.50000E+00	.12444E+01	.23747E+01	.28098E+00
.10000E+01	.11635E+01	.21594E+01	.27398E+00
.20000E+01	.11058E+01	.20664E+01	.27321E+00
.40000E+01	.10422E+01	.19426E+01	.27320E+00
.80000E+01	.10254E+01	.19033E+01	.27291E+00

## UNIAXIAL RELAXATION FUNCTION 016

.7599 EXP( -3.45898 \*T)

2.7509 EXP( -.02276 \*T)

## CONSTRAINED RELAXATION FUNCTION 017

1.2334 EXP( -3.27637 \*T)

3.1436 EXP( -.01969 \*T)

TIME (MIN.)	SHEAR MOD (MEGAPASC.)	BULK MOD (MEGAPASC.)	POIS. RATIO
.0	.13836E+01	.25321E+01	.26896E+00
.31000E-01	.13547E+01	.24497E+01	.26658E+00
.62000E-01	.13290E+01	.23745E+01	.26430E+00
.12500E+00	.12845E+01	.22421E+01	.25997E+00
.25000E+00	.12204E+01	.20448E+01	.25254E+00
.50000E+00	.11509E+01	.18180E+01	.24165E+00
.10000E+01	.11036E+01	.16574E+01	.23056E+00
.20000E+01	.10733E+01	.15928E+01	.22583E+00
.40000E+01	.10266E+01	.15397E+01	.22825E+00
.80000E+01	.10163E+01	.15206E+01	.22909E+00



## UNIAXIAL RELAXATION FUNCTION 018

.7696 EXP( -3.08525 \*T)  
2.8499 EXP( -.02071 \*T)

## CONSTRAINED RELAXATION FUNCTION 019

1.3622 EXP( -3.50302 \*T)  
3.4560 EXP( -.01954 \*T)

TIME (MIN.)	SHEAR MOD (MEGAPASC.)	BULK MOD (MEGAPASC.)	POIS. RATIO
.J	.13963E+01	.29562E+01	.29597E+00
.31000E-01	.13726E+01	.28459E+01	.29232E+00
.62000E-01	.13507E+01	.27473E+01	.28902E+00
.12500E+00	.13119E+01	.25779E+01	.28319E+00
.25000E+00	.12529E+01	.23365E+01	.27445E+00
.50000E+00	.11819E+01	.20833E+01	.26443E+00
.10000E+01	.11246E+01	.19307E+01	.25786E+00
.20000E+01	.10885E+01	.18734E+01	.25688E+00
.40000E+01	.10432E+01	.18094E+01	.25824E+00
.80000E+01	.10296E+01	.17931E+01	.25901E+00

## UNIAXIAL RELAXATION FUNCTION 020

2.7105 EXP( -.01756 \*T)  
.7799 EXP( -4.66051 \*T)

## CONSTRAINED RELAXATION FUNCTION 021

2.4472 EXP( -6.23685 \*T)  
3.7800 EXP( -.02519 \*T)

TIME (MIN.)	SHEAR MOD (MEGAPASC.)	BULK MOD (MEGAPASC.)	POIS. RATIO
.J	.12726E+01	.45298E+01	.37159E+00
.31000E-01	.12405E+01	.41400E+01	.36410E+00
.62000E-01	.12127E+01	.38196E+01	.35753E+00
.12500E+00	.11668E+01	.33347E+01	.34657E+00
.25000E+00	.11060E+01	.27964E+01	.33184E+00
.50000E+00	.10497E+01	.24415E+01	.31799E+00
.10000E+01	.10193E+01	.23317E+01	.31093E+00
.20000E+01	.10011E+01	.22589E+01	.30790E+00
.40000E+01	.97290E+00	.21225E+01	.30328E+00
.80000E+01	.96723E+00	.20774E+01	.30193E+00

## UNIAXIAL RELAXATION FUNCTION 022

.6658 EXP( -3.03202 \*T)

2.4942 EXP( -.02260 \*T)

## CONSTRAINED RELAXATION FUNCTION 023

1.2927 EXP( -3.86304 \*T)

3.4987 EXP( -.02277 \*T)

TIME (MIN.)	SHEAR MOD (MEGAPASC.)	BULK MOD (MEGAPASC.)	POIS. RATIO
.0	.11828E+01	.32147E+01	.33612E+00
.31000E-01	.11622E+01	.30934E+01	.33311E+00
.62000E-01	.11435E+01	.29864E+01	.33041E+00
.12500E+00	.11101E+01	.28062E+01	.32584E+00
.25000E+00	.10584E+01	.25596E+01	.31963E+00
.50000E+00	.99469E+00	.23200E+01	.31402E+00
.10000E+01	.94135E+00	.21917E+01	.31254E+00
.20000E+01	.90850E+00	.21329E+01	.31352E+00
.40000E+01	.87181E+00	.20416E+01	.31334E+00
.80000E+01	.86536E+00	.20168E+01	.31281E+00

## UNIAXIAL RELAXATION FUNCTION 032

.5034 EXP( -3.39397 \*T)

2.2716 EXP( -.02841 \*T)

## CONSTRAINED RELAXATION FUNCTION 033

1.7824 EXP( -3.76473 \*T)

2.5951 EXP( -.05160 \*T)

TIME (MIN.)	SHEAR MOD (MEGAPASC.)	BULK MOD (MEGAPASC.)	POIS. RATIO
.0	.10306E+01	.30029E+01	.34592E+00
.31000E-01	.10164E+01	.28217E+01	.33938E+00
.62000E-01	.10036E+01	.26601E+01	.33314E+00
.12500E+00	.98148E+00	.23831E+01	.32148E+00
.25000E+00	.95020E+00	.19905E+01	.30185E+00
.50000E+00	.91791E+00	.15766E+01	.27294E+00
.10000E+01	.89947E+00	.13065E+01	.23921E+00
.20000E+01	.88931E+00	.11555E+01	.20824E+00
.40000E+01	.86523E+00	.96252E+00	.17430E+00
.80000E+01	.85618E+00	.91072E+00	.16513E+00



## UNIAXIAL RELAXATION FUNCTION 034

.7781 EXP( -2.95406 \*T)  
2.4524 EXP( -.02814 \*T)

## CONSTRAINED RELAXATION FUNCTION 035

1.5068 EXP( -4.04959 \*T)  
3.2468 EXP( -.02794 \*T)

TIME (MIN.)	SHEAR MOD (MEGAPASC.)	BULK MOD (MEGAPASC.)	POIS. RATIO
.0	.12163E+01	.31316E+01	.32808E+00
.31000E-01	.11940E+01	.29810E+01	.32343E+00
.62000E-01	.11735E+01	.28488E+01	.31927E+00
.12500E+00	.11365E+01	.26284E+01	.31220E+00
.25000E+00	.10786E+01	.23338E+01	.30246E+00
.50000E+00	.10048E+01	.20612E+01	.29352E+00
.10000E+01	.93946E+00	.19309E+01	.29134E+00
.20000E+01	.89702E+00	.18746E+01	.29362E+00
.40000E+01	.84973E+00	.17748E+01	.29409E+00
.80000E+01	.83855E+00	.17432E+01	.29391E+00

## UNIAXIAL RELAXATION FUNCTION 036

.7335 EXP( -3.26040 \*T)  
2.5434 EXP( -.02737 \*T)

## CONSTRAINED RELAXATION FUNCTION 037

1.7364 EXP( -4.45328 \*T)  
3.3146 EXP( -.02786 \*T)

TIME (MIN.)	SHEAR MOD (MEGAPASC.)	BULK MOD (MEGAPASC.)	POIS. RATIO
.0	.12224E+01	.34212E+01	.34039E+00
.31000E-01	.12006E+01	.32234E+01	.33450E+00
.62000E-01	.11807E+01	.30521E+01	.32924E+00
.12500E+00	.11453E+01	.27711E+01	.32017E+00
.25000E+00	.10916E+01	.24065E+01	.30724E+00
.50000E+00	.10267E+01	.20871E+01	.29402E+00
.10000E+01	.97285E+00	.19464E+01	.28763E+00
.20000E+01	.93581E+00	.18878E+01	.28761E+00
.40000E+01	.88760E+00	.17899E+01	.28772E+00
.80000E+01	.87487E+00	.17650E+01	.28797E+00



## UNIAXIAL RELAXATION FUNCTION 038

.5859 EXP( -2.77435 \*T)

2.3484 EXP( -.02773 \*T)

## CONSTRAINED RELAXATION FUNCTION 039

1.0738 EXP( -2.99313 \*T)

3.2165 EXP( -.02344 \*T)

TIME (MIN.)	SHEAR MOD (MEGAPASC.)	BULK MOD (MEGAPASC.)	POIS. RATIO
.0	.11058E+01	.28156E+01	.32632E+00
.31000E-01	.10885E+01	.27415E+01	.32469E+00
.62000E-01	.10723E+01	.26741E+01	.32321E+00
.12500E+00	.10430E+01	.25551E+01	.32058E+00
.25000E+00	.99735E+00	.23762E+01	.31656E+00
.50000E+00	.93922E+00	.21674E+01	.31182E+00
.10000E+01	.88711E+00	.20130E+01	.30868E+00
.20000E+01	.84920E+00	.19395E+01	.30890E+00
.40000E+01	.79972E+00	.18654E+01	.31154E+00
.80000E+01	.78282E+00	.18477E+01	.31248E+00

## UNIAXIAL RELAXATION FUNCTION 040

.6060 EXP( -2.37079 \*T)

2.2361 EXP( -.03184 \*T)

## CONSTRAINED RELAXATION FUNCTION 041

1.6123 EXP( -3.37739 \*T)

3.1743 EXP( -.04169 \*T)

TIME (MIN.)	SHEAR MOD (MEGAPASC.)	BULK MOD (MEGAPASC.)	POIS. RATIO
.0	.10447E+01	.33926E+01	.36044E+00
.31000E-01	.10309E+01	.32474E+01	.35655E+00
.62000E-01	.10182E+01	.31162E+01	.35297E+00
.12500E+00	.99453E+00	.28887E+01	.34656E+00
.25000E+00	.95574E+00	.25603E+01	.33666E+00
.50000E+00	.90177E+00	.22046E+01	.32466E+00
.10000E+01	.84572E+00	.19720E+01	.31576E+00
.20000E+01	.80228E+00	.18515E+01	.31222E+00
.40000E+01	.75655E+00	.16789E+01	.30745E+00
.80000E+01	.74591E+00	.16218E+01	.30613E+00

## UNIAXIAL RELAXATION FUNCTION 042

.4973 EXP( -2.48030 \*T)

2.3227 EXP( -.03064 \*T)

## CONSTRAINED RELAXATION FUNCTION 043

1.9459 EXP( -3.47533 \*T)

3.6249 EXP( -.03449 \*T)

TIME (MIN.)	SHEAR MOD (MEGAPASC.)	BULK MOD (MEGAPASC.)	POIS. RATIO
.0	.10154E+01	.42160E+01	.38854E+00
.31000E-01	.10039E+01	.40295E+01	.38506E+00
.62000E-01	.99317E+00	.38616E+01	.38183E+00
.12500E+00	.97345E+00	.35716E+01	.37600E+00
.25000E+00	.94147E+00	.31549E+01	.36685E+00
.50000E+00	.89782E+00	.27084E+01	.35533E+00
.10000E+01	.85310E+00	.24247E+01	.34603E+00
.20000E+01	.81554E+00	.22970E+01	.34243E+00
.40000E+01	.76888E+00	.21349E+01	.34066E+00
.80000E+01	.75692E+00	.20835E+01	.34012E+00

## UNIAXIAL RELAXATION FUNCTION 044

.7437 EXP( -4.15213 \*T)

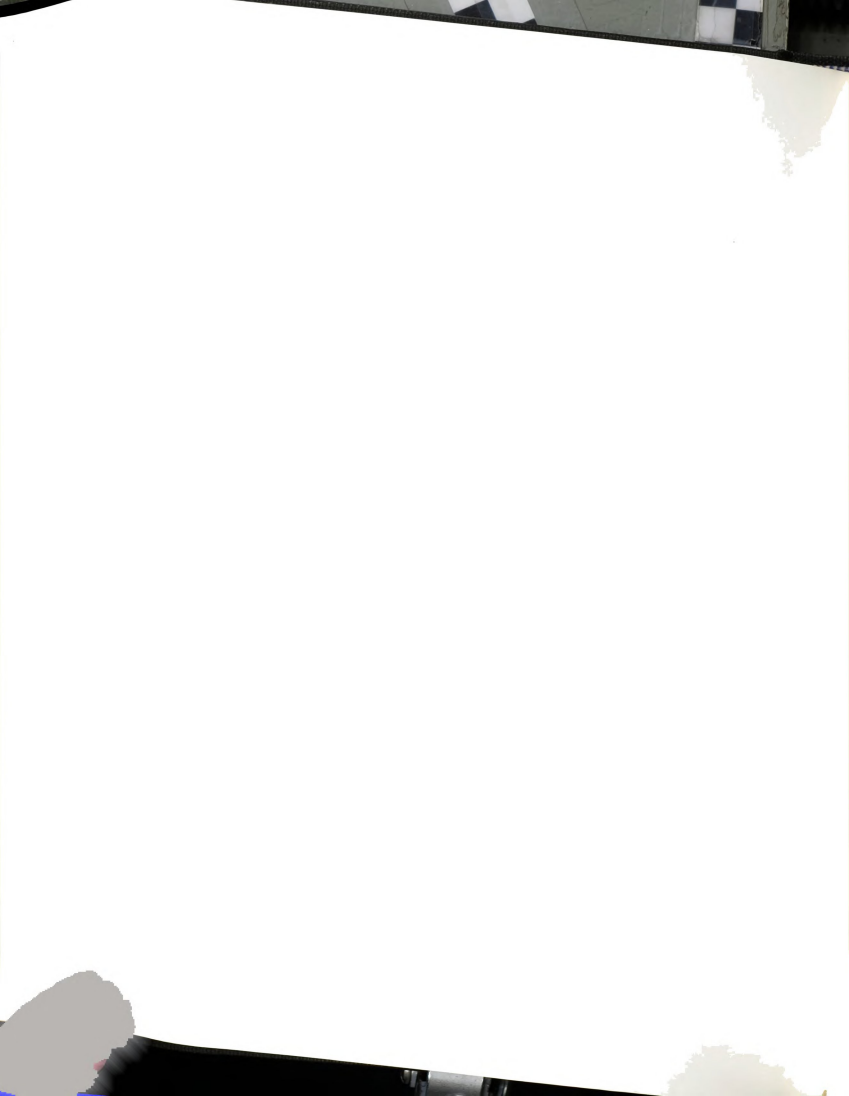
2.8628 EXP( -.02892 \*T)

## CONSTRAINED RELAXATION FUNCTION 045

2.0112 EXP( -4.63030 \*T)

3.3256 EXP( -.02840 \*T)

TIME (MIN.)	SHEAR MOD (MEGAPASC.)	BULK MOD (MEGAPASC.)	POIS. RATIO
.0	.13563E+01	.35285E+01	.32966E+00
.31000E-01	.13288E+01	.32932E+01	.32241E+00
.62000E-01	.13047E+01	.30895E+01	.31574E+00
.12500E+00	.12644E+01	.27553E+01	.30377E+00
.25000E+00	.12100E+01	.23206E+01	.28514E+00
.50000E+00	.11577E+01	.19336E+01	.26178E+00
.10000E+01	.11259E+01	.17507E+01	.24225E+00
.20000E+01	.10960E+01	.16813E+01	.23420E+00
.40000E+01	.10383E+01	.15929E+01	.23363E+00
.80000E+01	.10239E+01	.15698E+01	.23385E+00



## UNIAXIAL RELAXATION FUNCTION 046

.5797 EXP( -4.85286 \*T)

2.5519 EXP( -.02972 \*T)

## CONSTRAINED RELAXATION FUNCTION 047

3.1240 EXP( -5.25084 \*T)

3.0730 EXP( -.05344 \*T)

TIME (MIN.)	SHEAR MOD (MEGAPASC.)	BULK MOD (MEGAPASC.)	POIS. RATIO
.0	.11273E+01	.46935E+01	.38873E+00
.31000E-01	.11038E+01	.42509E+01	.38087E+00
.62000E-01	.10837E+01	.38733E+01	.37345E+00
.12500E+00	.10518E+01	.32707E+01	.35972E+00
.25000E+00	.10132E+01	.25220E+01	.33709E+00
.50000E+00	.98497E+00	.19050E+01	.30509E+00
.10000E+01	.97778E+00	.16256E+01	.27056E+00
.20000E+01	.96825E+00	.14704E+01	.24292E+00
.40000E+01	.93513E+00	.12428E+01	.21602E+00
.80000E+01	.92497E+00	.11812E+01	.20863E+00

## UNIAXIAL RELAXATION FUNCTION 050

.8353 EXP( -2.57384 \*T)

3.1536 EXP( -.03147 \*T)

## CONSTRAINED RELAXATION FUNCTION 051

1.3105 EXP( -3.42813 \*T)

3.8451 EXP( -.02748 \*T)

TIME (MIN.)	SHEAR MOD (MEGAPASC.)	BULK MOD (MEGAPASC.)	POIS. RATIO
.0	.15526E+01	.30850E+01	.28452E+00
.31000E-01	.15312E+01	.29785E+01	.28062E+00
.62000E-01	.15111E+01	.28832E+01	.27714E+00
.12500E+00	.14741E+01	.27202E+01	.27120E+00
.25000E+00	.14133E+01	.24906E+01	.26302E+00
.50000E+00	.13292E+01	.22565E+01	.25580E+00
.10000E+01	.12426E+01	.21264E+01	.25564E+00
.20000E+01	.11756E+01	.20732E+01	.26103E+00
.40000E+01	.11006E+01	.19823E+01	.26533E+00
.80000E+01	.10808E+01	.19545E+01	.26625E+00

## UNIAXIAL RELAXATION FUNCTION 052

.6996 EXP( -3.83343 \*T)  
3.0238 EXP( -.03406 \*T)

## CONSTRAINED RELAXATION FUNCTION 053

1.2360 EXP( -3.06739 \*T)  
3.8003 EXP( -.02267 \*T)

TIME (MIN.)	SHEAR MOD (MEGAPASC.)	BULK MOD (MEGAPASC.)	POIS. RATIO
.0	.14301E+01	.31292E+01	.30174E+00
.31000E+01	.13992E+01	.30558E+01	.30138E+00
.62000E+01	.13718E+01	.29879E+01	.30093E+00
.12500E+00	.13251E+01	.28651E+01	.29974E+00
.25000E+00	.12599E+01	.26732E+01	.29676E+00
.50000E+00	.11923E+01	.24345E+01	.29074E+00
.10000E+01	.11450E+01	.22458E+01	.28367E+00
.20000E+01	.11013E+01	.21658E+01	.28274E+00
.40000E+01	.10233E+01	.21097E+01	.29066E+00
.80000E+01	.10005E+01	.20939E+01	.29348E+00

## UNIAXIAL RELAXATION FUNCTION 054

.7501 EXP( -3.17312 \*T)  
2.9222 EXP( -.03818 \*T)

## CONSTRAINED RELAXATION FUNCTION 055

2.3671 EXP( -3.66107 \*T)  
4.2212 EXP( -.04113 \*T)

TIME (MIN.)	SHEAR MOD (MEGAPASC.)	BULK MOD (MEGAPASC.)	POIS. RATIO
.0	.13376E+01	.48044E+01	.37271E+00
.31000E+01	.13143E+01	.45766E+01	.36905E+00
.62000E+01	.12930E+01	.43730E+01	.36573E+00
.12500E+00	.12553E+01	.40237E+01	.35973E+00
.25000E+00	.11984E+01	.35282E+01	.35025E+00
.50000E+00	.11302E+01	.30081E+01	.33811E+00
.10000E+01	.10725E+01	.26818E+01	.32763E+00
.20000E+01	.10247E+01	.25229E+01	.32285E+00
.40000E+01	.95291E+00	.23189E+01	.32157E+00
.80000E+01	.93321E+00	.22615E+01	.32228E+00





## UNIAXIAL RELAXATION FUNCTION 056

.6686 EXP( -2.55635 \*T)  
2.7517 EXP( -.03327 \*T)

## CONSTRAINED RELAXATION FUNCTION 057

1.7637 EXP( -3.08777 \*T)  
3.0195 EXP( -.04004 \*T)

TIME (MIN.)	SHEAR MOD (MEGAPASC.)	BULK MOD (MEGAPASC.)	POIS. RATIO
.0	.13026E+01	.30463E+01	.31288E+00
.31000E-01	.12882E+01	.29009E+01	.30673E+00
.62000E-01	.12749E+01	.27687E+01	.30092E+00
.12500E+00	.12508E+01	.25357E+01	.29003E+00
.25000E+00	.12129E+01	.21873E+01	.27167E+00
.50000E+00	.11644E+01	.17839E+01	.24479E+00
.10000E+01	.11201E+01	.14878E+01	.21461E+00
.20000E+01	.10847E+01	.13444E+01	.19139E+00
.40000E+01	.10301E+01	.12058E+01	.17580E+00
.80000E+01	.10148E+01	.11685E+01	.17260E+00

## UNIAXIAL RELAXATION FUNCTION 060

.6872 EXP( -3.48049 \*T)  
2.5574 EXP( -.04137 \*T)

## CONSTRAINED RELAXATION FUNCTION 061

1.4710 EXP( -3.57430 \*T)  
3.6786 EXP( -.03413 \*T)

TIME (MIN.)	SHEAR MOD (MEGAPASC.)	BULK MOD (MEGAPASC.)	POIS. RATIO
.0	.12041E+01	.35438E+01	.34746E+00
.31000E-01	.11784E+01	.34201E+01	.34551E+00
.62000E-01	.11553E+01	.33090E+01	.34375E+00
.12500E+00	.11150E+01	.31172E+01	.34059E+00
.25000E+00	.10557E+01	.28418E+01	.33573E+00
.50000E+00	.98793E+00	.25455E+01	.32986E+00
.10000E+01	.93390E+00	.23510E+01	.32573E+00
.20000E+01	.88846E+00	.22523E+01	.32587E+00
.40000E+01	.81866E+00	.21243E+01	.32960E+00
.80000E+01	.80109E+00	.20862E+01	.33105E+00



## UNIAXIAL RELAXATION FUNCTION 064

.7654 EXP( -3.54544 \*T)  
2.8442 EXP( -.04543 \*T)

## CONSTRAINED RELAXATION FUNCTION 065

1.7495 EXP( -3.42369 \*T)  
3.4250 EXP( -.03241 \*T)

TIME (MIN.)	SHEAR MOD (MEGAPASC.)	BULK MOD (MEGAPASC.)	POIS. RATIO
.0	.13667E+01	.33521E+01	.32055E+00
.31000E-01	.13386E+01	.32099E+01	.31701E+00
.62000E-01	.13135E+01	.30817E+01	.31367E+00
.12500E+00	.12699E+01	.28583E+01	.30745E+00
.25000E+00	.12067E+01	.25317E+01	.29709E+00
.50000E+00	.11365E+01	.21704E+01	.28260E+00
.10000E+01	.10813E+01	.19308E+01	.26899E+00
.20000E+01	.10272E+01	.18425E+01	.26562E+00
.40000E+01	.93304E+00	.17728E+01	.27487E+00
.80000E+01	.90762E+00	.17551E+01	.27791E+00

## UNIAXIAL RELAXATION FUNCTION 066

.8096 EXP( -2.55665 \*T)  
2.6134 EXP( -.04454 \*T)

## CONSTRAINED RELAXATION FUNCTION 067

3.3013 EXP( -4.24651 \*T)  
3.4463 EXP( -.09141 \*T)

TIME (MIN.)	SHEAR MOD (MEGAPASC.)	BULK MOD (MEGAPASC.)	POIS. RATIO
.0	.12328E+01	.51023E+01	.38808E+00
.31000E-01	.12153E+01	.47100E+01	.38144E+00
.62000E-01	.11990E+01	.43552E+01	.37514E+00
.12500E+00	.11692E+01	.37897E+01	.36354E+00
.25000E+00	.11214E+01	.30156E+01	.34473E+00
.50000E+00	.10575E+01	.22779E+01	.31894E+00
.10000E+01	.99486E+00	.18658E+01	.29249E+00
.20000E+01	.94665E+00	.16074E+01	.26931E+00
.40000E+01	.89158E+00	.12067E+01	.23567E+00
.80000E+01	.87669E+00	.10893E+01	.22523E+00

















MICHIGAN STATE UNIV. LIBRARIES



31293106045382